

**Electrochemical and Surface Chemical Studies of
n-GaAs Photoanodes**

Thesis by

Bruce John Tufts

In Partial Fulfillment of the Requirements

for the Degree of

Doctor of Philosophy

California Institute of Technology

Pasadena, California

1991

(Defended 18 March 1991)

Acknowledgements

I had the unusual experience of starting my graduate career at Stanford and finishing it at Caltech. Life in the Lewis' Group was generally exciting, and at times downright wild. I wouldn't have traded it for anything else. Along the way, many people were sources of strength and inspiration to me. My mother, Mom, was enormously supportive during the entire time. This thesis is dedicated to her, for her strength of conviction and the clarity of her life. Thanks, Mom.

Many thanks are also due to the members of the Group. From the early days, I want to thank Lou Casagrande, Mary Rosenbluth, and Dr. Ian Abrahams for their rare and good friendship. Mike "Motorhead" Heben, Amit "W. W." Kumar, and honorary group member Kim Gupta were roommates of mine. I cannot say enough in appreciation: they are a great bunch of guys. I'm grateful to Gail Ryba for occasionally letting me pick her brain, and for being such a sensitive and useful sounding board. Drs. Reggie Penner, Mike Sailor, Gordon Miskelly, and Malcolm Forbes contributed enormously to a sense of vitality and fun in the group. The days of High Gutter and Low Schtick are sorely missed by me. Hee-Hurr! Thanks are due to the entire rest of the current group - Teri, Gary, Sharon, Dr. Rik, Russ, Dr. Tom, Dr. Andy, Bao, Ming, Chris, Sonbinh, and Ashish - for putting up with me while I was writing up and for their generally good attitudes. I want to thank the Bercaw group, especially W. Donnie Cotter, Dr. John Power, and Dr. Gui "Bill" Bazan, for many great and good times. Finally, I thank Drs. Mike Hecht and Rick Vasquez of the Jet Propulsion Laboratory for access to and aid with the XPS instrumentation in their group.

While doing science in the Group has been fun, all work and no play is a lousy way to lead your life. I think I would have long ago lost my perspective on work and fun were it not for the saving influence of Matt Pujolar and Andy Griffin, two of my best friends. They have the brilliant perspective of not doing science for a living, and have periodically forced such a point of view on me. I have never suffered any ill effects from such treatment, and recommend it highly to anyone in this business. It works. In a similar vein, I am enormously grateful to Joey Vittitoe and Mark Gregg for their friendship and hospitality. I don't know two nicer guys.

I wish also to acknowledge sources of faculty support and encouragement. Professor Mike Hochella, of the Stanford Geology department, taught me the basics of surface science. I admire Mike's methods and style, and I hope some of it rubbed off on me. I am grateful to Professor Sunney Chan for his attention, candor, and hospitality. The Laughing Buddha of Caltech is living proof that courtesy and care are not dead in the halls of high power academia. Finally, I would like to acknowledge the guidance and patience of my research advisor, Professor Nate "Fearless Leader" Lewis. While working for Nate is definitely not for the weak-willed, anyone with the spirit of reasoned argument in them can have an open audience with Mr. Big. Unflinching scientific honesty and the ability to separate personal opinion from the facts at hand are among Nate's best qualities. (As near as he knows.) Thanks Nate, you set an excellent standard. After seven plus years in the Group, I think I can do just about anything. Now that's a plus.

Abstract

The electrochemical response of n-type gallium arsenide (n-GaAs) photoanodes was monitored while in contact with aqueous basic selenide electrolytes before and after exposure to separate aqueous 0.010 M solutions of transition metal ions. Representative members of the transition metal complexes included $\text{RuCl}_3 \cdot x\text{H}_2\text{O}$, $\text{RhCl}_3 \cdot x\text{H}_2\text{O}$, $\text{IrCl}_3 \cdot x\text{H}_2\text{O}$, $\text{OsCl}_3 \cdot x\text{H}_2\text{O}$, $[\text{Co(III)(NH}_3)_6](\text{Br})_3$, $[\text{Ru(III)(NH}_3)_5(\text{Cl})](\text{Cl})_2$, and $[\text{Ru(II)(NH}_3)_5(\text{OH}_2)](\text{Cl})_2$. Several members of this group were shown to yield improved current-voltage (*I-V*) characteristics at the n-GaAs/KOH - $\text{Se}^{-/2-}(\text{aq})$ junction. A comparison of the current-voltage properties for p-type and n⁺-type GaAs electrodes in the dark, as well as for 10 % Sn-doped In_2O_3 electrodes, demonstrated that the source of the improved *I-V* response following metal ion exposure was a large decrease in the overpotentials, at a given current density, required for selenide oxidation.

An extensive surface analytic study revealed that Co(III) ammine complexes became adsorbed on GaAs surfaces from solutions of pH > 9 by a redox reaction involving sacrificial oxidation of the GaAs substrate. The product in all cases was an amorphous Co(OH)_2 surface layer. The stoichiometry of the redox reaction involves one equivalent of GaAs per six equivalent Co(III) species. Following immersion into the KOH - $\text{Se}^{-/2-}(\text{aq})$ electrolyte, the Co(OH)_2 surface layer was converted to a CoSe_2 -like phase that is believed to be the active electrocatalyst responsible for the reduced overpotential dependence following Co(III) ammine treatment.

Finally, the surface composition of n-GaAs electrodes that had been specifically etched to produce either a clean, a metallic arsenic covered, or a uniformly oxidized surface were probed by high resolution XPS and were correlated with the n-GaAs *I-V* properties in aqueous and non-aqueous electrolytes.

Table of Contents

Acknowledgements	ii
Abstract	iv
Table of Contents	v
List of Figures	vi
List of Tables	ix
General Introduction	1
Chapter 1. Photoelectrochemical Studies of Transition Metal Ion exposed n-GaAs/KOH - Se ₂ ²⁻ - Se ²⁻ Semiconductor/Liquid Junctions	3
References	43
Chapter 2. X-ray Photoelectron and Extended X-ray Absorption Fine Structure Spectroscopic Studies of the Reactions of Co(III) Ammine Complexes with GaAs Surfaces	47
References	113
Chapter 3. Correlations Between the Interfacial Chemistry and Current-Voltage Behavior of n-GaAs/Liquid Junctions	119
References	153
Thesis Summary	157

List of Figures

Chapter 1

- Figure 1. Idealized photoelectrochemical cell. 6
- Figure 2. Idealized current voltage curves and fill factors. 9
- Figure 3. *I-V* properties of n-GaAs(Os)/KOH-Se⁻²⁻ junction. 12
- Figure 4. *I-V* properties of RuCl₃·xH₂O exposed n-type, p-type, n⁺-type GaAs, and ITO electrodes in contact with KOH-Se⁻²⁻ electrolytes. 27
- Figure 5. *I-V* properties of [Co(III)(NH₃)₆](Br)₃ exposed n-type, p-type, n⁺-type GaAs, and ITO electrodes in contact with KOH-Se⁻²⁻ electrolytes. 29
- Figure 6. *I-V* properties of RhCl₃·xH₂O exposed n-type, p-type, n⁺-type GaAs, and ITO electrodes in contact with KOH-Se⁻²⁻ electrolytes. 31
- Figure 7. *I-V* properties of OsCl₃·xH₂O exposed n-type, p-type, n⁺-type GaAs, and ITO electrodes in contact with KOH-Se⁻²⁻ electrolytes. 33

Chapter 2

- Figure 1. Co 2p region XPS of GaAs samples exposed to basic aqueous solutions of [Co(III)(NH₃)₆]³⁺. 63
- Figure 2. Co 2p region XPS of model compounds [Co(III)(NH₃)₆](Br)₃ and Co(OH)₂. 68
- Figure 3. XPS of As 3d and Ga 3d regions of GaAs samples exposed to basic aqueous solutions of [Co(III)(NH₃)₆]³⁺. 70

- Figure 4. Co 2p region XPS of a GaAs substrate exposed to basic aqueous $[\text{Co(II)(OH}_2)_6](\text{Cl})_2$ solutions. 82
- Figure 5. Co 2p region XPS of GaAs samples exposed to basic aqueous solutions of $[\text{Co(III)(NH}_3)_6]^{3+}$, followed by exposure to $\text{KOH-Se}^{-/2-}$ electrolyte; and Co 2p region XPS of model CoSe compound. 85
- Figure 6. Co k-edge x-ray fluorescence edge, EXAFS, and Fourier transform of GaAs powder exposed to aqueous basic $[\text{Co(III)(NH}_3)_5(\text{OH}_2)]^{2+}$ solution. 90
- Figure 7. EXAFS and Fourier transform data of model compounds *roseo*- Co(II)(OH)_2 and Co(III)O(OH) . 92
- Figure 8. *In vacuo* and *in situ* comparison of Fourier transformed Co k-edge EXAFS of GaAs powder exposed to basic $[\text{Co(III)(NH}_3)_5(\text{OH}_2)]^{2+}(\text{aq})$ solution. 97
- Figure 9. EXAFS and Fourier transform data of GaAs powder exposed to an aqueous basic solution of $[\text{Co(II)(OH}_2)_6](\text{SO}_4)$. 99
- Figure 10. EXAFS and Fourier transform data of CoSe_2 model compound, and GaAs powder initially treated with basic aqueous solutions of $[\text{Co(III)(NH}_3)_6]^{3+}$, followed by exposure to $\text{KOH-Se}^{-/2-}$ electrolyte. 102

Chapter 3

- Figure 1. *I-V* curves of various n-GaAs surfaces in contact with the acetonitrile-based $\text{LiClO}_4\text{-FeCp}_2^{+/0}$ electrolyte, the $\text{KOH-Se}^{-/2-}$ electrolyte, and Au overlayers. 133

Figure 2. As 3d region XPS of a near stoichiometric and As⁰ rich GaAs interface. 137

Figure 3. XPS from the As 3d and Ga 3d regions of near stoichiometric, As⁰ rich, and uniformly oxidized GaAs interfaces before and after *I-V* cycling in acetonitrile-based LiClO₄-FeCp₂⁺⁰ and KOH-Se⁻²⁻ electrolytes. 139

List of Tables

Chapter 1

Table I. <i>I-V</i> characteristics of transition metal ion exposed (100)-oriented n-GaAs photoanodes in KOH-Se ⁻²⁻ electrolytes.	24
--	----

Chapter 2

Table I. X-ray photoelectron spectroscopy: Surface analysis materials parameters.	57
Table II. XPS peak positions: Model compounds and surface components of etched and reacted GaAs interfaces.	65
Table III. Surface coverage of reacted (100) GaAs surfaces.	72
Table IV. EXAFS derived nearest neighbor distances and coordination numbers.	93
Table V. Distribution of product ions by XRF analysis.	104
Table VI. ⁵⁷ Co coverage on single crystal GaAs.	107

Chapter 3

Table I. X-ray photoelectron spectroscopy: Surface analysis materials parameters.	130
Table II. XPS peak positions and intensities of etched and photoelectrochemically cycled (100) n-GaAs electrodes.	140
Table III. XPS surface composition of etched and photoelectrochemically cycled (100) GaAs electrodes.	145

General Introduction

The focus of this thesis is on the current-voltage (*I-V*) behavior of surface modified n-type gallium arsenide (GaAs) photoanodes in contact with aqueous and non-aqueous electrolytes. Two distinct classes of surface manipulation served to give direction to the body of this work: (i) GaAs electrodes exposed to an array of transition metal complexes in aqueous solution; and (ii) specific production of near-stoichiometric, elemental arsenic (As^0) covered, or uniformly oxidized, n-GaAs surfaces. Extensive use of surface sensitive analytic methods, specifically x-ray photoelectron spectroscopy (XPS), and extended x-ray absorption fine structure analysis (EXAFS), has revealed important correlations between surface composition, interfacial chemical transformations, and the *I-V* properties of surface modified n-GaAs electrodes. In order to keep the volume of this work to a reasonable size, a minimal amount of background material has been provided in the introductory sections of each chapter. Sufficient references have been provided to facilitate access to the more fundamental reviews available in the literature.

This dissertation is divided into three chapters. Chapter one details the effects exposure to certain transition metal ions has on the current-voltage properties of n-GaAs(M)/1.0 M KOH - 0.8 M K_2Se - 0.1 M K_2Se_2 aqueous junctions. The outcome of parallel treatments on p-type and n^+ -type GaAs electrodes and 10 % doped In_2O_3 (ITO) electrodes is used to differentiate between contradictory theoretical descriptions of the mechanism of transition metal induced *I-V* improvements. Chapter two reports an exhaustive surface chemical study of the interactions of GaAs surfaces with

$[\text{Co(III)(NH}_3)_5\text{X}]^{n+}$ ($\text{X} = \text{NH}_3, \text{OH}_2, \text{Br}^-, \text{Cl}^-, \text{N}_3^-$), $[\text{Co(II)(NH}_3)_6]^{2+}$, $[\text{Co(III/II)(bipy)}_3]^{3+/2+}$ (bipy = 2, 2'-bipyridine), and $[\text{Co(II)(OH}_2)_6]^{2+}$ complexes over the range $2 < \text{pH} < 13$. The data in chapter two prove sufficient to reveal the dominant pathway to, as well as the scope of and limitations on, chemisorption in the GaAs-cobalt metal ion complex system. Additionally, the fate of chemisorbed cobalt ions upon introduction of modified GaAs electrodes into the $\text{KOH-Se}^{-/2-}(\text{aq})$ electrolyte is also described. Chapter three presents the results of a combined XPS/specific surface etch study on n-GaAs photoanodes in contact with acetonitrile-based $\text{LiClO}_4 - \text{FeCp}_2^{+/0}$ ($\text{FeCp}_2 = \text{ferrocene}$) and $\text{KOH-Se}^{-/2-}(\text{aq})$ electrolytes. Correlations between the surface composition and current-voltage behavior of specifically prepared n-GaAs/liquid junctions serve to highlight significant shortcomings in current theories of semiconductor interface charge-carrier dynamics. Finally, the results illustrate the unique, reproducible, and non-destructive character of semiconductor/liquid junctions in tests of the chemical manipulability of electrically active surface recombination sites.

Chapter 1

Photoelectrochemical Studies of Transition Metal Ion exposed n-GaAs/KOH – Se²⁻ – Se²⁻ Semiconductor/Liquid Junctions

Abstract: Improvements observed (1979) in the current-voltage (*I-V*) characteristics of illuminated n-GaAs/KOH-Se²⁻(aq) junctions, due to electrode exposure to acidic (pH < 2) solutions of transition metal complexes, suggested that electrically active recombination sites at the n-GaAs surface could be manipulated chemically. In order to outline the general scope and magnitude of this activity, etched n-GaAs electrodes were exposed to a wide range of octahedral transition metal complexes and subsequently monitored under illumination in the KOH–Se²⁻(aq) electrolyte. Relative to untreated n-GaAs electrodes, improvement in *I-V* behavior was observed following exposure to Co(III), Co(II), Ru(IV), Ru(II), Pb(II), Rh(III), Os(IV), Os(III), and Ir(III) complexes. At 88 mW cm⁻² solar-simulated illumination, transition metal ion exposed, matte etched, n-GaAs/KOH-Se²⁻(aq) junctions gave absolute light to electrical power conversion efficiencies of up to 16 ± 1 %. Two compelling predictions concerning the role of surface treatments on electrically active interface states implied opposing trends for changes in surface recombination rate versus changes in hole transfer rate to Se²⁻ ion. A test of the changes in carrier dynamics was afforded by an exploration of the dark *I-V* behavior of untreated and transition metal complex exposed n⁺- and p-GaAs, and of tin-doped indium oxide (10 % Sn:In₂O₃; ITO) electrodes. A consistent analysis indicated that improvements in the *I-V* characteristic of transition metal ion-treated n-GaAs/KOH-Se²⁻(aq) junctions were due to increased rates of Se²⁻ oxidation, relative to the untreated case.

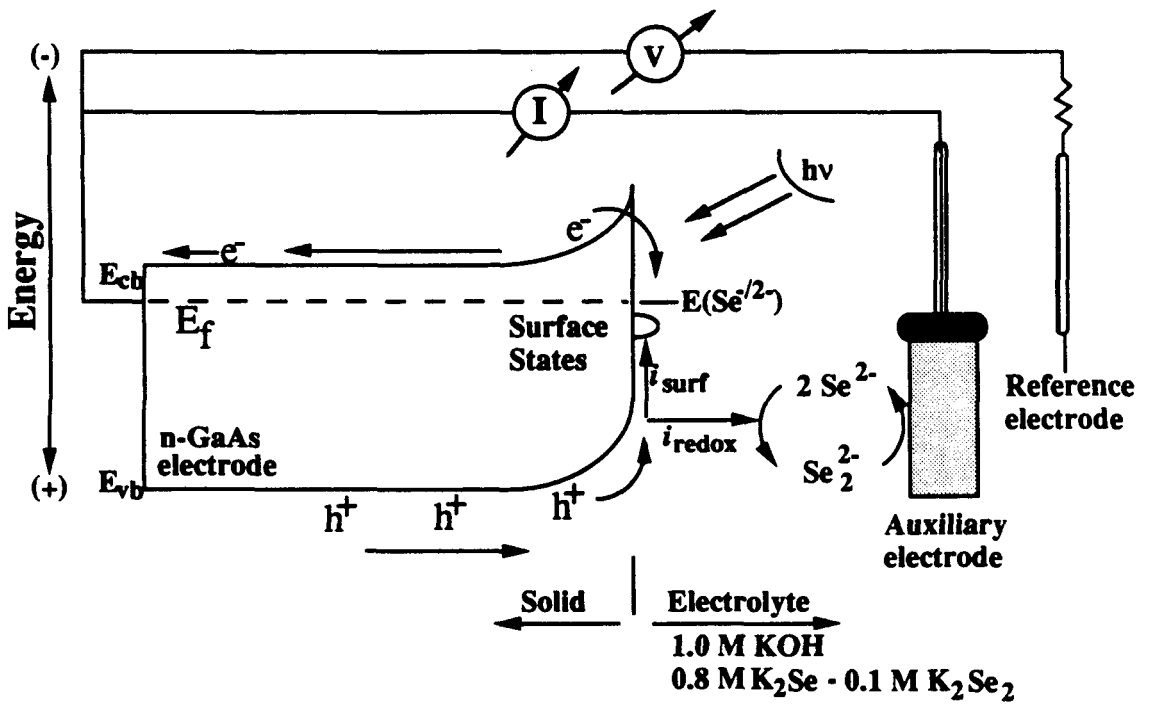
Introduction

Upon immersion of a semiconductor electrode into a redox active electrolyte, the initial difference in electrochemical potentials of the electrode (termed the Fermi level, E_f) and the solution (called the redox level, $E(A^+/A)$) induces a small amount of charge to flow from one to the other until equilibrium is achieved. With respect to the solution, the relative change in the concentrations of oxidized and reduced species upon equilibration with the semiconductor is negligible. The semiconductor, however, typically experiences relatively large changes in the magnitude and distribution of ionized dopants (donors or acceptors) held in the crystal lattice. The spread of ionized dopants is confined to the near surface region and is the source of the built-in electric field that is responsible for the rectifying current-voltage (I - V) behavior observed in semiconductor devices. Figure 1 displays a cut-away cartoon of an idealized n-GaAs/1.0 M KOH - 0.8 M K_2Se - 0.1 M K_2Se_2 liquid junction. The semiconductor is n-GaAs, while the species K_2Se_2 - K_2Se make up the redox couple. In Figure 1, the curved lines of the n-GaAs conduction (E_{cb}) and valence (E_{vb}) bands near the solid/liquid interface represent the presence of the built-in electric field. The figure also displays the auxiliary and reference electrodes that, together with the n-GaAs photoanode, form the basis of a three electrode photoelectrochemical cell.

When the n-GaAs electrode is in contact with the KOH- Se^{2-} (aq) electrolyte and is illuminated with sufficiently energetic light, photons may be absorbed and electrons excited across the band gap, from the valence band to the conduction band. In the process, a net deficit of electrons, termed holes, is created in the valence band. Photogenerated electrons and holes created near the solid/liquid interface are almost immediately separated in the presence of the built-in electric field. At an n-type semiconductor, photogenerated holes are swept to the solid/liquid interface and photogenerated electrons are swept into the crystal bulk. As shown in Figure 1, once at the surface the holes will experience one of at least

Figure 1: Idealized n-GaAs/1.0 M KOH - 0.8 M K₂Se - 0.1 M K₂Se₂ photoelectrochemical cell. The electrochemical potential of the solution is designated by $E(\text{Se}^{-2})$. E_f is the electrode electrochemical potential, also known as the Fermi level. E_{vb} is the semiconductor valence band edge. E_{cb} is the semiconductor conduction band edge. Current leading to surface recombination events is labeled i_{surf} , observed current is labeled i_{redox} .

Idealized Photoelectrochemical Cell:
n-GaAs/1.0 M KOH-0.8 M K₂Se-0.1 M K₂Se₂
Liquid Junction



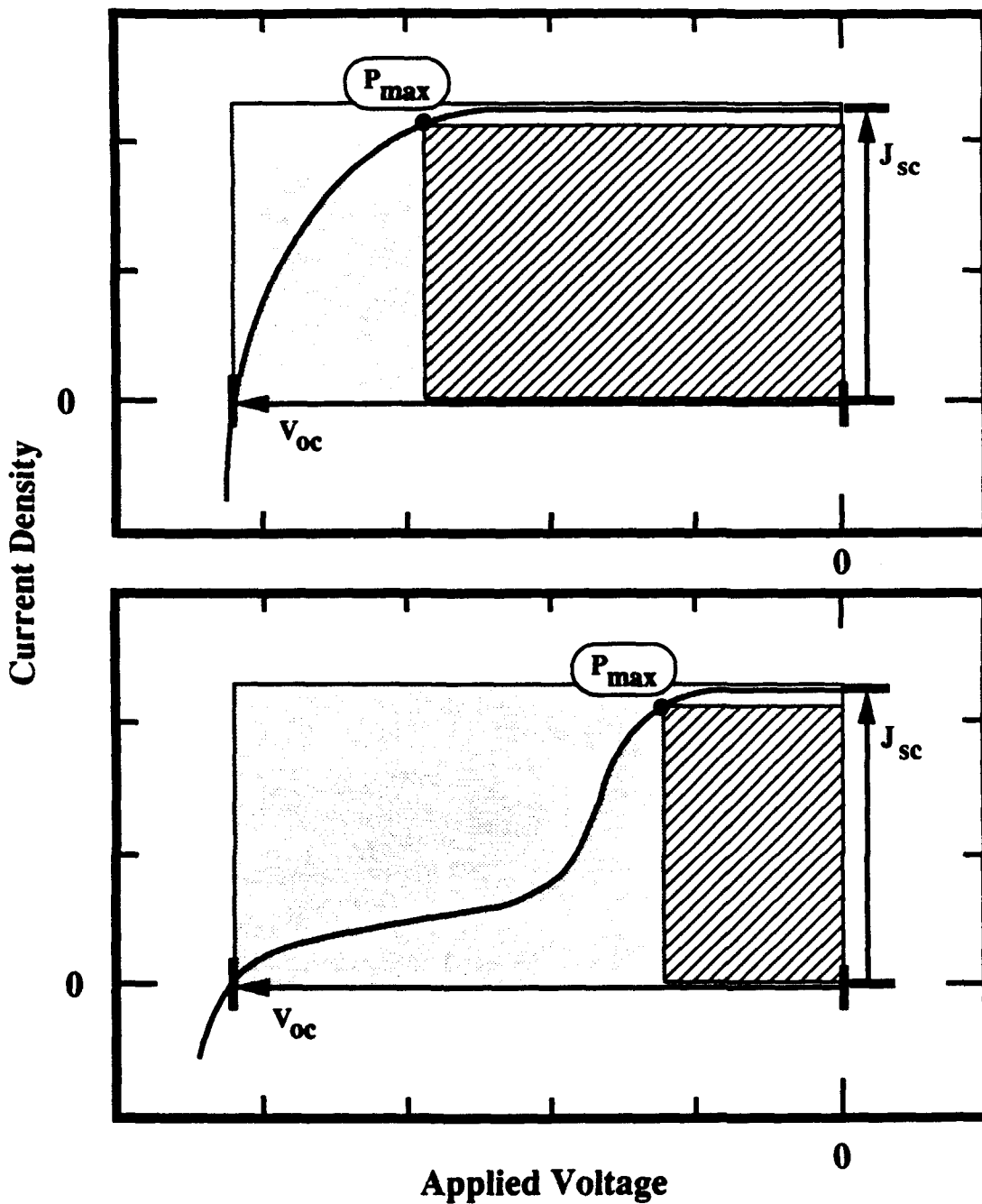
two possible fates. They can become trapped in surface states (ubiquitous poorly defined sites on the surface that have energies lying in the band gap), and eventually recombine with an electron. This surface recombination process results in no net current.

Alternatively, the hole can oxidize Se^{2-} from solution, giving rise to a net current. Use of a potentiostat and a three electrode configuration allows the full current-voltage characteristic of the n-GaAs/1.0 M KOH - 0.8 M K_2Se - 0.1 M K_2Se_2 junction to be collected while maintaining current continuity (by driving exactly the opposite current through the auxiliary electrode) in the cell.

In assessing the nature of current-voltage curves, among other observables, three principle figures of merit are employed: the open circuit photovoltage (V_{oc}), the short circuit photocurrent density (J_{sc}), and the maximum power point (P_{max}). These terms are illustrated in Figure 2. The V_{oc} is found on an I - V trace at the point of no net current flow. It is a measure of the free energy available to the cell to do work on an external load. V_{oc} scales with the logarithm of the photocurrent density, J_{ph} . (In this work, the characteristics of all I - V data collected at n-GaAs electrodes was such that $J_{\text{ph}} = J_{\text{sc}}$.) J_{sc} is found on an I - V trace at the point of zero driving force, *i.e.*, at zero net cell voltage. P_{max} is that point on the I - V curve where the maximum power available from the cell is developed. By definition, $P_{\text{max}} = V_{\text{max}} \cdot J_{\text{max}}$. These figures of merit are collected into one term, called the fill factor ($\text{FF} = P_{\text{max}}/[V_{\text{oc}} \cdot J_{\text{sc}}]$). This reflects the upper limit of the power that may be extracted from the photoelectrochemical cell, relative to the idealized power expected from a cell with no kinetic limitations on charge transport through the bulk semiconductor, or charge transfer at, or mass transport to, the cell's electrodes. In this sense the fill factor is a measure of the kinetic competence of a given photoelectrochemical cell. The theoretical maximum for the fill factor is $\text{FF} \approx 0.85$.

Figure 2: Idealized current-voltage (I - V) curves and fill factors showing a high quality (top) I - V characteristic and a poor (bottom) I - V characteristic. V_{oc} is the open circuit photovoltage, J_{sc} is the short circuit current density, and P_{max} represents that point on the I - V trace where the maximum power is generated in the system. The photovoltage and photocurrent density at P_{max} are referred to as V_{max} and J_{max} , respectively. By definition, $P_{max} = V_{max} \cdot J_{max}$. The shaded region gives graphically the cell power available at P_{max} . The ratio of the shaded area to the hypothetical larger rectangle defined by V_{oc} and J_{sc} is the fill factor ($FF = P_{max}/[V_{oc} \cdot J_{sc}]$).

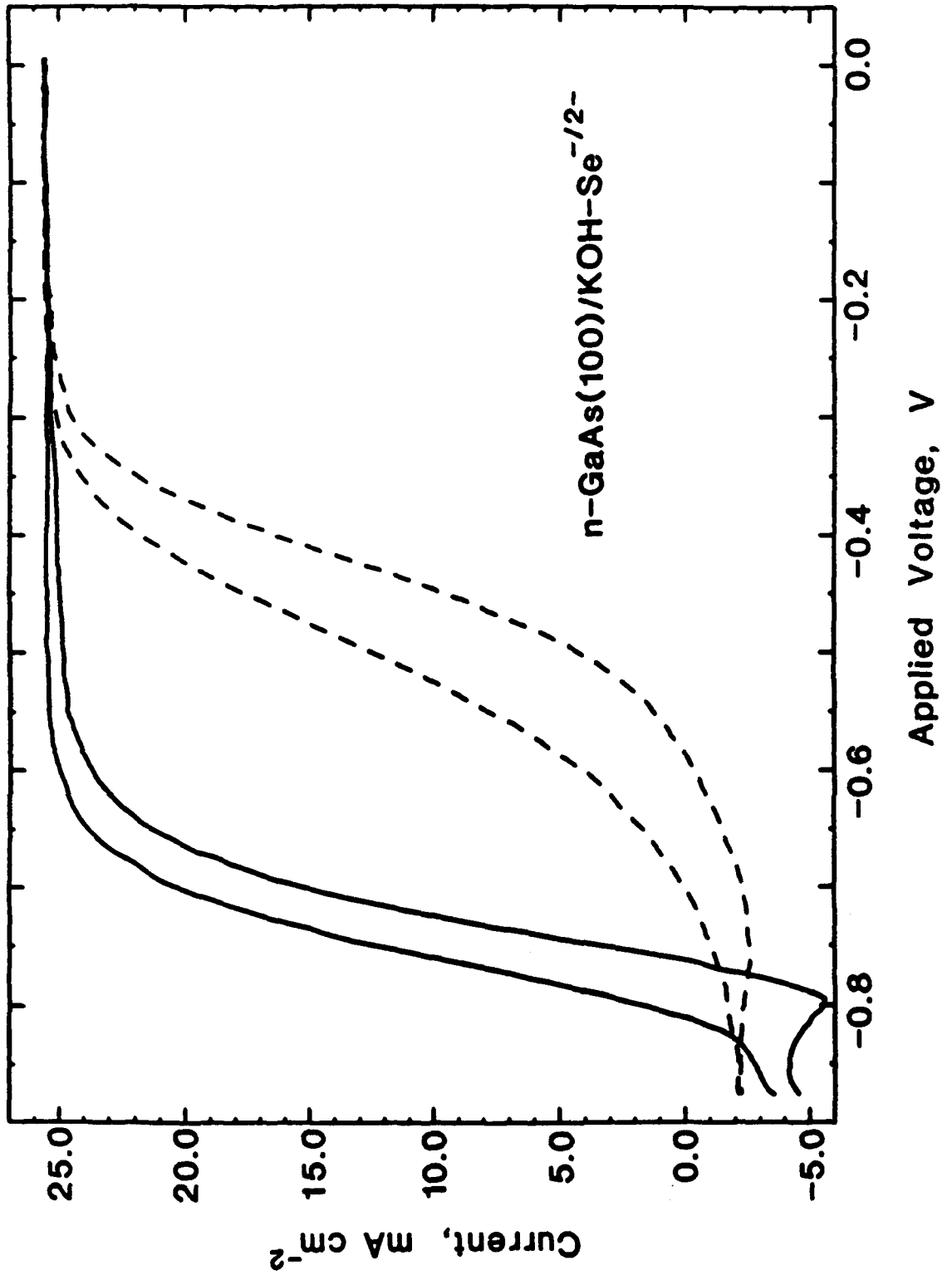
Idealized Fill Factors



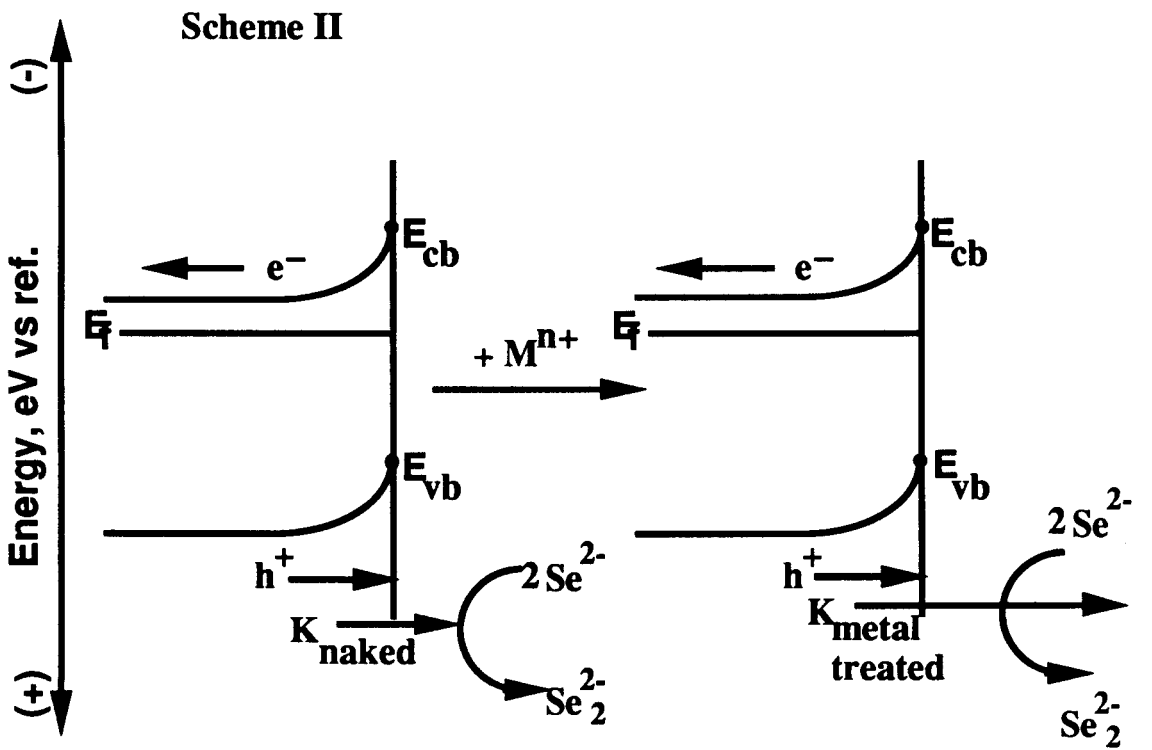
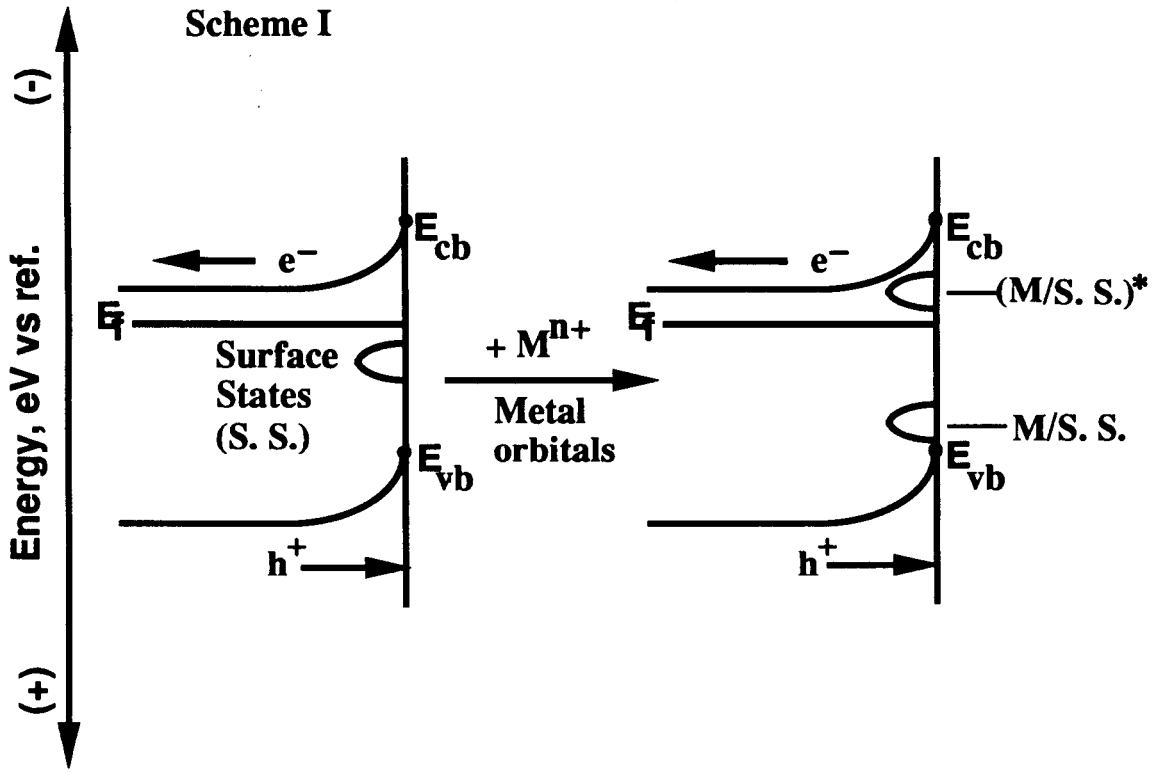
As the first small band gap ($E_g < 2.0$ eV, 1977) photoanode found to be stable in aqueous electrolytes,¹ the n-GaAs/1.0 M KOH–0.8 M K₂Se–0.1 M K₂Se₂/Pt photoelectrochemical cell attracted intense interest as a model system for tests of kinetic stability against photocorrosion² and implied that p-type GaAs-based systems might serve as potential platforms for hydrogen production schemes.³ During the course of early empirical studies on this system, it was observed that exposure of etched GaAs electrodes to acidic solutions (pH < 2) of certain transition metal ions led to large improvements in the current-voltage (*I-V*) characteristic of illuminated GaAs/KOH-Se^{-/2-} junctions.⁴ Figure 3 displays the effect OsCl₃·xH₂O exposure has on the *I-V* characteristic of a n-GaAs/KOH-Se^{-/2-} cell. Several theoretical attempts have been made to describe the nature of the metal ion-induced improvements at the n-GaAs-Se^{-/2-} junction,⁵ and these attempts have given rise to a pair of contradictory theoretical descriptions.^{5bd} The stability and moderate-to-high efficiency of the n-GaAs selenide system provide the experimentalist with a convenient system for mechanistic studies and allow an assessment of the dominant model describing the changes induced in the *I-V* behavior of metal ion-exposed GaAs/KOH-Se^{-/2-} interfaces.

The role of surface treatments that leads to improved cell performance is controversial.⁵ Evidence that the Ru(III) treatment described by Parkinson, Heller, and Miller⁴ reduces surface-state recombination rates has been obtained from surface recombination velocity (S_{recom}) measurements at the n-GaAs/air interface^{5c,6a} and from electron beam induced current (EBIC) measurements on polycrystalline GaAs/Schottky junctions.^{6b} These experiments have led to the suggestion that a decreased surface recombination velocity is responsible for the improvement in the *I-V* properties at the n-GaAs/KOH-Se^{-/2-} junction.^{5bc,6} Phenomenologically, the effect is ascribed to strong bonding between the metal center and surface orbitals that behave as electrically active recombination centers.^{5bc}

Figure 3: Photocurrent-voltage (I - V) properties of matte-etched (100)-oriented n-GaAs anodes in contact with 1.0 M KOH - 0.94 M K_2Se - 0.03 M K_2Se_2 aqueous electrolyte. The substrate consisted of a 10 μm thick n-GaAs layer epitaxially grown by organo-metallic vapor phase epitaxy on a n^+ -GaAs substrate. Illumination was provided by a calibrated ELH-type W-halogen bulb at 88 $mW\ cm^{-2}$ intensity; the solutions were magnetically stirred and the I - V data was collected potentiostatically (50 $mV\ s^{-1}$ scan rate). The reference electrode was a Pt wire poised at the equilibrium cell potential and the auxiliary electrode was a large area Pt foil. Dashed line: n-GaAs photoanode etched to a matte finish (30 seconds exposure to a quiescent 1:1 *vol.* con. H_2SO_4 :30 % H_2O_2 solution), and then rinsed with H_2O . Solid line: n-GaAs photoanode etched to a matte finish, rinsed with H_2O , immersed for 60 seconds in an aqueous (pH = 2, HCl) 0.010 M $OsCl_3 \cdot 3H_2O$ solution, and rinsed with H_2O . No corrections have been made for any optical absorption or reflection losses.



Reference to Scheme I illustrates these points. The unreacted surface is shown as having some density of surface states in the middle of the band gap. The theory of recombination processes reveals that states occupying energy levels in the middle of the band gap yield the highest surface recombination rates. Hence, in this framework the unreacted surface is expected to have a large surface recombination velocity ($S_{\text{recom}} \approx 10^6 \text{ cm s}^{-1}$). This supposition is supported by the observation that most GaAs junctions have large interfacial recombination rates ($10^4 < S_{\text{recom}} [\text{cm s}^{-1}] < 10^6$).^{5bc,7} Strong bond formation between the metal ion and the recombination site ought to lead to well separated bonding and anti-bonding molecular orbitals for each reacted pair, eventually leading to two new densities of states well removed from the band gap center. The net result is a decrease in surface state density at energies that sustain high rates of recombination, and therefore decreased rates of interfacial recombination. This interpretation of the recombination process may be understood by realizing that the interface kinetics are inherently bimolecular,⁸ depending on the concentration of available electrons and holes. The concentration of available electrons and holes is, in turn, exponentially sensitive to energy. At mid-gap energies, the $[e^-][h^+]$ product involved in the numerator of the rate law is a maximum. Therefore, surface traps residing at mid-gap give rise to the largest possible surface recombination rates. Within the split state model, bond formation between surface sites and metal ions shifts the energy of surface states away from mid-gap values. The result is that, while the concentration of one carrier-type will increase (up to a maximum that depends on the particular semiconductor), the concentration of the other carrier-type will decrease: the $[e^-][h^+]$ product falls very quickly at energies away from mid-gap. Consequently, the recombination rate for surface states at energies away from mid-gap is much smaller than for the same states at the center of the band gap. The overall result of splitting the density of surface states through metal ion bonding is to lower the magnitude of surface recombination losses, and hence to observe improved current-voltage characteristics from metal ion-treated electrodes.



In contrast, Allongue and co-workers have interpreted their results for the GaAs(Ru³⁺)/KOH-Se^{-/2-}/C cell in terms of Ru-induced electrocatalysis for Se²⁻ oxidation.^{5d} In this simplified framework, illustrated in Scheme II, photogenerated holes swept to the surface by the depletion region electric field are faced with two possible reaction channels. One involves hole transfer to a surface state (*cf.* Scheme I) and eventual annihilation via recombination with an electron, *i.e.*, a surface recombination reaction. The other option involves hole transfer to a solution hole acceptor (in this case the reduced form of the redox couple, Se²⁻), *i.e.*, an oxidation reaction. Modification of the surface by metal ion treatment is viewed as increasing the rate of the oxidation reaction relative to any changes in the rate of the recombination reaction.

In order to address the importance of electrocatalysis in this system, experiments have been conducted on the dark *I-V* behavior of n⁺-GaAs, p-GaAs, and tin-doped indium oxide (10 % Sn:In₂O₃; ITO) electrodes that have been previously exposed to a variety of metal ion complexes.⁹ For convenience, metal complex treated electrodes will be referred to in a parenthetical shorthand, *e.g.*, n-GaAs(M). These experiments also serve to comment on the surface state splitting model of Heller *et al.*^{5bc} Additionally, in an effort to assess the chemistry responsible for metal ion binding to n-GaAs surfaces, several new surface treatments were performed involving octahedral transition metal complexes having well established ligand substitution chemistries. The interaction of these octahedral complexes with n-GaAs electrodes and the electrodes' subsequent behavior in KOH-Se^{-/2-} electrolyte served to distinguish between mechanistic possibilities involving purely electrostatic, substitutional, or charge transfer based binding modes.

Experimental

A. Chemicals.

All solvents and etches used were either J. T. Baker MOS grade or Mallinckrodt Transistar stock. A Barnstead NANOpure water purifier provided 18 M Ω deionized water, used for all aqueous solutions.

The chloride and bromide salts of $[\text{Co(III)(NH}_3)_5\text{X}]^{n+}$ ($\text{X} = \text{N}_3^-$, NH_3 , OH_2 , Br^-),^{10,11} $[\text{Co(III)(bipy)}_3]^{3+}$,¹³ and $[\text{Co(II)(bipy)}_3]^{2+}$ ¹³ were prepared as described in the literature. The perchlorate salts of the above complexes were made by dissolving a small amount (0.5-1.0 g) of the halide salt in a minimum amount of hot (60-70 °C) water, and then adding concentrated perchloric acid dropwise to effect precipitation of the complex with perchlorate as the counter ion. The resulting solids were rinsed with 1.0 M perchloric acid on a Büchner funnel until no chloride was observed by a silver ion test, and then were washed with cold water and stored in a dessicator. The nitrate salt of $[\text{Co(III)(NH}_3)_5(\text{OH}_2)]^{3+}$ was made in a similar fashion. $[\text{Ru(III)(NH}_3)_6](\text{Cl})_3$ was purchased from Strem chemicals and used without further purification. The ruthenium complexes $[\text{Ru(III)(NH}_3)_5(\text{Cl})](\text{Cl})_2$,^{14a} $[\text{Ru(II)(NH}_3)_5(\text{OH}_2)](\text{PF}_6)_2$,^{14b} $[\text{Ru(II)(NH}_3)_6](\text{Cl})_2$,^{14c} the rhodium complexes $[\text{Rh(III)(NH}_3)_5(\text{OH}_2)](\text{ClO}_4)_3$,^{15a} $[\text{Rh(III)(NH}_3)_5(\text{Cl})](\text{ClO}_4)_3$,^{15b} , and $[\text{Rh(III)(NH}_3)_6](\text{ClO}_4)_3$,^{15c} were prepared as described in the literature. *In-situ* conversions of the ruthenium and rhodium complexes were used to generate $[\text{Ru(III)(NH}_3)_5(\text{OH}_2)]^{3+}$,^{14a} $[\text{Ru(II)(NH}_3)_5(\text{pyr})]^{2+}$ (by the addition of weak triflic acid solutions of pyridine (pyr) to $[\text{Ru(II)(NH}_3)_5(\text{OH}_2)]^{2+}$,^{14b}) $[\text{Ru(II)(NH}_3)_5(\text{Cl})]^+$,^{14a} . All water soluble cobalt ammine complexes, ruthenium ammine and hexaaquo complexes, rhodium ammine complexes, and the chromium and nickel ammine complexes were recrystallized twice from hot water (deaired where necessary) and were characterized by their electronic absorption spectra. Crystals of x-ray quality

$[\{\text{Ru(IV)}\}_2\text{OCl}_6](\text{PhCN})_4$ were kindly provided by Drs. Kaspar Evertz and John M. Power of Professor Bercau's group. The complexes $[\text{Co(II)(OH}_2)_6](\text{Cl})_2$ (J. T. Baker), $[\text{Co(II)(OH}_2)_6](\text{SO}_4)$ (J. T. Baker), $[\text{Co(II)(OH}_2)_6](\text{ClO}_4)_2$ (GFS chemicals), $\text{Pd}(\text{NO}_3)_2$ (Alfa), $\text{RuCl}_3 \cdot x\text{H}_2\text{O}$ (Alfa), $\text{RhCl}_3 \cdot x\text{H}_2\text{O}$ (Alfa and Johnson Matthey), $\text{IrCl}_3 \cdot x\text{H}_2\text{O}$ (Johnson Matthey), $\text{OsCl}_3 \cdot x\text{H}_2\text{O}$ (Alfa), $(\text{K})_2[\text{Os(IV)(Cl)}_6]$ (Engelhard), $\text{Bi}(\text{NO}_3)_3 \cdot x\text{H}_2\text{O}$ (Alfa), $[\text{Pb(II)(NO}_3)_2]$ and $[\text{Pb(II)(Cl)}_2]$ (Alfa), 1.0 M $[\text{Hg(II)(Me)(OH)}]$ in H_2O (Aesar), and $\text{Hg}(\text{NO}_3)_2$ (J. T. Baker) were used without further purification. No hazards were encountered from the manipulation of the perchlorate salts used in this work. Reagent grade KOH was obtained from J. T. Baker, and Al_2Se_3 used in preparing the selenide based electrolyte was obtained from Alfa. Concentrated HCl was obtained from Fischer, con. HClO_4 from GFS Chemicals, and trifluoroacetic acid from Aldrich.

B. GaAs Electrodes, Surface Preparations, and Photoelectrochemistry.

Several different electrode substrates were used in this study. Single crystals of (100)-oriented n-GaAs were either grown by organo-metallic vapor phase epitaxy (OMVPE) to give $N_D = 2 \times 10^{17} \text{ cm}^{-3}$ Se doped 10 μm thick epilayers, or were Czochralski grown to give $N_D = 1 - 4 \times 10^{17} \text{ cm}^{-3}$ Si doped bulk samples. Crystals of (100)-oriented n⁺-GaAs ($N_D > 5 \times 10^{18} \text{ cm}^{-3}$) were grown by OMVPE to give 5 μm thick epilayers on an n⁺-GaAs ($5 \times 10^{17} \text{ cm}^{-3}$ [Se]) substrate. Substrates of (100)-oriented p-GaAs (2×10^{17} [Zn]) were grown by OMVPE to yield a 10 μm thick epilayer on a p⁺-GaAs substrate. The Sn-doped (10 %) In_2O_3 (ITO) electrodes were fabricated as thin films ($1.2 \times 10^3 \text{ \AA}$) deposited onto glass slides. The composition of the ITO films was confirmed by electron microprobe analysis.

Ohmic contacts for the n- and n⁺-GaAs substrates were established by filament evaporation (Consolidated Vacuum Corporation, LCI-14B) of 1000 \AA of a

Au (96 %)-Ge (4 %) alloy onto the crystal back, followed by annealing in flowing N₂ (95 %)-H₂ (5 %) gas at 475 °C for 5 minutes. Evaporated metal film thicknesses were tracked simultaneously during film deposition with an oscillating quartz crystal acoustic impedance thickness monitor (R. D. Mathis, TM-100). Back contact to p-GaAs samples was made by filament evaporation of 1000 Å of a Au (95 %)-Zn (5 %) alloy, followed by annealing in flowing N₂ (95 %)-H₂ (5 %) gas at 450 °C for 5 minutes.

Electrodes were made by attaching a coiled Cu/Sn (tin clad copper) wire to the back ohmic contacts of the GaAs substrates or to the ITO surface with Ag print, and passing the end of the Cu/Sn wire through a glass tube to provide insulation from the solution. The exposed Cu/Sn wire and back contact were then sealed with white epoxy cement (Hysol Corporation) so that only the electrode face was left uncovered. (All ITO mounted in this fashion displayed Nernstian *I-V* behavior, with the expected sheet resistance properties,¹⁶ in an aqueous 1.00 M KCl-0.100 M Fe(CN)₆³⁻-0.100 M Fe(CN)₆⁴⁻ cell.) Exposed areas ranged from 0.05 - 0.2 cm², as determined to within ± 5 % by enlarged photomicrographs of the exposed electrode surfaces.

Pyrex glass Schlenk vessels were used as (photo)electrochemical cells. In photoelectrochemical studies, light was directed horizontally through the side of the cell onto electrode surfaces kept no more than 5 mm away from the inside wall. All solutions were stirred magnetically.

The 1.0 M KOH-0.8 M K₂Se-0.1 M K₂Se₂ electrolyte was prepared by scavenging H₂Se gas (pK_{a1} = 4.0)¹² in an aqueous 3.0 M KOH solution. (Caution! Stench agent! Severe poison! H₂Se gas is extremely toxic if inhaled, more so than HCN(g) or H₂S(g). It is colorless, smells intensely of rotten pumpkins, and is insidious; at non-lethal concentrations it deadens one's sense of smell. Conduct this protocol only in an efficient fume hood, and preferably in the presence of a labmate.) Note that H₂Se and

selenide salts are moderately air sensitive, eventually yielding Se^0 as the main air oxidation product. A two-neck round-bottom flask containing *ca.* 1.4 equivalents of Al_2Se_3 chunks (do not use powder!) charged with a strong magnetic stir bar was attached by ground glass joints to a custom made all glass gas train. The glass gas train was attached by ground glass joints to the inlet tube of a large (350 mL) bubbler cell, to the bottom of which was attached a ground glass stopcock joint connected to a 250 mL receiving flask having a side arm stopcock. The inlet tube passed down the length of the bubbler and terminated in a cluster of four medium porosity gas bubbling tubes. An all glass mineral oil bubbler was attached to the outlet side of the main bubbler cell. Gasses exiting the mineral oil bubbler were passed, via Tygon tubing, to a simple inverted tube bubbler immersed in 10 M $\text{KOH}(\text{aq})$ solution. Except on the exit side of the bubbler, Tygon tubing or Teflon seals have been avoided because they are O_2 permeable. The entire set-up was sparged with high purity N_2 for at least half an hour prior to gas collection. H_2Se gas was generated by the slow ($1/4$ to $1/2 \text{ mL min}^{-1}$, via a small syringe through a rubber septum sealing the second neck of the Al_2Se_3 -charged flask) dropwise addition of a N_2 -sparged 2 M HCl solution onto the Al_2Se_3 chunks. (Bubbles that escape the main bubbler are mostly composed of H_2 , the product of a side reaction.) Usually a several fold excess of acidic H_2O solution must be added to the Al_2Se_3 chunks, as a viscous $\text{Al}(\text{OH})_3$ solution is produced during the course of the reaction that slows down the rate of H_2Se evolution. At the end of the reaction (typically several hours) the solution was drained from the bubbler, under N_2 over pressure, to the receiving flask (over pressure in the receiving flask was relieved via a separate mineral oil bubbler attached to its side arm joint). The total selenium content was then assayed gravimetrically. Air was passed through an aliquot of $\text{KOH-K}_2\text{Se}$ solution in order to oxidize the selenide to yield flakes of Se^0 . The Se^0 was collected on a very fine Büchner funnel, and weighed. From the weight of Se^0 per aliquot, the concentration of Se^{2-} was determined. A final adjustment by addition of O_2 (to give K_2Se_2) or more $\text{KOH}(\text{aq})$ solution was then made to produce the final

1.0 M KOH-0.8 M K_2Se -0.1 M K_2Se_2 electrolyte. The electrolyte solutions were stable for extended periods of time (> 12 months) under a N_2 atmosphere.

Individual (photo)electrochemical cells were prepared by the transfer of *ca.* 10 mL of KOH- Se^{2-} electrolyte from the storage flask to the test cell via anaerobic syringe techniques. Severe effects of cross-contamination of KOH- Se^{2-} cells with the various metal ions were observed. Extreme care in the suppression of trace metal ion contamination of these solutions required that a separate set of etches, cells, KOH- Se^{2-} solutions, and electrodes be used for metal ion treatments with any one particular transition metal complex. For example, previous observations of improved *I-V* behavior (beyond the first cycle) for n-GaAs photoanodes exposed to Pb^{2+} ions were not supported by these studies.^{4b,17a} GaAs photoanodes exposed to 0.010 M solutions of $Pb(NO_3)_2$ or $PbCl_2$ over $0 < pH < 14$ consistently showed no improvement in *I-V* properties subsequent to the initial cycle. Trace contamination with other ions (Ru^{3+}) used in those studies is believed to be the source of the reported improvements. Additionally, the n-GaAs photoelectrochemical properties were found to be a function of the applied potential limits in the KOH- Se^{2-} electrolyte. *I-V* data collected in this work for n-GaAs electrodes were obtained with triangular voltage waveforms cycled between -0.750 and 0.050 V versus the KOH- Se^{2-} cell potential (*ca.* -0.96 V vs. SCE), except for n-GaAs($Os^{4+,3+}$), n-GaAs($Ru^{4+,3+}$), and n-GaAs($Co^{3+,2+}$) electrodes, which were cycled between -0.850 and 0.050 V.

Mirror-finished GaAs surfaces were prepared by initially etching each electrode in a freshly prepared solution of con. $H_2SO_4:30\% H_2O_2:H_2O$ (*vol.* 4:1:1, cooled to room temperature), for 3 - 5 seconds, followed by a rinse with H_2O , then blown dry in a stream of N_2 , and repeated once more. Matte-finished n-GaAs surfaces were prepared by placing 1 - 2 drops of con. $H_2SO_4:30\% H_2O_2$ (1:1) on the surface of a mirror-finished electrode for 30 seconds, and then rinsing and drying as above. These etches yield

surfaces which are herein referred to as naked or untreated GaAs surfaces. The electrode is then introduced into a KOH-Se⁻²⁻ cell within 15 seconds of the final rinse. Naked ITO electrodes were etched in 6 M HCl for 10 seconds, and then rinsed with deionized H₂O prior to introduction to selenide electrolytes. Metal ion treated electrodes were first subjected to the initial etch procedures. The resultant surfaces were then exposed for 1 minute to 10 mL aqueous solutions containing 10 mM of the test complexes RuCl₃·xH₂O (pH = 2), [Ru(III)(NH₃)₆](Cl)₃ (pH = 2), [Ru(III)(NH₃)₅(OH₂)](ClO₄)₃ (pH = 0.7, 2.0), [Ru(III)(NH₃)₅(Cl)](Cl)₂ (pH = 2, 12), [Ru(II)(NH₃)₆](Cl)₂ (pH = 2.4), [Ru(II)(NH₃)₅(OH₂)](Trif)₂ (pH = 2.1), [Ru(II)(NH₃)₅(pyr)]²⁺ (pH = 2.1, 4 - 10), [Ru(II)(NH₃)₅(Cl)]⁺ (pH = 2.9), RhCl₃·xH₂O (pH = 2, 0.10 M NaOH), [Rh(III)(NH₃)₅(OH₂)](ClO₄)₃ (pH = 1, 12.6), [Rh(III)(NH₃)₆](ClO₄)₃ (pH = 2), [Rh(III)(NH₃)₅(Cl)](ClO₄)₃ (pH = 2), IrCl₃·xH₂O (pH = 2), OsCl₃·xH₂O (pH = 2, 10, 12), (K)₂[Os(IV)(Cl)₆] (pH = 2, 10, 12), (all the cobalt complexes were tested over 2 ≤ pH ≤ 13, please see chapter 2 for complete details) [Co(III)(NH₃)₆](Cl)₃, [Co(III)(NH₃)₆](Br)₃, [Co(III)(NH₃)₆](ClO₄)₂, [Co(III)(NH₃)₅(OH₂)](NO₃)₃, [Co(III)(NH₃)₅Br](Br)₂, [Co(III)(NH₃)₅(N₃)](Cl)₂, [Co(II)(OH₂)₆](ClO₄)₂, [Co(II)(OH₂)₆](SO₄), [Co(II)(OH₂)₆](Cl)₂, Pd(NO₃)₂ (pH = 2), BiCl₃·xH₂O (pH = 2), [Pb(II)(NO₃)₂] (pH = 2, 12), and [Pb(II)(NO₃)₂] (pH = 2, 12). Etched electrodes were also exposed for 1 minute to 0.010 M aqueous solutions, over the range 0 < pH < 14, of the complexes [Co(III)(bipy)₃](ClO₄)₃, [Co(II)(bipy)₃](ClO₄)₂, Pb(NO₃)₂, PbCl₂, HgCl₂, and a 1.0 M solution of [Hg(II)(Me)(OH)]; and a 0.010 M solution (1:1 acetonitrile:methanol, 10 minute electrode exposure) of [{Ru(IV)}₂OCl₆](PhCN)₄. Following exposure, each electrode was rinsed with 18 MΩ H₂O (acetonitrile in the Ru(IV) case), blown dry in a stream of N₂ and immersed in the KOH-Se⁻²⁻ electrolyte. Electrode exposure to Ru(II) and immersion into the KOH-Se⁻²⁻ cell were performed under Ar(g) ambient in a glove bag. The pH of each solution was adjusted with stock solutions made with KOH or NaOH, or HCl, HClO₄, or triflic acid.

Potential control was accomplished with a PAR model 173 potentiostat equipped with a model 175 voltage programmer. Current-voltage traces were recorded on a Houston Instruments model 2000 X-Y recorder at scan rates of 50 mV s^{-1} , and current-time measurements were recorded with a Linear, Inc., model 555 strip chart recorder. The current and voltage conventions adopted in this work are such that the energy of a hypothetical electron in vacuum is negative (by *ca.* 4.5 eV) of the standard H_2/H^+ couple; positive (negative) values of the current represent anodic (cathodic) polarization of the working electrode. Accurate values of the open-circuit voltage (V_{oc}) were obtained with either a Fluke model 27 multimeter or a Keithley model 177 voltmeter. The short-circuit current density (J_{sc}), and point of maximum power (P_{max}) were obtained by converting the raw current-voltage traces to computer data files by use of a line digitizer (Houston Instruments Hi-Pad) and subsequent software (customized code) analysis. In these experiments, J_{sc} was always observed to be equivalent to the light limited photocurrent density, J_{ph} .

Light sources were either an ELH-type tungsten-halogen bulb (3350 K black body temperature, dichroic rear reflector), or an ENH-type tungsten-halogen bulb (3250 K black body temperature, dichroic rear reflector; used for stability runs) with a line-of-sight ground glass diffuser. For the GaAs/KOH- Se^{-2} - system, an ELH-type irradiation source has been shown to provide acceptable solar simulation when the incident light intensity is calibrated with a Si secondary standard cell. In this study, irradiation intensities were measured with a Solarex Si secondary standard solar cell of area 4 cm^2 . For efficiency measurements, the ELH bulb was always maintained at line voltage and the distance of the source was adjusted to achieve the required light intensity (as measured by the short-circuit current of the Solarex cell).

Results

1. The Current-Voltage Behavior of n-GaAs Electrodes in Aqueous KOH-Se⁻²⁻ Solutions.

A. Naked Surfaces.

The current-voltage traces of untreated n-GaAs electrodes immersed in the KOH-Se⁻²⁻ electrolyte display several general features (Figures 4a, 5a, 6a, and 7a). For surfaces that had not been deliberately exposed to any metal ion solutions, all etched (con. H₂SO₄:30 % H₂O₂:H₂O; vol. 4:1:1) (100)-oriented n-GaAs electrodes exhibited an inflection point in the *I-V* behavior of the junction formed in KOH-Se⁻²⁻ electrolyte. At a light limited photocurrent density of $20 \pm 0.5 \text{ mA cm}^{-2}$ the open circuit photovoltages typically observed were $660 \pm 20 \text{ mV}$ vs. the cell rest potential ($V_{\text{cell}} = -0.96 \pm 0.03 \text{ V}$ vs. SCE). This is in accord with the results⁴ of Parkinson, Heller, and Miller but is in contrast to the findings of Allongue *et al.*^{5d} A possible explanation for the discrepancy is the observation that only extremely small quantities ($< \mu\text{M}$) of Ru³⁺ or other trace metal ions^{4b,17} (*vide supra*) in the KOH-Se⁻²⁻ solution are sufficient to produce improvements in the *I-V* behavior of n-GaAs surfaces. In this work, strict precautions were taken to ensure that the KOH-Se⁻²⁻ solutions were not contaminated with trace transition metal ions prior to conducting current-voltage experiments.

B. Metal Ion Exposed Surfaces.

Significant improvements in the current-voltage properties of GaAs(M)/KOH-Se⁻²⁻ (aq) liquid junctions have been observed following exposure of etched (100)-oriented n-GaAs photoelectrodes to aqueous solutions of RuCl₃·xH₂O,

Table I: *I-V* Characteristics of Transition Metal Ion Exposed (100)-Oriented n-GaAs Photoanodes^a in KOH-Se^{-/2-} Electrolytes

Metal Ion Treatment	J_{sc}^b (mA cm ⁻²)	V_{oc}^c (mV)	V_{max}^d (mV)	J_{max}^e (mA cm ⁻²)	Fill Factor ^f	η_{rel}^g (%)
naked ^h	20.0	660	306	17.2	0.40	0.51
Os(III) ⁱ	20.0	819	627	18.4	0.70	1.12
Co(III) ^j	20.0	752	611	18.3	0.74	1.08
Ru(III) ⁱ	20.0	743	559	18.5	0.70	1.00
Ru(IV) ^k	20.0	813	608	18.6	0.70	1.09
Rh(III) ^l	20.0	690	540	18.7	0.73	0.98
Ir(III) ⁱ	20.0	712	473	18.1	0.60	0.83

a. All surfaces were mirror-finished; each experiment was performed at least three times.

In all cases, the concentration of metal ion complex was 0.010 M.

b. Short circuit photocurrent density, ± 0.5 mA cm⁻². In this work, $J_{sc} = J_{ph}$.

c. Open circuit photovoltage, ± 10 mV, unless otherwise noted.

d. Photovoltage developed at the maximum power point, ± 10 mV.

e. Photocurrent developed at the maximum power point, ± 0.5 mA cm⁻².

f. Fill factor: $FF = (V_{max} \cdot J_{max}) / (V_{oc} \cdot J_{sc})$, ± 0.5 .

g. Efficiency at the maximum power point, relative to the absolute efficiency at the maximum power point of the GaAs(Ru³⁺)/KOH-Se^{-/2-} cell, ± 0.5 %.

h. Entry for the untreated GaAs/KOH-Se^{-/2-} junction; observed variation in V_{oc} was ± 20 mV.

i. GaAs electrodes treated with the appropriate $MCl_3 \cdot xH_2O$ complex (aqueous solution, pH = 2.0 ± 0.1).

j. GaAs electrodes treated with Co(III)(NH₃)₆³⁺ or Co(II)(H₂O)₆²⁺ ions (aqueous solution, pH = 10).

k. GaAs electrodes treated with [$\{Ru(IV)\}_2OCl_6\}(\text{PhCN})_4$ complex in 1:1 ACN:MeOH.

l. GaAs electrodes treated with either the RhCl₃·xH₂O, [Rh(III)(NH₃)₅(OH₂)](ClO₄)₃, [Rh(III)(NH₃)₅(Cl)](ClO₄)₃, or [Rh(III)(NH₃)₆](ClO₄)₃ complexes.

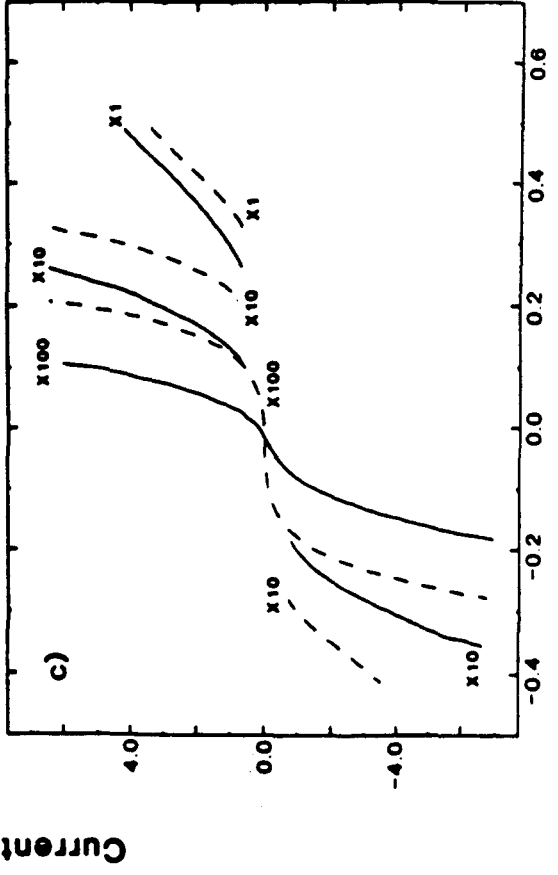
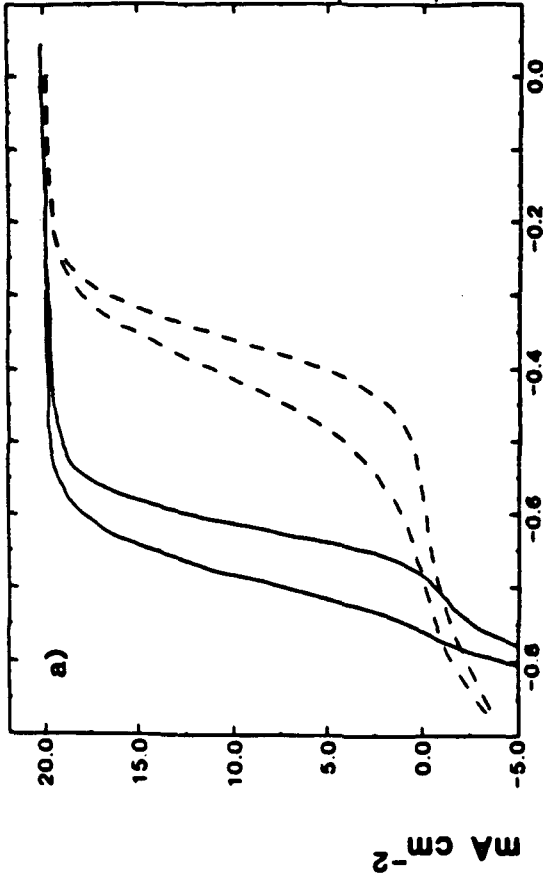
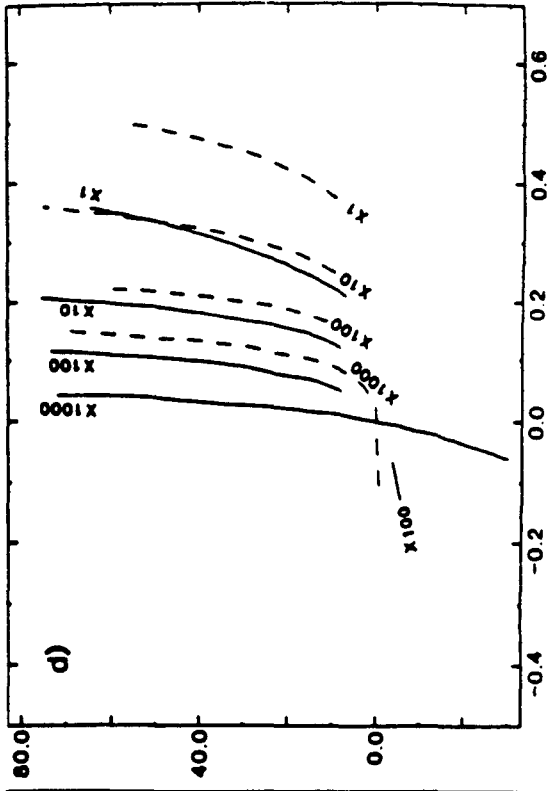
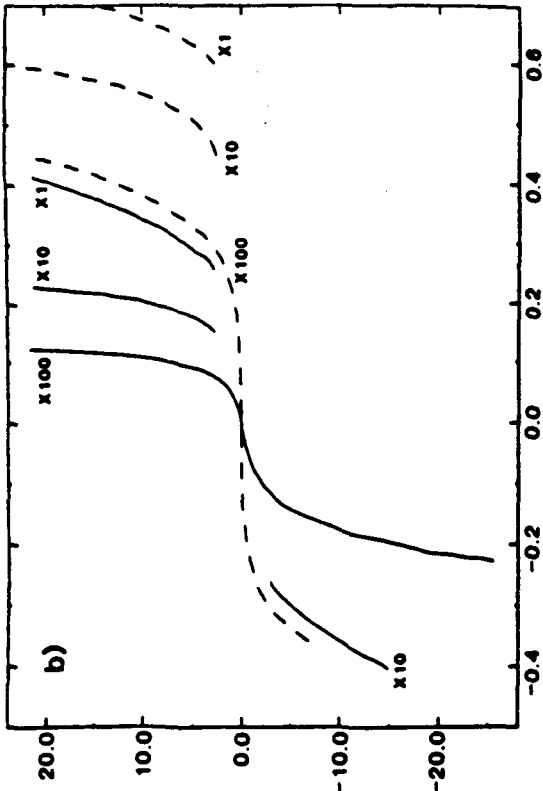
[Ru(III)(NH₃)₅(OH₂)](ClO₄)₃ (pH = 0.7), OsCl₃·xH₂O, RhCl₃·xH₂O, [Rh(III)(NH₃)₅(OH₂)](ClO₄)₃, [Rh(III)(NH₃)₅(Cl)](ClO₄)₃, [Rh(III)(NH₃)₆](ClO₄)₃, IrCl₃·xH₂O, Co(III)(NH₃)₅X (X = NH₃, OH₂, Br⁻, Cl⁻, N₃⁻) complex ions, Co(II)(OH₂)₆ salts, and [(Ru(IV))₂OCl₆](PhCN)₄ complex from acetonitrile/methanol. The *I-V* properties of n-GaAs photoanodes as a function of metal ion pretreatment have been summarized in Table I. The data are tabulated as the relative efficiency of n-GaAs(M) electrodes compared to n-GaAs(Ru³⁺) junctions at identical photocurrent densities (20 mA cm⁻²). Except where indicated otherwise, the *I-V* data were stable for several hours; in the case of pretreatment with OsCl₃·xH₂O (*vide supra*), long term stability runs performed on matte-etched (100)-oriented epitaxially grown n-GaAs electrodes treated with Os³⁺ and potentiostatically held at the maximum power point (under 88 mW cm⁻² solar simulated insolation) indicated no change in power output for > 3000 C cm⁻² (*i.e.*, in excess of 48 hours).¹⁹ Note that for these electrodes, only 20 C cm⁻² would have been required to consume the entire photoactive n-GaAs epilayer (10 μm thick) by a 6-electron photocorrosion reaction.

Figures 4a, 5a, 6a, and 7a display representative current-voltage curves for several illuminated n-GaAs(M)/KOH-Se^{-/2-} interfaces. In general, the initial current-voltage traces following GaAs(M) formation displayed superior fill factors relative to the untreated case, and continued to show improvement over successive *I-V* scans (typically over 30 - 50 cycles) to yield a stable final *I-V* trace. Improved final state *I-V* curves were characterized by consistent differences with respect to naked n-GaAs/KOH-Se^{-/2-} junction behavior. At identical photocurrent densities, increases of up to 160 mV in V_{oc} were observed, in addition to a characteristic absence of inflection point, for these metal ion-treated n-GaAs photoanodes compared to the untreated case. The magnitude of the increases in V_{oc} and the shape of the final state current-voltage traces were indicative of the specific GaAs(M) treatment. Furthermore, following metal ion treatment, it was observed

Figure 4: Current-voltage (*I-V*) behavior of various electrode surfaces in contact with 1.0 M KOH - 0.8 M K₂Se - 0.1 M K₂Se₂ aqueous electrolyte. Dashed lines represent etched mirror-finished GaAs surfaces, while solid lines indicate responses obtained after etching and exposure to an aqueous 0.010 M RuCl₃·3H₂O solution (pH = 2, HCl) for 60 seconds, followed by a H₂O rinse. The (100)-oriented GaAs electrodes were etched with 4:1:1 (*vol. con.* H₂SO₄:30 % H₂O₂:H₂O) solution, while the 10 % Sn-doped In₂O₃ (ITO) electrodes were etched in 6 M HCl for a total of 10 seconds; immediately after etching, each electrode was rinsed in H₂O. All *I-V* data were collected using a three-electrode potentiostatic configuration (Pt wire reference electrode poised at the equilibrium cell potential and large area Pt foil auxiliary electrode, 50 mV s⁻¹ scan rate). Each solution was magnetically stirred. The units that accompany the individual curves (b - d) indicate the appropriate increase in sensitivity scale of the current.

RuCl₃·3H₂O exposed electrodes:

- (a) Photocurrent-voltage properties of (100)-oriented n-GaAs anodes. The short circuit current density was set to 20 mA cm⁻² with an ELH-type W-halogen bulb.
- (b) *I-V* behavior of ITO electrodes.
- (c) Dark *I-V* behavior of degenerately doped ($N_D > 5 \times 10^{18} \text{ cm}^{-3}$) (100)-oriented n⁺-GaAs electrodes.
- (d) Dark *I-V* behavior of (100)-oriented p-GaAs electrodes.

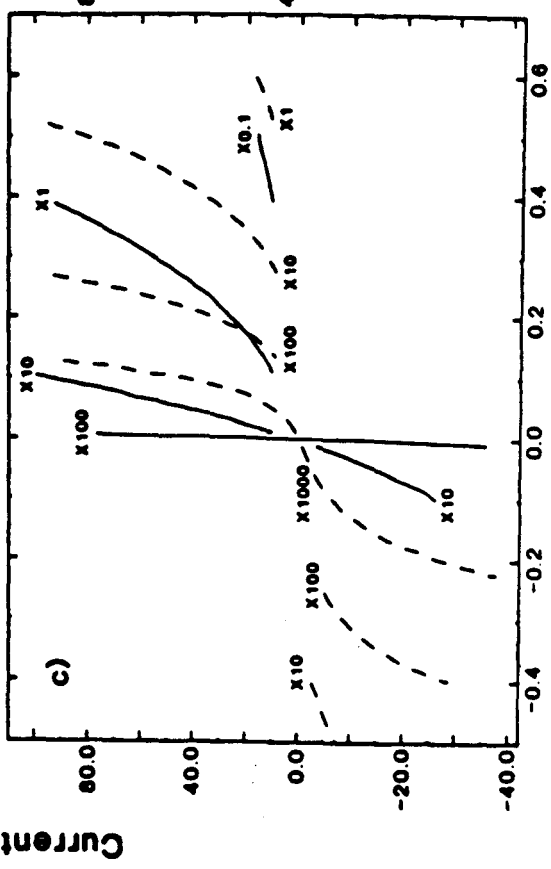
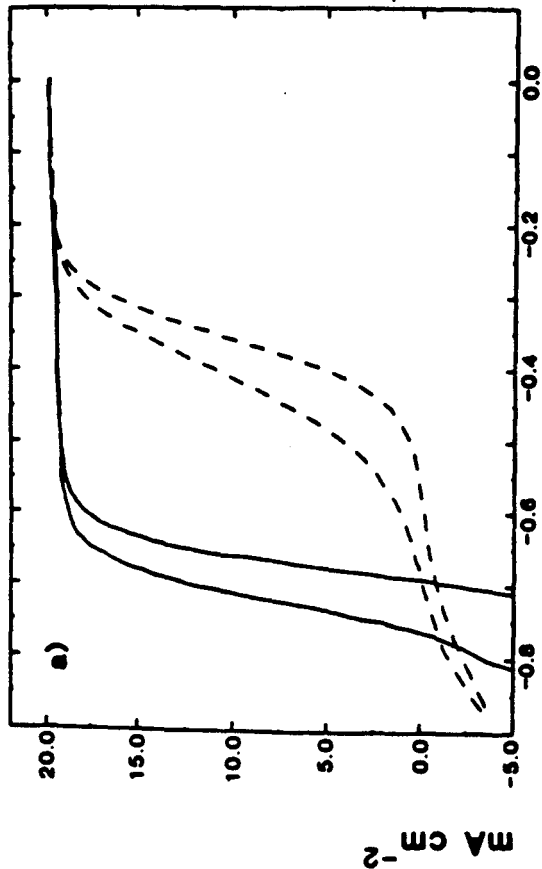
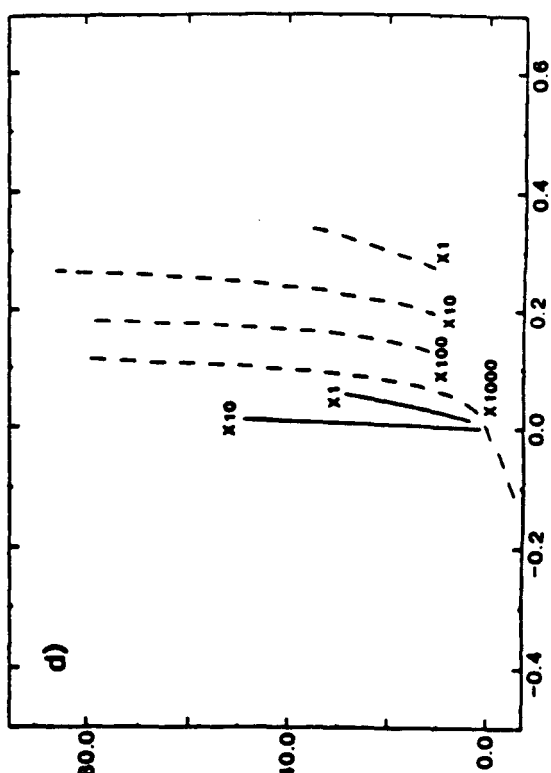
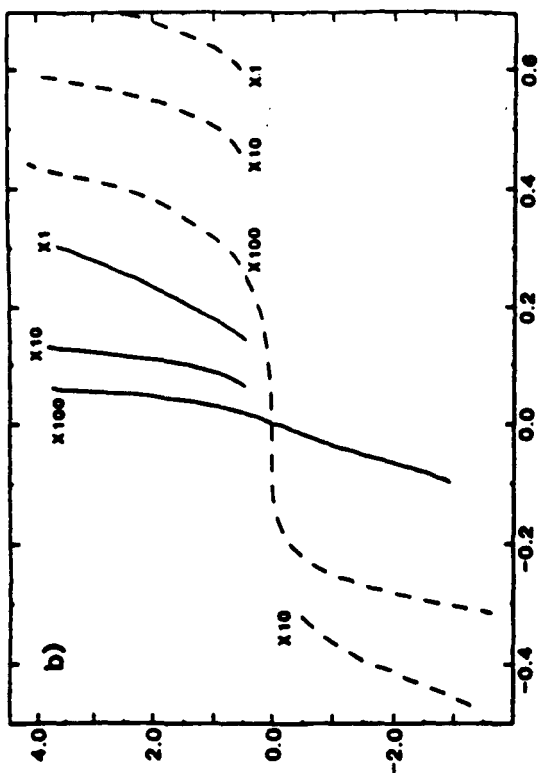


Applied Voltage, V

Figure 5: Current-voltage (*I-V*) behavior of various electrode surfaces in contact with 1.0 M KOH - 0.8 M K₂Se - 0.1 M K₂Se₂ aqueous electrolyte. Dashed lines represent etched mirror-finished GaAs surfaces, while solid lines indicate responses obtained after etching and exposure to an aqueous 0.010 M [Co(III)(NH₃)₆](Br)₃ solution (pH = 10, KOH) for 60 seconds, followed by a H₂O rinse. The (100)-oriented GaAs electrodes were etched with 4:1:1 (*vol. con.* H₂SO₄:30 % H₂O₂:H₂O) solution, while the 10 % Sn-doped In₂O₃ (ITO) electrodes were etched in 6 M HCl for a total of 10 seconds; immediately after etching, each electrode was rinsed in H₂O. All *I-V* data were collected using a three-electrode potentiostatic configuration (Pt wire reference electrode poised at the equilibrium cell potential and large area Pt foil auxiliary electrode, 50 mV s⁻¹ scan rate). Each solution was magnetically stirred. The units that accompany the individual curves (b - d) indicate the appropriate increase in sensitivity scale of the current.

[Co(III)(NH₃)₆](Br)₃ exposed electrodes:

- (a) Photocurrent-voltage properties of (100)-oriented n-GaAs anodes. The short circuit current density was set to 20 mA cm⁻² with an ELH-type W-halogen bulb.
- (b) *I-V* behavior of ITO electrodes.
- (c) Dark *I-V* behavior of degenerately doped ($N_D > 5 \times 10^{18}$ cm⁻³) (100)-oriented n⁺-GaAs electrodes.
- (d) Dark *I-V* behavior of (100)-oriented p-GaAs electrodes.



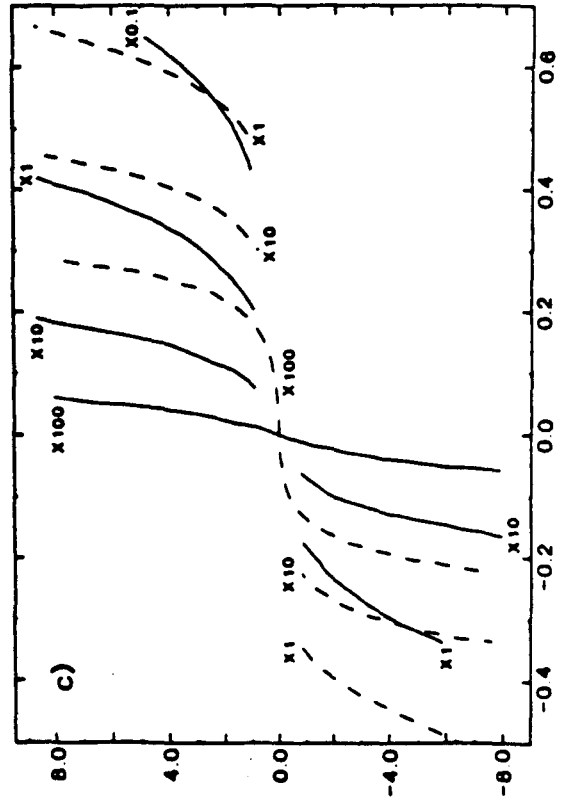
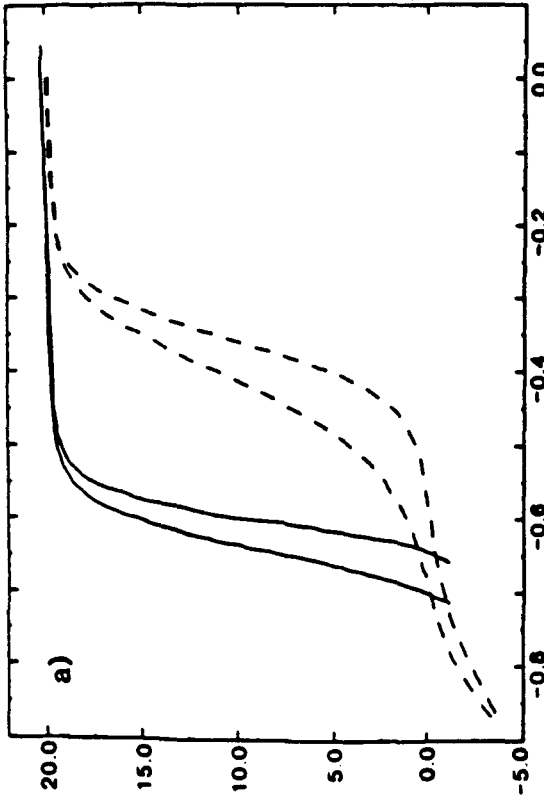
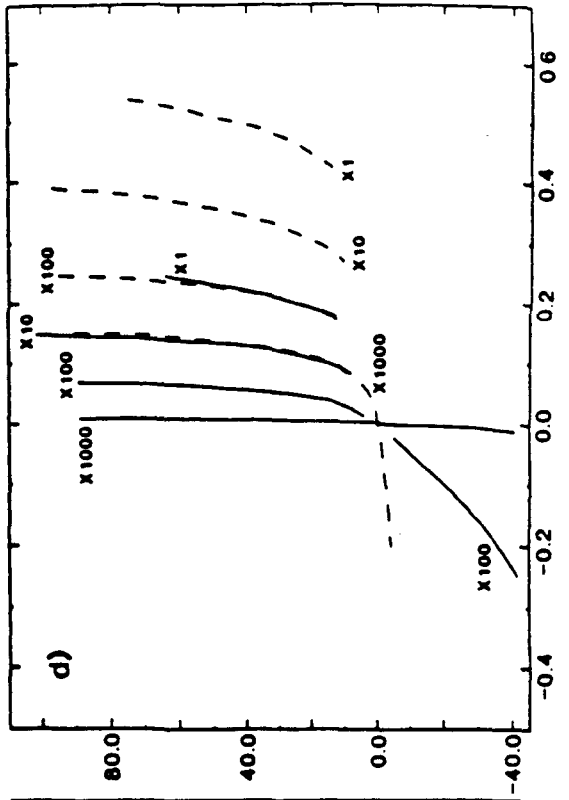
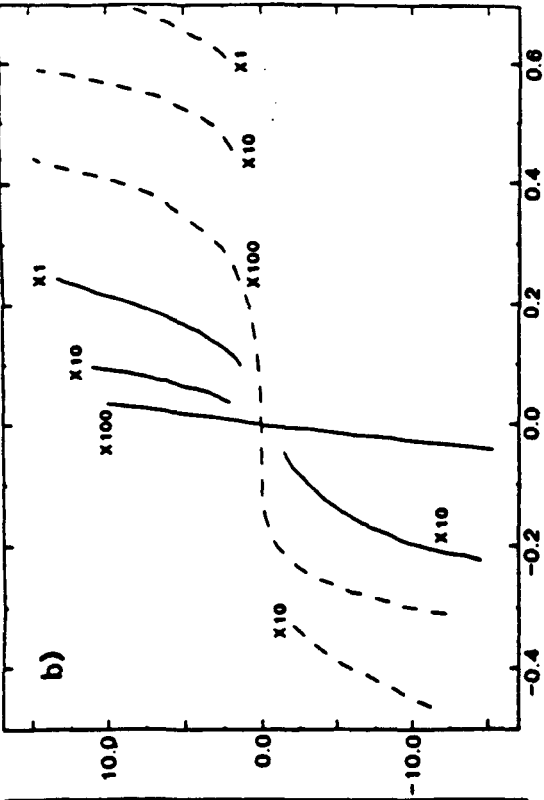
Applied Voltage, V

Current, mA cm⁻²

Figure 6: Current-voltage (*I-V*) behavior of various electrode surfaces in contact with 1.0 M KOH - 0.8 M K₂Se - 0.1 M K₂Se₂ aqueous electrolyte. Dashed lines represent etched mirror-finished GaAs surfaces, while solid lines indicate responses obtained after etching and exposure to an aqueous 0.010 M RhCl₃·3H₂O solution (pH = 2, HCl) for 60 seconds, followed by a H₂O rinse. The (100)-oriented GaAs electrodes were etched with 4:1:1 (*vol. con.* H₂SO₄:30 % H₂O₂:H₂O) solution, while the 10 % Sn-doped In₂O₃ (ITO) electrodes were etched in 6 M HCl for a total of 10 seconds; immediately after etching, each electrode was rinsed in H₂O. All *I-V* data were collected using a three-electrode potentiostatic configuration (Pt wire reference electrode poised at the equilibrium cell potential and large area Pt foil auxiliary electrode, 50 mV s⁻¹ scan rate). Each solution was magnetically stirred. The units that accompany the individual curves (b - d) indicate the appropriate increase in sensitivity scale of the current.

RhCl₃·3H₂O exposed electrodes:

- (a) Photocurrent-voltage properties of (100)-oriented n-GaAs anodes. The short circuit current density was set to 20 mA cm⁻² with an ELH-type W-halogen bulb.
- (b) *I-V* behavior of ITO electrodes.
- (c) Dark *I-V* behavior of degenerately doped ($N_D > 5 \times 10^{18} \text{ cm}^{-3}$) (100)-oriented n⁺-GaAs electrodes.
- (d) Dark *I-V* behavior of (100)-oriented p-GaAs electrodes.



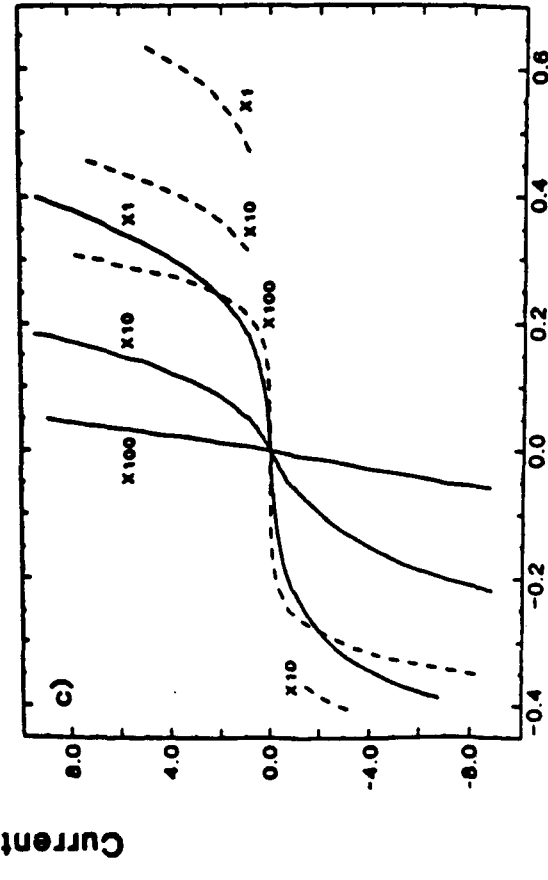
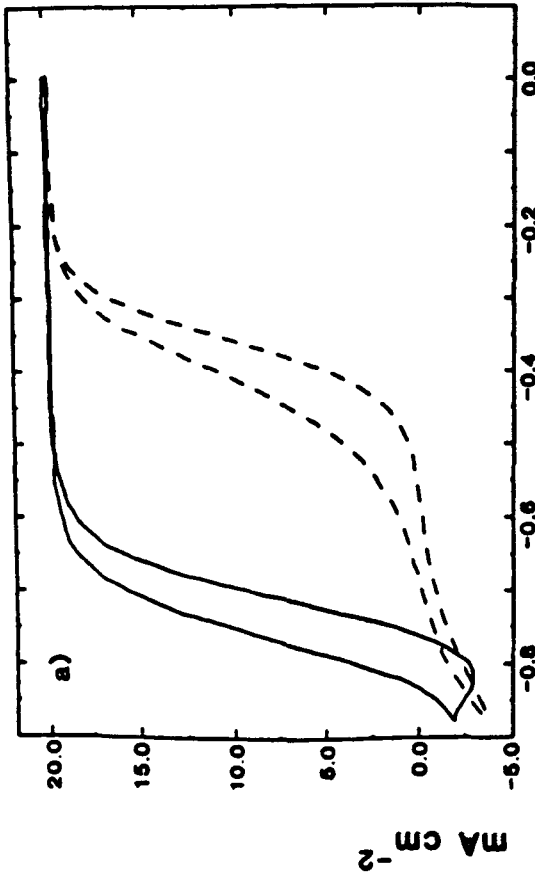
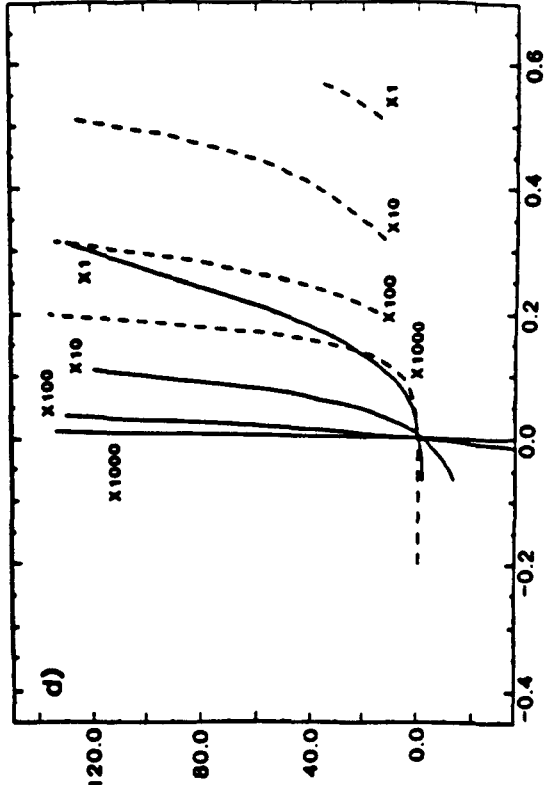
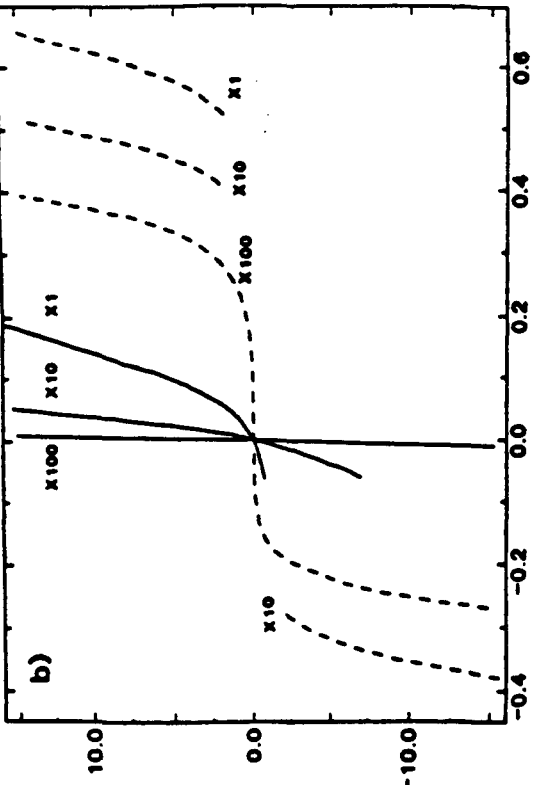
Applied Voltage, V

Current, mA cm⁻²

Figure 7: Current-voltage (*I-V*) behavior of various electrode surfaces in contact with 1.0 M KOH - 0.8 M K₂Se - 0.1 M K₂Se₂ aqueous electrolyte. Dashed lines represent etched mirror-finished GaAs surfaces, while solid lines indicate responses obtained after etching and exposure to an aqueous 0.010 M OsCl₃·3H₂O solution (pH = 2, HCl) for 60 seconds, followed by a H₂O rinse. The (100)-oriented GaAs electrodes were etched with 4:1:1 (*vol. con.* H₂SO₄:30 % H₂O₂:H₂O) solution, while the 10 % Sn-doped In₂O₃ (ITO) electrodes were etched in 6 M HCl for a total of 10 seconds; immediately after etching, each electrode was rinsed in H₂O. All *I-V* data were collected using a three-electrode potentiostatic configuration (Pt wire reference electrode poised at the equilibrium cell potential and large area Pt foil auxiliary electrode, 50 mV s⁻¹ scan rate). Each solution was magnetically stirred. The units that accompany the individual curves (b - d) indicate the appropriate increase in sensitivity scale of the current.

OsCl₃·3H₂O exposed electrodes:

- (a) Photocurrent-voltage properties of (100)-oriented n-GaAs anodes. The short circuit current density was set to 20 mA cm⁻² with an ELH-type W-halogen bulb.
- (b) *I-V* behavior of ITO electrodes.
- (c) Dark *I-V* behavior of degenerately doped ($N_D > 5 \times 10^{18} \text{ cm}^{-3}$) (100)-oriented n⁺-GaAs electrodes.
- (d) Dark *I-V* behavior of (100)-oriented p-GaAs electrodes.



Applied Voltage, V

that small bubbles formed on the n-GaAs electrode surface during electrochemical cycling at the far negative range of the I - V scan, in contrast to untreated n-GaAs surfaces. Bubble formation generally correlated with large increases of cathodic current following metal ion exposure. This cathodic current was well in excess of the mass transport limit prior to metal ion treatment. While a head gas analysis has not been conducted, it is most reasonable to expect that the bubbles are composed¹⁸ of H_2 formed by the reduction of water. Especially in the case of n-GaAs(Rh) treatments, the appearance of a bubble formation onset in the dark paralleled the upper limit on V_{oc} observed at photocurrent densities near 20 mA cm^{-2} .

The outstanding I - V properties of the n-GaAs(Os)/KOH- Se^{-2} junction warranted a combined stability and absolute light-to-electrical power conversion efficiency study.¹⁹ (100)-oriented OMVPE grown epitaxial n-GaAs electrodes were matte-etched with 1:1 (*vol.*) con. H_2SO_4 :30 % H_2O_2 to produce a microscopically roughened non-reflective surface.^{5c} Following exposure to a 0.010 M solution of $OsCl_3 \cdot xH_2O$ (*vide supra*), a typical electrode was then immersed into a cell charged with 1.0 M KOH - 0.8 M K_2Se - 0.1 M K_2Se_2 electrolyte. Current-voltage scans for the long term stability runs were collected with the n-GaAs(Os) electrode under 88 mW cm^{-2} solar simulated illumination from a tungsten-halogen ENH bulb, while an ELH bulb was used to measure absolute light-to-electrical power conversion efficiencies; the incident light intensity at the plane of the electrode was measured by a calibrated Si p-n junction secondary standard. (The ENH bulb has a slightly cooler blackbody color temperature maximum than the ELH bulb. The typical lifetime of an ELH bulb was insufficient to last through the course [> 48 hours] of the stability experiment.) The I - V scans for a pair of untreated and Os-treated n-GaAs/KOH- Se^{-2} junctions are displayed in Figure 3. The measured J_{sc} of 25.0 mA cm^{-2} under 88 mW cm^{-2} of illumination scales to 28.4 mA cm^{-2} under 1 Sun AM1.0 (100 mW cm^{-2}) conditions; thus, the observed J_{sc}

represents 86 % of the theoretical photocurrent density attainable from the incident photons available above gallium arsenide's band gap of 1.42 eV (33 mA cm⁻² at AM1.0). Typical efficiencies observed in this system were 15.5 - 16.5 %, but efficiencies as high as 17.2 % have been observed with optimized values of J_{sc} and the fill factor. These efficiencies represent the highest accurate light-to-electrical power conversion values reported for a liquid junction photoelectrochemical cell, to date. Note that no special attempts have been made to achieve these record level conversions by manipulation of solution path length, use of anti-reflective coatings, or specialized vessel materials or cell designs.

Transient improvements in $I-V$ traces were observed²⁰ for n-GaAs photoanodes exposed to Pb(II) salts over the range $1 < \text{pH} < 14$, and $[\text{Ru(II)(NH}_3)_5(\text{OH}_2)]^{2+}$ (pH = 2), $[\text{Ru(II)(NH}_3)_5(\text{Cl})]^+$ (pH = 2.9), $[\text{Ru(III)(NH}_3)_5(\text{OH}_2)]^{3+}$ (pH > 2), $[\text{Ru(II)(NH}_3)_5(\text{Cl})]^+$ (pH = 2, 12). Typically, a significant change over the untreated case was only obvious on the first $I-V$ scan, and in all cases behavior identical to the untreated case was observed after three complete and any subsequent current-voltage cycles.

Exposure of n-GaAs electrodes to 0.010 M solutions of the ruthenium complexes $[\text{Ru(III)(NH}_3)_6](\text{Cl})_3$ (pH = 2), $[\text{Ru(II)(NH}_3)_6](\text{Cl})_2$ (pH = 2.4), $[\text{Ru(II)(NH}_3)_5(\text{pyr})]^{2+}$ (pH = 2.1, 4 - 10), and the complexes (over the range $1 < \text{pH} < 14$) $[\text{Co(III)(bipy)}_3](\text{ClO}_4)_3$, $[\text{Co(II)(bipy)}_3](\text{ClO}_4)_2$, $\text{Bi}(\text{NO}_3)_3 \cdot x\text{H}_2\text{O}$, $\text{Pd}(\text{NO}_3)_2$, $\text{Hg}(\text{NO}_3)_2$, and 1.0 M $[\text{Hg(II)(Me)(OH)}]$ in H_2O , yielded no observable improvements in the $I-V$ behavior of n-GaAs/KOH-Se⁻²⁻ junctions.²¹

2. The I - V Behavior of Sn:In₂O₃, p-GaAs, and n⁺-GaAs Electrodes in Aqueous KOH-Se⁻²⁻ Solutions.

To investigate whether chemisorbed metal ions are effective electrocatalysts for the oxidation of Se²⁻ in aqueous KOH-Se⁻²⁻ solutions, I - V data were collected for p-type GaAs, n⁺-GaAs, and Sn-doped (10 %) In₂O₃ (ITO) electrodes that had been exposed to a variety of metal ion complexes.

A. ITO Electrode Properties.

ITO surfaces were observed to exhibit large kinetic overpotentials for the oxidation and reduction of Se⁻²⁻ species in the aqueous KOH electrolyte. Therefore, ITO electrodes provided a useful surface with which to probe possible electrocatalytic effects of metal ion chemisorption. It was observed that exposure of ITO electrode surfaces to aqueous solutions of the simple halo salts of Ru³⁺, Co²⁺, Pb²⁺, Rh³⁺, Os³⁺, Ir³⁺, or Co(NH₃)₆³⁺ ions led to pronounced decreases in the overpotential for Se²⁻ oxidation in the ITO/KOH-Se⁻²⁻ cell (Figures 4b, 5b, 6b, and 7b). In the most favorable cases, the current density at low overpotentials increased by greater than 10³ after the metal ion treatment. These results clearly indicate the beneficial effects of electrocatalysis on the I - V properties in the KOH-Se⁻²⁻ electrolyte.

B. n⁺-GaAs Electrode Properties.

The I - V properties of various unilluminated n⁺-GaAs(M) electrodes were investigated in an attempt to determine whether improved charge-transfer kinetics might be observed for thermally generated carriers at degenerately doped GaAs surfaces. Such surfaces are expected to have interfacial chemistries very similar to n-GaAs surfaces, and hence represent a link between reductions in the overpotential observed for Se²⁻ oxidation at ITO(M)/KOH-Se⁻²⁻(aq) interfaces and the corresponding GaAs(M)/KOH-Se⁻²⁻(aq)

junctions. Figures 4c, 5c, 6c, and 7c show the I - V characteristics of several specific n^+ -GaAs(M)/KOH- Se^{2-} (aq) interfaces, and clearly demonstrate the reduction of Se^{2-} oxidation overpotentials at n^+ -GaAs surfaces following selected metal ion exposure.

C. p-GaAs Electrode Properties.

Experiments at p-type GaAs electrodes in the absence of illumination are useful in assessing metal ion chemisorption effects on interfacial charge transfer (*vide infra*). The data for representative p-GaAs(M) surfaces in KOH- Se^{2-} electrolytes are presented in Figures 4d, 5d, 6d, and 7d. The anodic current density at a given applied potential increased substantially after metal ion chemisorption; specifically, Co^{2+} and Os^{3+} yielded the highest anodic current densities observed for a given applied potential. Another interesting feature of the I - V features in Figures 4d, 5d, 6d, and 7d is that the reverse bias saturation current density (*i.e.*, cathodic limiting current) increased for the p-GaAs(M) electrodes that displayed increased anodic currents.

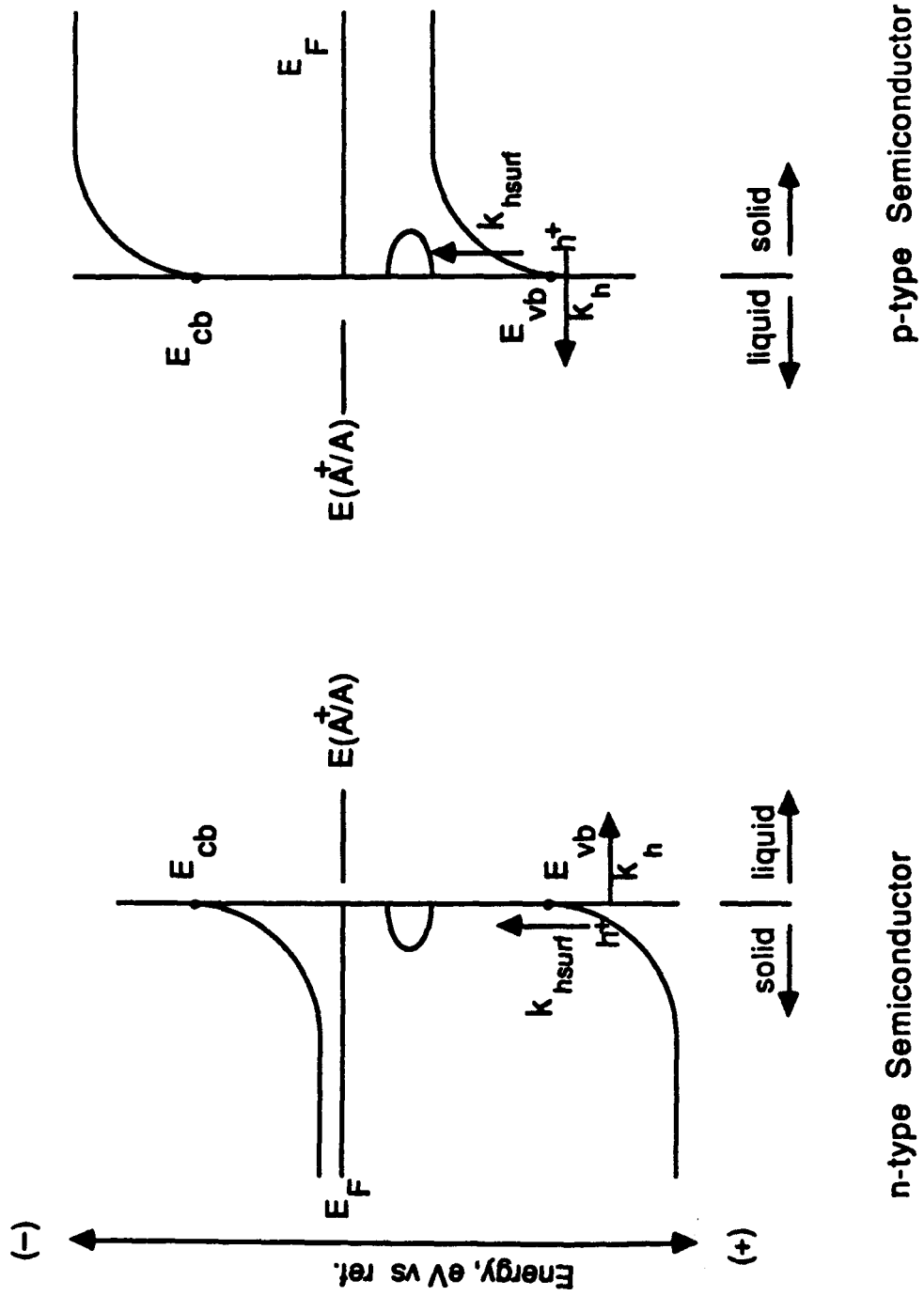
Discussion

All ions investigated in this study that were observed to be effective electrocatalysts at ITO electrodes were found to reduce the overpotential for Se^{2-} oxidation at both unilluminated n^+ -GaAs and p-GaAs surfaces and also were found to be effective in improving the I - V characteristics of the n-GaAs/KOH- Se^{2-} /Pt cell. This strongly indicates that improvements in the I - V behavior of the n-GaAs/KOH- Se^{2-} system are dominated by electrocatalytic effects of the chemisorbed metal ion. Of the ions investigated herein, no exceptions to this proposal have been found; *i.e.*, no metal ion that is not an effective electrocatalyst at ITO or n^+ -GaAs surfaces has been observed to yield improved I - V properties at the n-GaAs/KOH- Se^{2-} interface.

Of particular relevance to this work is the fate of holes driven to the interface of GaAs/KOH- Se^{2-} junctions. The system observable, anodic current flow, depends upon the relative rate constants (the branching ratio) for hole transfer to Se^{2-} species in solution or for hole recombination at surface states. Hole transfer at illuminated n-type GaAs or unilluminated n⁺-GaAs electrodes is a minority carrier process, but is a majority carrier process at unilluminated p-type GaAs electrodes. This difference in carrier class allows a mechanistic test of the two principal theories that attempt to describe the effect of metal ion chemisorption on GaAs surfaces, suppression of surface recombination rate^{5bc} or enhancement of the Se^{2-} oxidation rate.^{5d,9} These kinetic possibilities are illustrated in Scheme III. Specifically, for a photoanode the anodic I - V characteristic results from competition between the hole injection current into the electrolyte (i_{redox}) and the surface-related hole recombination current (i_{surf}): subsequent to metal ion treatment, an increase in the collected anodic photocurrent is consistent with an increase in the ratio $i_{\text{redox}}/i_{\text{surf}}$. Note that, for an n-type photoanode, this ratio increases in response to either hole electrocatalysis (increased i_{redox}) or to passivation of surface states (decreased i_{surf}). A distinction in the two cases is made possible upon appeal to I - V data obtained at p-GaAs(M)/KOH- Se^{2-} (aq) junctions.

For a p-type electrode used as an anode in the absence of illumination, holes are majority carriers and therefore the total anodic current represents the *sum* of the hole currents i_{redox} and i_{surf} . After metal ion treatment, a decrease in surface recombination would *decrease* the anodic current, while an increase in i_{redox} would *increase* the anodic current. Within this framework, passivation of surface recombination is expected to reduce the interfacial "leakage" pathways, yielding a better junction at both n-type and p-type GaAs/liquid interfaces (increased n-type anodic photocurrents and decreased p-type dark anodic and cathodic currents), while electrocatalysis is expected to produce increased anodic currents at both types of electrode surfaces.

Scheme III:



n-type Semiconductor

p-type Semiconductor

Upon review of the results at p-GaAs(M)/KOH-Se⁻²⁻(aq) interfaces, it is clear that the *I-V* data for those junctions are inconsistent with the notion that passivation of hole surface recombination processes is the dominant effect that metal ion chemisorption has on p-GaAs(M) surfaces in KOH-Se⁻²⁻ electrolytes. The n-GaAs and p-GaAs data are both consistent with the metal ion chemisorption effecting an increase in the valence band exchange current density. On the basis of these observations, it is suggested that the chemisorbed metal ions in contact with the KOH-Se⁻²⁻(aq) electrolyte introduce interfacial states with energies near the top of the GaAs valence band edge and that the role of these states is to improve communication between the holes (photogenerated or thermally generated) in GaAs and the KOH-Se⁻²⁻(aq) electrolyte.

The data at n⁺-GaAs(M)/KOH-Se⁻²⁻ junctions supports the proposal of chemisorbed transition metal ions inducing the electrocatalysis of Se²⁻ oxidation at GaAs interfaces. The improvements observed in the *I-V* properties of n⁺-GaAs(M)/KOH-Se⁻²⁻ junctions subsequent to metal ion treatment also confirm the supposition that etched, metal-free n-GaAs surfaces possess substantial kinetic overpotentials for Se²⁻ oxidation; thus, these kinetic overpotentials could produce the observed poor fill factors when naked n-GaAs surfaces are employed as photoanodes in the KOH-Se⁻²⁻(aq) electrolyte (Figure 1).

It is possible that the increased exchange current densities observed for the p-GaAs(M) electrodes could also be produced by shifts in the flat-band potential without the introduction of additional electrocatalytic states.²² However, at degenerately doped surfaces, improvements in interfacial kinetics due to flat-band shifts are expected to be minimal, because of effective screening⁷ of the accumulated surface charge by the highly doped semiconductor. From the n⁺-GaAs(M) data, an additional increase in the hole exchange current density at the nondegenerately doped samples (either n-type or p-type

GaAs) cannot be invoked to rule out a shift in flat-band potential. Such shifts in surface potential may well be responsible for the previously observed decrease in surface recombination velocity after Ru^{3+} treatment implied by the time-resolved photoluminescence data of Nelson *et al.* at GaAs(Ru)/air interfaces^{6a}. Suggestions for such flat-band shifts can be found in the electrochemical data of Figures 3 – 6 by noting that although V_{oc} for n-GaAs photoanodes increases in the order $\text{Rh}^{3+} < \text{Ru}^{3+} < \text{Co}(\text{NH}_3)_6^{3+}$, the ITO electrocatalysis effect and the reverse bias saturation current at p-GaAs samples increase in the order $\text{Ru}^{3+} < \text{Rh}^{3+} < \text{Co}(\text{NH}_3)_6^{3+}$.

As a caveat to the generalization of the conclusions obtained in this section, note that the correlations of the I - V characteristics employed have assumed that the metal ion chemisorption reactions are similar at n-GaAs, n⁺-GaAs, and p-GaAs surfaces. Such an assumption would appear to be warranted by the close correlation in I - V properties of the various electrode surfaces with the different metal ion treatments. It has been verified by x-ray photoelectron spectroscopic (XPS) analysis that chemisorption of $\text{Co}(\text{NH}_3)_6^{3+}$ ions yields identical XP Co 2p signals on n-GaAs surfaces and on unintentionally doped GaAs powder (see also chapter 2).²³ It is expected that similar correlations hold between GaAs(M) surfaces for the other metal ions as well.²⁴ While it need not follow that the chemistry at ITO surfaces be identical to that at GaAs surfaces, the correlations between the I - V behavior of n-GaAs, n⁺-GaAs, and p-GaAs appear to be secure.

In general, the close correlation between metal ions that are effective electrocatalysts for Se^{2-} oxidation at ITO electrodes and those transition metal ions that yield improved fill factors at n-GaAs photoanodes confirms the usefulness of this hypothesis in designing improved photoelectrochemical cells in the $\text{KOH-Se}^{2-}(\text{aq})$ electrolyte. Specifically, the chemisorption of transition metal ions has been shown to effect decreases in the kinetic overpotentials for Se^{2-} oxidation at ITO electrodes. Additionally, chemisorption of transition metal ions has also been observed to yield increased anodic and cathodic currents

at p-GaAs electrodes in the KOH-Se⁻²⁻(aq) electrolyte. The behavior of the p-GaAs(M)/KOH-Se⁻²⁻(aq) junctions is consistent with metal ion chemisorption introducing electrocatalytic states having energies near the valence band edge at GaAs surfaces, but is inconsistent with the passivation of hole surface recombination processes as a basis for explaining the dominant *I-V* effects found for GaAs electrodes in the KOH-Se⁻²⁻(aq) electrolyte. Furthermore, naked degenerately doped n⁺-GaAs electrodes exhibit large kinetic overpotentials for Se²⁻ oxidation, while metal ion chemisorption yields improved anodic currents and verifies the notion that chemisorbed metal ions can act as electrocatalysts for Se²⁻ oxidation at GaAs surfaces. With respect to the n-GaAs(M)/KOH-Se⁻²⁻(aq) junction, these interfaces have been observed to yield outstanding photovoltaic performance, providing efficiencies that are superior to those reported to date for conventional solid state surface barrier devices (semiconductor/metal or metal/insulator/semiconductor systems) employing GaAs or other *III-V* semiconductor materials.^{7ac} These high efficiencies underscore the ability of properly constructed photoelectrochemical cells to provide superior photovoltaic performance as compared to their Schottky barrier analogs. The bulk diffusion/recombination limited value of V_{oc} for these n-GaAs samples is 1.05 V at 300 K and J_{sc} = 20 mA cm⁻²;^{7c} thus, an improved understanding of surface chemical interactions at GaAs surfaces might be expected to yield even further enhancements in the performance of n-GaAs/KOH-Se⁻²⁻(aq) junctions.

References

1. Chang, K. C.; Heller, A.; Schwartz, B.; Menezes, S.; Miller, B. *Science (Washington, D. C.)* **1977**, *196*, 1097.
2. (a) Ellis, A. B.; Bolts, J. M.; Kaiser, S. W.; Wrighton, M. S. *J. Am. Chem. Soc.* **1977**, *99*, 2848. (b) Harvey, W. W. *J. Electrochem. Soc.* **1967**, *114*, 472. (c) Vanmaekelbergh, D.; Gomes, W. P.; Cardon, F. *Ber. Bunsenges. Phys. Chem.* **1985**, *89*, 987. (d) Rajeshwar, K. *J. Appl. Electrochem.* **1985**, *15*, 1.
3. (a) Heller, A.; Aspnes, D. E.; Porter, J. D.; Sheng, T. T.; Vadimsky, R. G. *J. Phys. Chem.* **1985**, *89*, 4444. (b) Heller, A.; Vadimsky, R. G. *Phys. Rev. Lett.* **1981**, *46*, 1153. (c) Heller, A.; Miller, S. *Electrochim. Acta* **1980**, *25*, 29.
4. (a) Parkinson, B. A.; Heller, A.; Miller, B. *Appl. Phys. Lett.* **1978**, *33*, 521. (b) Parkinson, B. A.; Heller, A.; Miller, B. *J. Electrochem. Soc.* **1979**, *126*, 954.
5. (a) Peter, L. M. *Electrochemistry* **1984**, *9*, 66. (b) Heller, A. *Accs. Chem. Res.* **1981**, *14*, 154. (c) Heller, A., "Chemical Control of Surface and Grain Boundary Recombination in Semiconductors," In *Photoeffects at Semiconductor-Electrolyte Interfaces*; Nozik, A., Ed.: ACS Symposium Series 146, American Chemical Society: Washington, D. C., 1981; pp 57 - 77. (d) Allongue, P.; Cachet, H. *J. Electrochem. Soc.* **1984**, *131*, 2861. (e) Peter, L. M.; Li, J.; Peat, R. *J. Electroanal. Chem.* **1984**, *165*, 29. (f) Peter, L. M.; Li, J.; *J. Electroanal. Chem.* **1986**, *199*, 1.
6. (a) Nelson, R. J.; Williams, J. S.; Leamy, H. J.; Miller, B.; Parkinson, B. A.; Heller, A. *Appl. Phys. Lett.* **1980**, *36*, 76. (b) Johnston, Jr., W. D.; Leamy, H. J.; Parkinson, B. A.; Heller, A.; Miller, B. *J. Electrochem. Soc.* **1980**, *127*, 90.

7. (a) Sze, S. M. *Physics of Semiconductor Devices*; Wiley: New York, 1981.
(b) Fonash, S. J. *Solar Cell Device Physics*; Academic Press: New York, 1981.
(c) Fahrenbruch, A. L.; Bube, R. H. *Fundamentals of Solar Cells*; Academic Press: New York, 1983. (d) Hovel, H. J. In *Semiconductors and Semimetals*; Willardson, R. K., Beer, A. C., Eds.; Academic Press: New York, 1975; Vol. 11, Solar Cells.
8. (a) Shockley, W.; Read, W. T. *Phys. Rev.* **1952**, *87*, 835. (b) Hall, R. N. *Phys. Rev.* **1952**, *87*, 387. (c) Henry, C. R.; Logan, R. A.; Merritt, F. R. *J. Appl. Phys.* **1978**, *44*, 3530.
9. Tufts, B. J.; Abrahams, I. L.; Casagrande, L. G.; Lewis, N. S. *J. Phys. Chem.* **1989**, *93*, 3260.
10. Literature preparation of $[\text{Co(III)(NH}_3)_6](\text{Cl})_3$: Bjerrum, J.; McReynolds, J. P. *Inorg. Synth.* **1946**, *2*, 217.
11. Literature preparation of: (a) $[\text{Co(III)(NH}_3)_5\text{Cl}](\text{Cl})_2$: Schlessinger, G. *Inorg. Synth.* **1967**, *9*, 160. (b) $[\text{Co(III)(NH}_3)_5\text{Br}](\text{Br})_2$ and $[\text{Co(III)(NH}_3)_5(\text{OH}_2)](\text{Br})_3$: Diehl, H.; Clark, H.; Willard, H. H. *Ibid.* **1939**, *1*, 186.
(c) $[\text{Co(III)(NH}_3)_5(\text{N}_3)](\text{Cl})_2$: Linhard, M.; Flygare, H. Z. *Anorg. Chem.* **1950**, *262*, 328.
12. Gordon, A. J., Ford, R. A., Eds. *The Chemists's Companion*; Wiley: New York, 1972; p 58.
13. (a) Blau, F. *Monatsh. Chem.* **1889**, *10*, 372. (b) Blau, F. *Monatsh. Chem.* **1898**, *19*, 647. (c) Burstal, F. M.; Nyholm, R. S. *J. Chem. Soc. (London)* **1952**, 3570.

14. (a) Vogt, L. H., Jr.; Katz, J. L.; Wiberley, S. E. *Inorg. Chem.* **1965**, *4*, 1157. (b) Kuehn, C. G.; Taube, H. *J. Am. Chem. Soc.* **1976**, *98*, 689. (c) Endicott, J. F.; Taube, H. *Inorg. Chem.* **1965**, *4*, 437.
15. (a) Bushnell, G. W.; Lalor, G. C.; Moelwyn-Hughes, E. A. *J. Chem. Soc. (London) A* **1966**, 712. (b) Osborne, J. A.; Thomas, K.; Wilkinson, G. *Inorg. Syn.* **1971**, *13*, 213. (c) Bromely, R.; Figgis, B. N. *J. Chem. Soc. (London) A* **1967**, 861.
16. Sze, S. M. *Physics of Semiconductor Devices*, 2nd ed.; Wiley: New York, 1981; p 31.
17. (a) Heller, A.; Lewerence, H. J.; Miller, B. *Ber. Bunsenges. Phys. Chem.* **1980**, *84*, 592. (b) Noufi, R.; Tench, D. *J. Electrochem. Soc.* **1980**, *127*, 188.
18. Uosaki, K.; Kita, H. *Chem. Lett.* **1984**, 953.
19. Tufts, B. J.; Abrahams, I. L.; Santangelo, P. G.; Ryba, G. N.; Casagrande, L. G.; Lewis, N. S. *Nature (London)* **1987**, *326*, 861.
20. A transient response was also noted for the complex *cis*-[Pt(II)(NH₃)₂(Cl)₂] (pH = 4.6, 9.2). The complex is listed here because the identity of the species in solution under the reaction conditions is in doubt.
21. Several other metal ion exposures also gave a null response. These complexes are listed here because the identity of the species in solution under the reaction conditions is in doubt. [Cr(III)(NH₃)₅(OH₂)](NH₄OH·NO₃) (pH = 12), [Ni(II)(NH₃)₆](Br)₂ (pH = 12), K₂Ni(CN)₄ (0.10 M NaOH solution), Na₂[Fe(III)(CN)₅(NH₃)] (pH = 2), Na₃[Fe(II)(CN)₅(NH₃)] (pH = 2), Na₆[{Co(II)}₂(CN)₁₀] (pH = 2 - 12), CuSO₄ (pH = 13), and the EDTA complexes of Pb(II), Fe(II), Co(II), Cr(III). Dr. M. J. Sailor, formerly of the Lewis Group, has exposed n-GaAs photoanodes to well characterized

[Ru(III)(OH₂)₆](Trif)₃ and [Ru(II)(OH₂)₆](Trif)₂ complexes (pH = 2), and not observed any *I-V* improvement after immersion of the electrode into the selenide electrolyte.

Additionally, unambiguous x-ray photoelectron spectroscopic signatures for Ni, Cr, Ir, Rh, and Co are found on GaAs surfaces exposed to the corresponding complexes used in this study and those listed in reference note 21.

22. (a) Pleskov, Yu. V.; Gurevich, Yu. Ya. *Semiconductor Photoelectrochemistry*, 2nd ed.; Plenum Press (Consultants Bureau): New York, 1986. (b) Gerischer, H. In *Physical Chemistry, an Advanced Treatise*; Eyring, H. Y., Henderson, D., Jost, W., Eds.; Academic Press: New York, 1970; Vol. 9A, pp 463 - 542.

23. (a) Abrahams, I. L.; Tufts, B. J.; Lewis, N. S. *J. Am. Chem. Soc.* **1987**, *109*, 3472. (b) Tufts, B. J.; Abrahams, I. L.; Caley, C. E.; Lunt, S. R.; Miskelly, G. M.; Sailor, M. J.; Santangelo, P. G.; Lewis, N. S.; Roe, A. L.; Hodgson, K. O. *J. Am. Chem. Soc.* **1990**, *112*, 5123.

24. (a) Holmes, P. J. *The Electrochemistry of Semiconductors*; Academic Press: New York, 1962. (b) Langmuir, M. E.; Parker, M. A.; Rauh, R. D. *J. Electrochem. Soc.* **1982**, *129*, 1705.

Chapter 2

X-ray Photoelectron and Extended X-ray Absorption Fine Structure Spectroscopic Studies of the Reactions of Co(III) Ammine Complexes with GaAs Surfaces

Abstract: The chemisorption of Co(II) and Co(III) complexes onto GaAs surfaces has been investigated by x-ray photoelectron spectroscopy (XPS) and radiotracer techniques. XPS of (100)-oriented n-GaAs single crystals that had been exposed to aqueous ($\text{pH} > 10$) $[\text{Co(III)(NH}_3)_5\text{X}]^{n+}$ ($\text{X} = \text{NH}_3, \text{Br}^-, \text{HO}^-$) or $[\text{Co(II)(OH}_2)_6]^{2+}$ solutions indicated the deposition of a Co(II)-oxo overlayer of approximate stoichiometry Co(OH)_2 , with a coverage of $(0.2\text{--}2.4) \times 10^{-9}$ mol (Co) cm^{-2} projected area of GaAs. Quantitative chemical and x-ray fluorescence analysis of the products from reaction of Co(III) and GaAs confirmed a reaction stoichiometry of six Co(III) to one equivalent of GaAs. X-ray absorption spectroscopy indicated that the oxidation state of the adsorbed Co (from either Co(III) or Co(II) sources) from aqueous $\text{pH} = 12$ electrolytes was Co(II). Extended x-ray absorption fine structure (EXAFS) spectroscopy at 298 K in contact with aqueous 0.010 M KOH indicated that Co had (6 ± 1) O or N scatterers at $(2.08 \pm 0.05 \text{ \AA})$ and (7 ± 1) Co (or possibly Ga or As) scatterers at $(3.13 \pm 0.05 \text{ \AA})$. EXAFS and XPS methods also indicated that exposure of the Co(III) or Co(II) treated GaAs surfaces to 1.0 M KOH-0.8 M Se^{2-} -0.1 M Se_2^{2-} for photoelectrochemical measurements yielded a new Co surface phase, with an approximate composition of $\text{CoSe}_{1.8}$.

Introduction

Although chemical modification of semiconductor surfaces can have a major effect on the behavior of photoelectrochemical cells, advanced optoelectronic devices, and chemical sensors,¹⁻³ at present there is no information concerning the chemical state of any bound metal complex at a semiconductor surface. Key systems of importance in this area include the chemisorption of $\text{RuCl}_3 \cdot x\text{H}_2\text{O}$ onto GaAs surfaces,⁴ the binding of amines and olefins to CdSe and CdS surfaces,⁵ the coating of GaAs with $\text{Na}_2\text{S} \cdot 9\text{H}_2\text{O}$,⁶ and the reaction of WSe_2 with phosphines.⁷ All of these treatments have yielded improved electrical surface properties, and several have resulted in large improvements in the efficiency of photoelectrochemical devices. However, spectroscopic and structural data on these types of systems will be necessary before a useful correlation between the surface chemistry and (photo)electronic properties of a given semiconductor can be achieved.

In chapter one it was shown that the interaction of selected group VIII B coordination complexes with n-GaAs electrodes yielded a range of improvements in the current-voltage behavior of the n-GaAs/KOH- K_2Se - K_2Se_2 junction.⁸ Complexes such as $[\text{M}(\text{III})(\text{NH}_3)_5\text{X}]^{n+}$ ($\text{M} = \text{Co}, \text{Rh}, \text{Ir}, \text{Ru}; \text{X} = \text{NH}_3, \text{N}_3^-, \text{Cl}^-, \text{Br}^-, \text{H}_2\text{O}, \text{pyr}$) were observed to adsorb onto GaAs electrode surfaces; furthermore, these treatments have been shown to yield extremely high (14-16%) solar-to-electrical energy conversion efficiencies in n-GaAs/KOH- Se^{2-} photoelectrochemical cells.^{8,9} Questions of interest concern the oxidation state and ligand environment of the bound metal ion, the mechanism of metal ion coordination, the nature of the surface ligating atoms, and the quantity of adsorbed metal. Also of concern are possible changes in chemical state that may occur when, in order to monitor the photoelectrochemical behavior of the surface, the GaAs/(M) surface is exposed to an aqueous 1.0 M KOH-0.8 M Se^{2-} -0.1 M Se_2^{2-} solution. To address these issues, x-ray photoelectron spectroscopic (XPS) and x-ray absorption fine structure (EXAFS) studies of the binding of Co(III) ammine complexes to etched (100) GaAs surfaces have

been performed. The XPS measurements have provided oxidation state and coverage information on the surface-bound metal ions, and are consistent with extended x-ray absorption fine structure (EXAFS) measurements conducted by many members of the Lewis Group.^{8c} The EXAFS data provided an important *in situ* characterization of the coordination sphere of the metal complex bound onto the semiconductor electrode surface, demonstrating that *ex-situ* measurements made in ultra high vacuum (UHV) are representative of the treated GaAs surface in contact with solution.

Experimental

A. Chemicals.

All solvents and etches were either J. T. Baker MOS grade or Mallinckrodt Transistar stock. A Barnstead NANOpure water purifier provided 18 MΩ deionized water. All solutions were deaerated by sparging with a stream of dry N₂ gas for at least 15 minutes.

For x-ray fluorescence (XRF) experiments, As and Ga standards were made from atomic absorption standards supplied by Aldrich, with KBr (Mallinckrodt) used as an internal XRF standard. 1,10-phenanthroline (phen), 2,2'-bipyridine (bipy), and the buffer agents CAPS (pH = 10.6; 3-cyclohexylamino-1-propanesulfonic acid), HEPES (pH = 7.4; 4-(2-hydroxyethyl)-1-piperazineethanesulfonic acid), and MES (pH = 6.15; 2-(N-morpholino)ethanesulfonic acid) were supplied by Aldrich. Phosphate based pH = 7.0 buffer was obtained from VWR. Hydroxylamine hydrochloride was obtained from J. T. Baker.

The chloride and bromide salts of [Co(III)(NH₃)₅X]ⁿ⁺ (X = N₃⁻, NH₃, OH₂, Br⁻),^{10,11} [Co(III)(bipy)₃]³⁺,¹² [Co(II)(bipy)₃]²⁺¹² and tris(1,10-phenanthroline)iron(II),¹³ [Fe(II)(phen)₃]²⁺, were prepared as described in the

literature. The perchlorate salts of the above complexes were made by dissolving a small amount (0.5-1.0 g) of the halide salt in a minimum amount of hot (60-70 °C) water, and then adding concentrated perchloric acid dropwise to effect precipitation of the complex with perchlorate as the counter ion. The resulting solids were rinsed with 1.0 M perchloric acid on a Büchner funnel until no chloride was observed by a silver ion test, and then were washed with cold water and stored in a dessicator. The nitrate salt of $[\text{Co(III)(NH}_3)_5(\text{OH}_2)]^{3+}$ was made in a similar fashion. $\text{CoCl}_2 \cdot 6\text{H}_2\text{O}$, $\text{CoSO}_4 \cdot 6\text{H}_2\text{O}$, $\text{FeSO}_4 \cdot 7\text{H}_2\text{O}$, and FeCl_3 were used as received from J. T. Baker. $[\text{Co(II)(OH}_2)_6](\text{ClO}_4)_2$ was obtained from GFS chemicals. All water soluble cobalt ammine complexes were recrystallized twice from hot water and were characterized by their electronic absorption spectra. No hazards were encountered from the manipulation of the perchlorate salts used in this work.

Model compounds *roseo*- Co(OH)_2 ¹⁴ and CoO(OH) ^{15a} were prepared as described previously. CoSe_2 was obtained by reacting stoichiometric amounts of powdered Co and Se (1:2 mol ratio) in evacuated ($\approx 10^{-4}$ torr) sealed quartz tubes held at either 600 °C or 800 °C for 164 hours.^{16a} A mineralogical sample of CoAs_3 , Skutterudite (Joint Council on Powder Diffraction Standards: JCPDS# 10-328),¹⁷ was provided by the Stanford Geology department. All of these model compounds were characterized by their powder x-ray diffraction patterns, which were obtained on either a Scintag Pad-V or a Rigaku Geigerflex XRD-131 powder x-ray diffractometer.

For use in EXAFS studies, the model compounds Co(OH)_2 , $[\text{Co(II)(OH}_2)_6](\text{ClO}_4)_2$, CoSe_2 , and CoAs_3 were ground to a fine powder with an agate mortar and pestle in an N_2 purged glove bag. The ground powders were then mixed with a dry boron nitride (Alfa) powder to give a dilute (1-3% by weight) suspension of the complex of interest in a non-interfering matrix.

B. GaAs Surfaces and Electrodes.

Preparation of the GaAs electrodes, the 1.0 M KOH-0.8 M K₂Se-0.1 M K₂Se₂ electrolyte, and descriptions of the electrode etching procedures, electrochemical cells, and equipment used to record current-voltage parameters have been described in chapter two and in the literature.¹⁸

Single crystals of (100)-oriented n-GaAs were either grown by organo-metallic vapor phase epitaxy to $N_D = 2 \times 10^{17} \text{ cm}^{-3}$ Se doped epilayers, or were Czochralski grown to give $N_D = 1-4 \times 10^{17} \text{ cm}^{-3}$ Si doped bulk samples. High surface area GaAs powder was made by grinding 99.9999+% GaAs chunks (Aesar) under an N₂ atmosphere (Vac Atmospheres dry box) in a ball mill or in a mortar (reserved solely for GaAs). The fraction of powder that passed a brass 240 mesh sieve (Scienceware) was then retained for further use.

Typical single crystal samples for XPS experiments were initially cleaved to *ca.* 1 cm x 1 cm pieces, degreased by sequential rinsing in trichloroethylene, acetone, and methanol, and then blown dry with N₂. Degreased samples were etched in 4:1:1 (vol) con. H₂SO₄:30% H₂O₂:H₂O, rinsed with H₂O, dried with N₂, and passed into an N₂ purged glove bag. All solutions placed in the glove bag had been previously deaerated and sealed. In order to strip any GaAs oxides formed during transfer, these pieces were then immersed in deaerated 14.8 M NH₄OH solution for 30 seconds, then rinsed with DI water, and dried in N₂. These specimens were then exposed for 1 min to 10 mL aqueous solutions containing 10 mM of either [Co(III)(NH₃)₆](Cl)₃, [Co(III)(NH₃)₆](Br)₃, [Co(III)(NH₃)₆](ClO₄)₂, [Co(III)(NH₃)₅OH₂](NO₃)₃, [Co(III)(NH₃)₅Br](Br)₂, [Co(III)(NH₃)₅(N₃)](Cl)₂, [Co(II)(OH₂)₆](ClO₄)₂, or [Co(II)(OH₂)₆](Cl)₂. The Co solutions were made up over a range (1.0-12.9) of pH values. The treated samples were then lightly (3-4 mL) rinsed with 18 MΩ water and blown dry with a stream of N₂.

Treated GaAs pieces were then mounted on an XPS sample stub and sealed in air-tight vials for transport to the spectrometer.

To eliminate the possibility that photoreactions of the GaAs or the Co(III) complexes are responsible for the observed surface reactivity, several GaAs samples were exposed to $[\text{Co(III)(NH}_3)_5\text{X}]^{n+}$ ($\text{X} = \text{NH}_3, \text{Br}^-, \text{OH}_2$) solutions in the absence of room light. These samples displayed spectroscopic and electrochemical behavior that was identical to samples that had been manipulated in ambient room light.

Powders of GaAs were treated in a similar fashion. In a glove bag, portions of GaAs powder (*ca.* 100 mg) were added to 10 mL of the Co(III) and Co(II) solutions (*vide supra*) for 5 or 10 minutes. The solid suspensions were then filtered, and the filtrate was analyzed by XRF or UV-VIS methods, or the collected solids were rinsed with H_2O , CH_3OH , and then dried with N_2 under suction. Depending upon the pH of the Co complex ion solution, this procedure led to a loading of the powders with up to 4% (by weight) Co. Treated powdered samples intended for XPS studies were pressed into a sample of In foil (Alfa) that was molded onto the top of an XPS sample mount.

To investigate potential chemical reactions in the electrochemical solutions of interest, parallel sets of Co-ion treated GaAs powders or single crystals were subsequently exposed to 5 mL solutions of 1.0 M KOH-0.8 M K_2Se -0.1 M K_2Se_2 for 1 minute. The samples were then rinsed, dried, mounted as described above and subjected to XPS analysis. No difference in reaction behavior was observed for identical manipulations performed in the dark relative to those performed under ambient room light.

C. ^{57}Co Studies.

2 mCi of γ -active $^{57}\text{CoCl}_2 \cdot 6\text{H}_2\text{O}$ was purchased from ICN Chemicals, and was used to synthesize¹⁰ a 3.46 mM solution (as determined by UV-VIS spectrophotometry)

of ^{57}Co enriched $[\text{Co(III)(NH}_3)_6](\text{Cl})_3$. The activity of the final stock solution of the complex was $34.0 \mu\text{Ci ml}^{-1}$. In the same manner as above, *ca.* 1 cm^2 pieces of (100) n-GaAs were exposed, in air, to 2 ml of the ^{57}Co enriched stock solution at $\text{pH} = 1.0$ (HCl) or $\text{pH} = 12.0$ (KOH). These GaAs samples were then either immersed in $\text{pH} = 1.0$ (HCl) solution for 30 sec and the acidic solution assayed for ^{57}Co , or were etched in 5 mL of 4:1:1 (vol) con. H_2SO_4 :30% H_2O_2 : H_2O for 10 seconds, and then rinsed with H_2O . In the later procedure, care was taken to collect the rinse water into the etch solution, and the etch solution and rinse water were then analyzed for γ -activity. Counting was done with a Beckman Model 8000 γ -ray scintillation counter. Standards were prepared from known concentrations of the ^{57}Co -enriched $[\text{Co(III)(NH}_3)_6](\text{Cl})_3$ solution and were used to calibrate the counts observed from the Co-treated GaAs samples. No activity above detectability limits (signal to background 2:1; $\leq 3 \times 10^{-11} \text{ mol(Co) cm}^{-2}(\text{GaAs})$) was observed from etch solutions of untreated GaAs or from ^{57}Co -exposed GaAs that had been deliberately etched prior to the ^{57}Co analysis described above.

D. XPS.

I. **Experimental Procedures.** X-ray photoelectron spectra were obtained on a Vacuum Generators Mark II ESCALAB. All spectra were acquired at a base pressure of $< 10^{-10}$ torr using non-monochromatic Al $\text{K}\alpha$ ($h\nu = 1486.6 \text{ eV}$) irradiation. The x-ray source was typically operated at 20 mA and 12.5 kV.

A Ag stub was used to determine the instrumental linewidth, which was observed to be 1.1 eV in narrow scan mode from the FWHM of the Ag 3d doublet peaks at 367.9 and 373.9 binding energy (BeV). All corrected binding energies discussed in this work were referenced to the C 1s line of adventitious carbon at 284.6 BeV. Peak deconvolutions were performed using standard software routines provided by Vacuum Generators. The

surface analysis was slightly compromised, in that on oxidized GaAs substrates the Ga 3d and O 2s lines overlap, often precluding reliable calculation of stoichiometric ratios relative to Ga.

Unless otherwise noted, all samples were prepared and mounted on sample stubs under an N₂ atmosphere (in a glove bag) and were transported to the XPS instrument in sealed, gas-tight, vials. Mounted samples were loaded into the instrument's N₂ purged fast entry lock either by quick transfer in air or by transfer into a N₂-purged glove bag sealed around the entry port. Total exposure to air during instrument transfer was effectively less than one second when the samples were protected by a glove bag, and typically less than 10 seconds when they were unprotected. Etched GaAs that was exposed only to 1.0 M KOH or to pH = 11.0, 0.05 M KClO₄ solutions displayed peaks for lattice As 3d at (41.3 ± 0.5) BeV and lattice Ga 3d at (19.4 ± 0.5) BeV, and had oxide region peak intensities consistent with < 3 × 10⁻¹⁰ mol cm⁻² (*i.e.*, < 1/2 monolayer) of arsenic oxides and of gallium oxides (*cf.* Figure 3). These low background values required careful anaerobic handling of the GaAs through all etching steps and subsequent solution manipulations; however, under these conditions, the appearance of large Ga or As oxide-based XPS signals reliably indicated exposure of the GaAs to additional oxidants (*i.e.*, the Co(III) complexes), and not the trivial case due to air oxidation.

II. Data Analysis. Estimates of the Co 2p photoelectron escape depth (λ) were obtained using the method of Seah and Dench,¹⁹ with photoelectron differential cross-sections as given by Scofield.²⁰ All GaAs samples exposed to aqueous solutions of [Co(III)(NH₃)₅X]ⁿ⁺ (X = N₃⁻, NH₃, OH⁻, Br⁻), [Co(III)(NH₃)₆]³⁺, and [Co(III)(OH₂)₆]²⁺ complexes at pH > 8 invariably displayed Co 2p signal intensity solely due to Co(II) sources (*vide infra*). In each case, the Co 2p peak structure was very similar to that of Co(OH)₂, and hence the local environment about each Co(II) source was assumed to be similar to Co(OH)₂, thus establishing an estimate for the number densities

(gram atom cm^{-3}) of Co and O in the Co 2p signal source. This yielded a value of $\lambda_{\text{Co}2p} = 18 \text{ \AA}$. Employing the simple homogeneous overlayer model of photoelectron attenuation,²¹ the surface coverage was then determined with respect to the intensity, photoelectron escape depth ($\lambda_{\text{As}3d} = 25 \text{ \AA}$), and molar density ($n_{\text{As}} = 3.68 \times 10^{-2} \text{ mol cm}^{-3}$) for As in the substrate GaAs, the integrated Co 2p_{3/2} peak intensity, and the known values of the sample-detector angle, and the atomic number density ($3.87 \times 10^{-2} \text{ mol cm}^{-3}$) for Co in Co(OH)_2 .²²

Sources of As 3d signal attributable to As_2O_3 were assumed to have a molar density equivalent to that of vitreous arsenic oxide ($\rho = 1.89 \times 10^{-2} \text{ mol cm}^{-3}$)²³; the corresponding value of the photoelectron escape depth is $\lambda_{\text{As}3d} = 36 \text{ \AA}$. Sources of Ga 3d signal due to gallium oxide (Ga_2O_3) were often obscured by a broad peak due to the O 2s core level. The density of surface Ga_2O_3 was taken as the average of the molar densities of the α and the β phases, $\rho = 3.30 \times 10^{-2} \text{ mol cm}^{-3}$;²⁴ this yielded an escape depth of $\lambda_{\text{Ga}3d} = 28 \text{ \AA}$. XPS signals from the C 1s region showed that more than one type of hydrocarbon was in the surface overlayer. The value of the hydrocarbon molar density was estimated as $\rho = 1.5 \times 10^{-2} \text{ mol (C) cm}^{-3}$ and the carbon atomic number density was estimated as $\rho = 3.3 \times 10^{-2} \text{ gram-atom cm}^{-3}$. In determining the amount of carbonaceous material at each surface, the experimentally determined value²⁶ of $\lambda_{\text{C}1s} = 35 \text{ \AA}$ for the mean free path of the photoelectrons in an organic film was used.

Surface morphology and relative stoichiometry were obtained by comparison of XPS peak intensities between the substrate As 3d or Ga 3d lines, the O 1s line, and the Co 2p lines on (100)-oriented n-GaAs over a range of sample-detector angles.²⁶ The simple XPS substrate/overlayer intensity model of Fadley²⁷ was applied, assuming that substrate oxides were closest to the GaAs interface, followed by a cobalt-oxo or seleno layer, and finally an adventitious hydrocarbon layer. In determining the stoichiometric ratio of Co:O in the overlayer, a correction for sources of O other than Co(OH)_2 was made to the

raw O 1s intensity. The sources were clearly identified from their peak positions: the oxides of GaAs ($\lambda_{O1s}(As_2O_3) = 29 \text{ \AA}$ and $\lambda_{O1s}(Ga_2O_3) = 22 \text{ \AA}$), signals for carboxy-O in the C 1s region at $\geq 286 \text{ BeV}$ ($\lambda_{O1s}(C-O) = 37 \text{ \AA}$), and those for H₂O in the O 1s region at $\geq 534 \text{ BeV}$ ($\lambda_{O1s}(H_2O) = 22 \text{ \AA}$). The λ_{O1s} escape depths were estimated from the method of Seah and Dench.¹⁹ Assuming an atomic O density $\rho = 2.8 \times 10^{-2} \text{ gram-atom cm}^{-3}$ for carboxy-O and $\rho = 5.6 \times 10^{-2} \text{ gram-atom cm}^{-3}$ for H₂O, a background O 1s intensity was determined and subtracted from the raw O 1s signal. Deviations from the expected stoichiometric ratios were interpreted as evidence of a non-uniform surface phase.²⁸ It has been assumed that a non-uniform surface phase may be modeled as a void-filled thin film, the density of which varied in the direction normal to the surface.

For those GaAs samples subsequently exposed to Se⁻²⁻ electrolyte, estimates of Co coverage were based on the integrated Co 3p_{3/2} and 3p_{1/2} intensities (the two core levels give rise to a single line in the XPS spectrum).²⁹ The Co 3p and Se 3d lines were used to derive a stoichiometric relationship between Co and Se because these lines are only 4 eV apart in binding energy. The closeness of the lines minimizes the systematic error due to differences in the spectrometer transmission response as a function of photoelectron energy. Following the procedure described above, using the atomic density of Co in Trogalyte, CoSe₂ ($\rho = 3.3 \times 10^{-2} \text{ gram-atom cm}^{-3}$),^{16bc} the photoelectron escape depths for Co and Se were estimated as $\lambda_{Co3p} = 20 \text{ \AA}$ and $\lambda_{Se3d} = 20 \text{ \AA}$. Table I summarizes all of the estimated and calculated parameters used in the determination of surface coverages and surface chemical compositions.

E. EXAFS.

Cobalt K edge EXAFS spectra were obtained on beam lines II-3, IV-2 (unfocussed), and VII-3 at the Stanford Synchrotron Radiation Laboratory (SSRL).

Table I:**X-ray Photoelectron Spectroscopy: Surface Analysis Materials Parameters**

Compound	line ^a	n (g-atom cm ⁻³) ^b	$\sigma_{\text{Scofield}}^c$	λ (Å) ^d	Γ (mole cm ⁻²) ^e	d (Å) ^e
GaAs	As 3d	3.68×10^{-2}	$\Sigma^f = 1.821$	25	1.31×10^{-9}	---
	Ga3d	3.68×10^{-2}	$\Sigma = 1.085$	25		
As ₂ O ₃ (vitreous)	As 3d	3.78×10^{-2}	$\Sigma = 1.821$	36	8.4×10^{-10}	4.4
	O 1s	5.67×10^{-2}	2.93	29		
Ga ₂ O ₃ ($\alpha + \beta$) ^g	Ga 3d	6.59×10^{-2}	$\Sigma = 1.085$	28	1.2×10^{-9}	3.7
	O 1s	9.89×10^{-2}	2.93	22		
Co(OH) ₂	Co 2p _{3/2}	3.87×10^{-2}	12.62	18	1.4×10^{-9}	3.5
	O 1s	7.75×10^{-2}	2.93	21		
CoSe ₂	Co 3p	3.30×10^{-2}	$\Sigma = 1.93$	20	1.22×10^{-9}	3.7
	Se 3d	6.60×10^{-2}	$\Sigma = 2.294$	20		
C _x H _y O _z ^h	C 1s	3.3×10^{-2}	1.000	35	7.3×10^{-10}	4.8
	O 1s	2.8×10^{-2}	2.93	37		
OH ₂	O 1s	5.6×10^{-2}	2.93	22	1.73×10^{-9}	3.1

a. Detected line due to photoemission from the relevant core level.

b. Elemental equivalent in a cubic centimeter of solid compound.

c. Core level differential photoelectron cross section, as calculated by Scofield.²⁰

d. Photoelectron escape depth at the given core line energy in the compound material.

e. Mole equivalent in a monolayer thick film and idealized thickness for the compound material.

f. Σ is used when lines from core levels with net spin overlap, and indicates the sum of the pertinent Scofield differential photoelectron cross sections.

g. Average of $\alpha + \beta$ phases of Ga₂O₃.

h. Generic oxygen-containing carbonaceous material.

Synchrotron radiation (derived from a ring electron current of 30-80 mA and *ca.* 3.0 GeV energy) was passed through a scanning Si (220) double-crystal monochromator prior to sample illumination. EXAFS data on the model compounds were obtained under 10^{-6} torr at 10 K in the transmission mode. These data were collected from *ca.* 7400 eV, through the Co K edge of the internal calibration Co foil at 7709.30 eV, to *ca.* 8800 eV using N₂ ionization detectors. EXAFS data for Co-treated GaAs powders were collected under 10^{-6} torr at 10 K, 77 K, and 298 K by monitoring the fluorescence lines of Co K_{a1,2} at 6930 and 6915 eV using an ionization-type fluorescence detector^{30ab} and an Fe sheet high pass filter supplied by the SSRL Biotechnology group.

Absorbance (or fluorescence) vs. wavelength data were collected in 20-to-30 minute scans, with several scans collected and averaged to improve the signal-to-noise ratio. Derivative spectra of the edge region contained several small inflection points; the energy at half-height of the absorption jump was therefore taken as the edge position. Bond distances and the number of scatterers were calculated by fitting the oscillatory part of the EXAFS spectra to the EXAFS equation,^{30c-f} using phase factors and scattering amplitudes determined experimentally from the model compounds. The average Co-O distance in [Co(II)(OH₂)₆](ClO₄)₂ was taken as the average Co-O distance from the crystallographically determined Co-O bond lengths in [Co(II)(OH₂)₆](NH₄SO₄)₂,^{31a} [Co(II)(OH₂)₆](NO₃)₂,^{31b} and [Co(II)(OH₂)₆](SiF₆).^{31c}

Immediately before data collection, either a cobalt model compound/BN powder blend or a Co-ion treated GaAs powder was pressed into a sample holder that was fashioned from a 3mm x 25mm slot cut through a 3mm-thick Cu plate. The powder sample was sealed in place with Kapton tape. The loaded sample holder was mounted onto the cold head of an Air Products Displex 10 K closed cycle He gas refrigerator or of a home-made liquid nitrogen cooled cold finger. This sample assembly was evacuated to

$\leq 10^{-6}$ torr before data collection was initiated. Kapton film (1-2 mil) was used as the refrigerator window material to allow for x-ray excitation and for detection of both transmission (BN matrix) and fluorescence (GaAs powder) EXAFS spectra.

F. Quantitative Chemical Analysis.

Reaction vials, wrapped in aluminum foil to keep out light, were charged in the glove box with freshly ground GaAs (10-20 mg, fraction passing a 240 mesh sieve) and were stoppered. Standard syringe techniques were used to transfer *ca.* 6 mL of degassed 5.0 mM $[\text{Co(III)(NH}_3)_6]^{3+}$ solutions at either 0.10 M HCl (pH = 1.0), 50 mM HEPES (pH = 7.4), 50 mM CAPS (pH = 10.6), or 14.8 M NH_4OH (pH = 12.9) to one set of vials. Another set of vials charged with GaAs was treated with the various pH solutions containing no Co complex. At least three vials were used for each combination of blank and Co complex at each pH. A parallel set of trials at 0.10 M HCl was carried out using Fe^{3+} , from ferric chloride, in place of the Co(III) complex.

Reaction vials were stored in the dark for 15-24 hours and typically were stirred for 6-8 hours. At the end of the reaction period, the sample was analyzed under N_2 for Co(II) ion, by removing an aliquot of the reaction solution via gas tight syringe and converting any Co(II) ions in the analyte to the Co(II) thiocyanate complex via a slightly modified method.³² In place of acetylacetone, a (2:5) mixture of water:acetone was used in the final analyte solution to form the cobalt complex. Co(II) thiocyanate ($\lambda_{\text{max}} = 622 \text{ nm}$) was spectrophotometrically detected³² with a Hewlett-Packard (HP) 8452A diode array UV-VIS spectrophotometer. A series of calibration curves, determined for a range of Co(III) and Co(II) concentrations ($4.3 \times 10^{-5} \text{ M}$ to $2.50 \times 10^{-3} \text{ M}$) at each pH, was used to convert measured absorbances to initial reactant concentrations. The limits of detectability of the HP UV-VIS made it possible to monitor both Co(II) and Co(III) complex ions simultaneously, down to concentrations of 30 μM and 150 μM respectively. The

GaAs-driven conversion of Fe^{3+} to Fe^{2+} at 0.10 M HCl was monitored by converting any iron(II) aquo ions to the tris(phenanthroline)iron(II) complex. The oxidation state and concentration of the resulting Fe complex was observed by UV-VIS spectrophotometry. The UV-VIS detectability limit for the Fe(II) complex was 30 μM .

Product As and Ga ions formed in the reaction solution were determined by x-ray fluorescence (XRF) analysis. Both arsenic (III) and gallium (III) oxides are amphoteric, and therefore are soluble at either low or high pH conditions.³³ Concentrations of arsenic (III) or gallium (III) ions, up to and including the maximum observed values of *ca.* 1 mM, were routinely handled and not found to be solubility product limited. Using anaerobic syringe techniques, a typical reaction solution was filtered (0.2 μm filter) to remove suspended GaAs. A 1.00 mL aliquot of the filtrate was transferred by micropipet to a thin (1 mil) polyethylene-bottomed x-ray fluorescence sample cup to which 10.0 μL of 30.0 mM KBr solution was added for use as an internal XRF standard. XRF analysis was performed on a KEVEX 0700 XES instrument. Co, Ga, and As ions were probed by x-rays from a Ag target operated at 35 kV and 0.35 mA. Fe ions were detected with a Ge target operated at 20 kV and 0.2 mA. Acquisition times of 300s or 500s were used to obtain areas from the intensities of the x-ray fluorescence peaks. Employing standard computer deconvolution techniques, the measured intensities were converted to solution concentrations by comparison to intensities obtained from stock solutions of As, Ga, Co, and Fe at known concentrations under identical instrumental conditions. The detectability limits ($S/N < 2$, $\pm 50\%$ of the detectability limit) using this method were 10 μM , 80 μM , 750 μM , and 840 μM for As, Ga, Co, and Fe respectively.

Determination of the complete stoichiometry of the redox reaction at pH = 10.6 (CAPS buffer) was not feasible by these techniques. The amount of observed Co(II) ion could not be correlated with the disappearance of Co(III) or with the final As and Ga ion concentrations. In the absence of stabilizing ligands (*e.g.*, NH_3), *roseo*-Co(OH)₂ is

insoluble ($K_{sp} = 1.99 \times 10^{-15}$) at $\text{pH} = 10.6$,³⁴ which likely accounts for the irreproducible variations in the [As]:[Ga]:[Co(II)] ratio of soluble ions observed in the XRF experiments at this pH.

The pH stability of a Co-containing surface layer on GaAs was probed by first reacting the $[\text{Co(III)(NH}_3)_6]^{3+}$ complex with GaAs powder in 0.010 M KOH as above, removing the reaction solution, and then subjecting the resulting solids to 0.10 M HCl, VWR phosphate buffer ($\text{pH} = 7.0$), or 0.010 M KOH solutions for 30 seconds. The resulting solution was then syringe filtered ($0.45 \mu\text{m}$), any Co(II) in the analyte was converted to the Co(II) thiocyanate complex (*vide supra*) and determined spectrophotometrically.

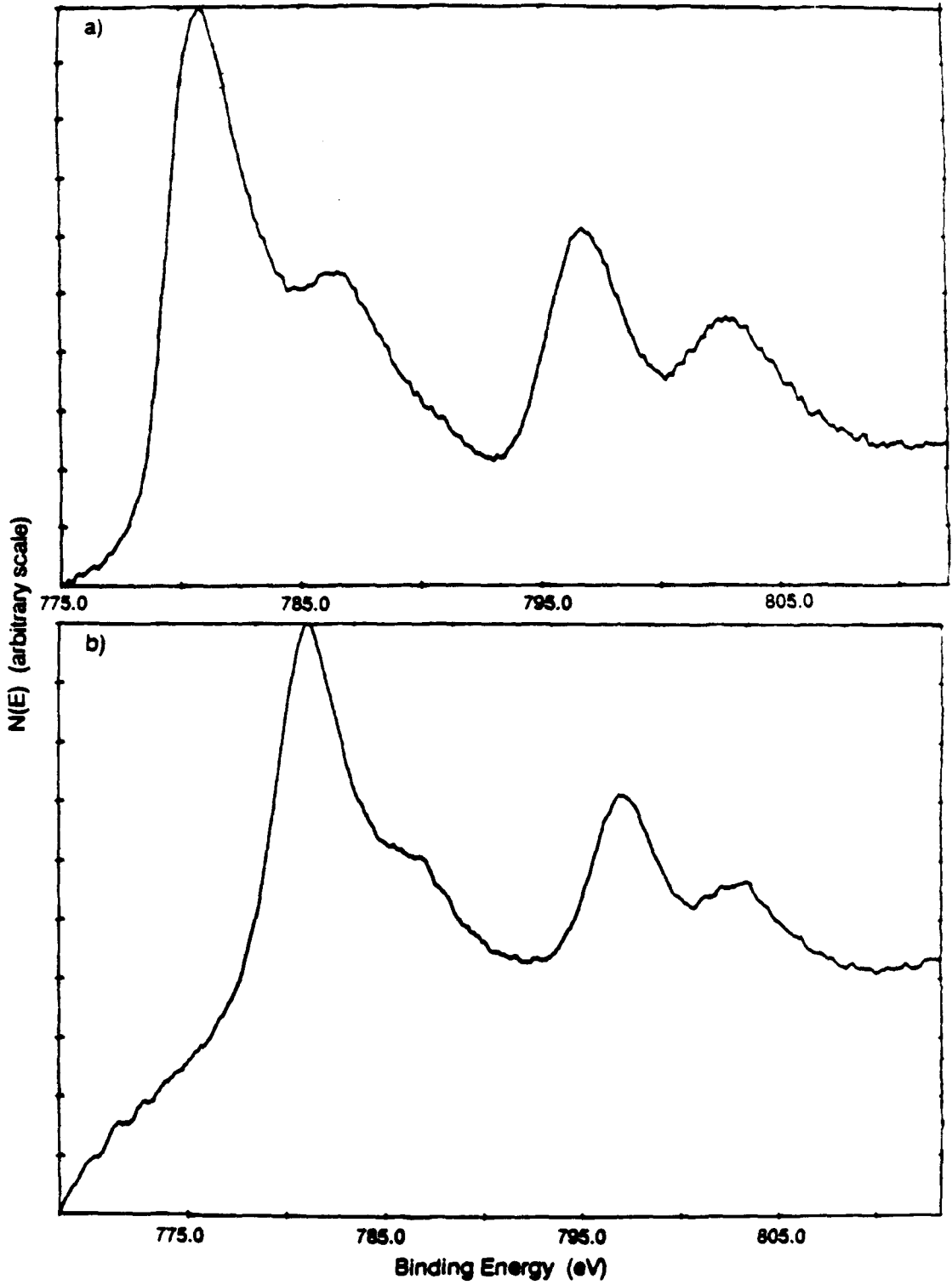
Results

1. XPS Studies of Co Chemisorption on GaAs

A. Co(III) Complexes: XPS Spectra in the Co 2p, As 3d, and Ga 3d Regions.

Both single crystal and powdered GaAs samples were observed to bind Co after exposure to basic 0.010 M KOH aqueous Co(III) ammine solutions. Figure 1 displays the x-ray photoelectron (XP) spectra that were obtained from these samples. Note that the peak structure observed for the most intense lines in the XP spectra of transition metal complexes, especially in those cases of the metal ion having net electron spin density, are highly characteristic of both the oxidation state and spin state of the metal ion. The relevant diagnostics are the separation between the parent peak pair (Δ), and the absence or presence of a satellite peak pair, each satellite line being displaced to higher binding energy with respect to its associated parent peak. In the present case, $\Delta \equiv \text{BeV}(\text{Co } 2p_{1/2}) - \text{BeV}(\text{Co } 2p_{3/2})$. The spectra exhibited two primary

Figure 1: Co 2p region XPS of GaAs samples exposed to basic (pH > 10) aqueous solutions of $[\text{Co(III)(NH}_3)_6]^{3+}$ complex. The raw data are displayed after being corrected for binding energy relative to C 1s. (a) (100)-oriented n-GaAs single crystal substrate. (b) GaAs powder on In foil.



signals (relative to adventitious carbon defined to be C 1s \equiv 284.6 BeV) in the Co 2p region (781.1 and 797.0 BeV, $\Delta_{\text{Co}2\text{p}} = 15.9$ eV) and two satellite peaks (786.2 and 802.8 BeV). A wide scan displayed the expected additional Co XP and Auger lines, but did not reveal signals corresponding to the presence of N, Cl, or elements other than C, O, Ga, As, and Co. Variation in the identity of the sixth ligand ($X = \text{N}_3^-, \text{Br}^-, \text{OH}_2, \text{NH}_3$) did not produce any change in the XPS spectrum of the Co 2p region, nor did such variation yield any new peaks in the XPS wide scans. Table II summarizes the peak positions obtained for representative samples in this series of XPS experiments.

XPS data were also obtained for several pure Co(II) and Co(III) coordination compounds. *roseo*-Co(OH)₂, displayed in Figure 2a, exhibited parent lines at 780.6 and 796.8 BeV ($\Delta_{\text{Co}2\text{p}} = 16.2$ eV) and daughter peaks at 785.6 and 802.5 BeV. The XPS of [Co(III)(NH₃)₆](Br)₃, cooled to 180 K, produced a spectrum with lines at 781.6 and 796.6 BeV ($\Delta_{\text{Co}2\text{p}} = 15.0$ eV) and displayed no satellite peak structure (Figure 2b). No noticeable photoreduction of Co(III) to Co(II) was observed on this sample. The spectra of these complexes are in agreement with the general expectations of parent peak splittings of $\Delta = 16.1 \pm 0.3$ eV and satellite structure for high spin ($S = 3/2$) Co(II)³⁵ complexes, and parent peak splittings $\Delta = 15.0 \pm 0.3$ eV and no satellite structure for low spin ($S = 0$) Co(III) compounds.³⁵

The peak positions and satellite structure of the Co 2p lines in Figures 1 and 2a, and the similarity to the known XP spectra for Co(II) complexes,³⁵ indicate that the oxidation state of the GaAs-bound Co is Co(II). This implies that the mechanism of Co(III) binding to the GaAs involves a redox reaction. The loss of XP signals attributable to either coordinated amines or to other inner sphere ligands of [Co(III)(NH₃)₅X]ⁿ⁺ ($X = \text{N}_3^-, \text{Br}^-, \text{HO}^-, \text{NH}_3$) is consistent with the lability of the Co(II) oxidation state,³⁶ and confirms the involvement of electron transfer steps in the chemisorption of these complexes.

Table II: XPS Peak Positions^a: Model Compounds and Surface Components of Etched and Reacted GaAs Interfaces

Sample	Co 2p Core Lines (BeV) ^a				
	Parent		Satellite		O 1s
	Co 2p _{3/2}	Co 2p _{1/2}	(2p _{3/2})	(2p _{1/2})	
[Co(III)(NH ₃) ₆](Br) ₃	781.6	796.6	----	----	----
		$\Delta^b = 15.0$	N 1s = 399.7	Br 3d = 68.5	
CoSe (sputtered)	777.9	792.8	----	----	----
		$\Delta^b = 14.9$	Se 3d = 54.4	Co 3p = 58.8	
<i>roseo</i> -Co(OH) ₂	780.6	796.8	785.6	802.5	530.6
		$\Delta^b = 16.2$		$\Delta^b = 16.9$	
(100) GaAs ^d + [Co(III)(NH ₃) ₆](ClO ₄) ₃ 0.010 M KOH	781.1 ± 0.5	797.0 ± 0.4	786.2 ± 0.4	802.8 ± 0.4	531.3 ± 0.5
		$\Delta^b = 15.9 \pm 0.1$		$\Delta^b = 16.6 \pm 0.3$	
(100) GaAs ^d + [Co(III)(NH ₃) ₅ (OH)](NO ₃) ₃ 0.010 M KOH	780.8	797.0	786.4	802.8	531.0
		$\Delta^b = 16.2$		$\Delta^b = 16.4$	
(100) GaAs ^d + [Co(III)(NH ₃) ₆](ClO ₄) ₃ pH = 12.9 (sat'd. NH ₃)	(781) ^c	e	e	e	532.1
240 mesh GaAs ^d + [Co(III)(NH ₃) ₅ Br](Br) ₂ pH = 11.0	781.0	797.1	786.3	802.7	531.0
		$\Delta^b = 16.1$		$\Delta^b = 16.4$	
240 mesh GaAs ^d + [Co(III)(NH ₃) ₅ N ₃](Cl) ₂ pH = 10.7	781.6	797.6	787.0	803.6	531.3
		$\Delta^b = 16.0$		$\Delta^b = 16.6$	

Table II (continued)

Sample	Co 2p Core Lines				O 1s
	Parent		Satellite		
	Co 2p _{3/2}	Co 2p _{1/2}	(2p _{3/2})	(2p _{1/2})	
(100) GaAs ^d + [Co(III)(NH ₃) ₅ N ₃](Cl) ₂ pH = 6.2 (MES buffer)	e	e	e	e	531.9
(100) GaAs ^d + [Co(III)(NH ₃) ₆](Br) ₃ pH = 2.0	e	e	e	e	531.7
(100) GaAs ^d + [Co(III)(bipy) ₃](ClO ₄) ₃ pH = 11.3	(781) ^c	e	e	e	531 ± 0.1
(100) GaAs ^d + [Co(II)(OH ₂) ₆](Cl) ₂ 0.010 M KOH	781.1 ± 0.4	797.2 ± 0.4 $\Delta^b = 16.1 \pm 0.1$	786.4 ± 0.4	802.9 ± 0.4 $\Delta^b = 16.5 \pm 0.1$	531.0 ± 0.3
(100) GaAs ^d + [Co(II)(OH ₂) ₆](Cl) ₂ pH = 12.9 (sat'd. NH ₃)	(782) ^c	(798) ^c $\Delta^b = 16$	e	e	532.2
(100) GaAs ^d + [Co(II)(bipy) ₃](Cl) ₂ pH = 12.0	(781) ^c	(797) ^c $\Delta^b = 16$	e	e	532.7
(100) GaAs ^d + [Co(III)(NH ₃) ₆](ClO ₄) ₃ (0.010 M KOH) + KOH-Se ^{-1/2-}	778.4	793.3 $\Delta^b = 14.9$ Co 3p = 59.0	e	e	531.2 Se 3d = 54.2 ± 0.3

a. XPS core lines referenced against C 1s = 284.6 Binding eV (BeV). Data listed from multiple experiments include ± 1 standard deviation.

b. Separation between Parent lines and between Satellite lines.

c. Edge of poorly defined peak barely discernible above background.

d. No peaks due to N 1s or counter ion sources were observed from this experiment.

e. No signal detected above background.

Figure 2: Co 2p region XPS of model compounds; the raw data are displayed after being corrected for binding energy relative to C 1s. (a) *roseo*-Co(OH)₂ on In foil.
(b) [Co(III)(NH₃)₆](Br)₃ on In foil at T = 180 K.

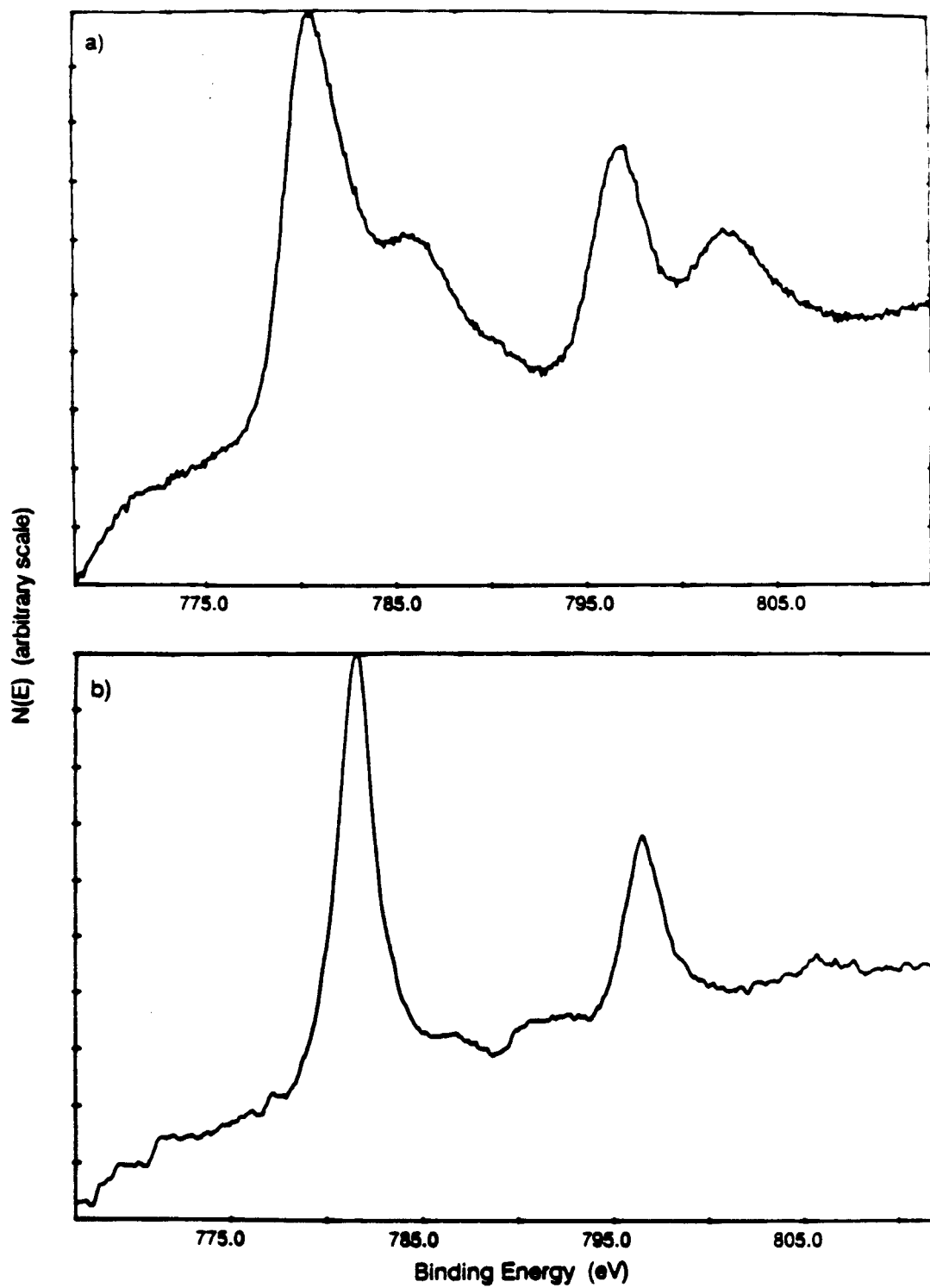
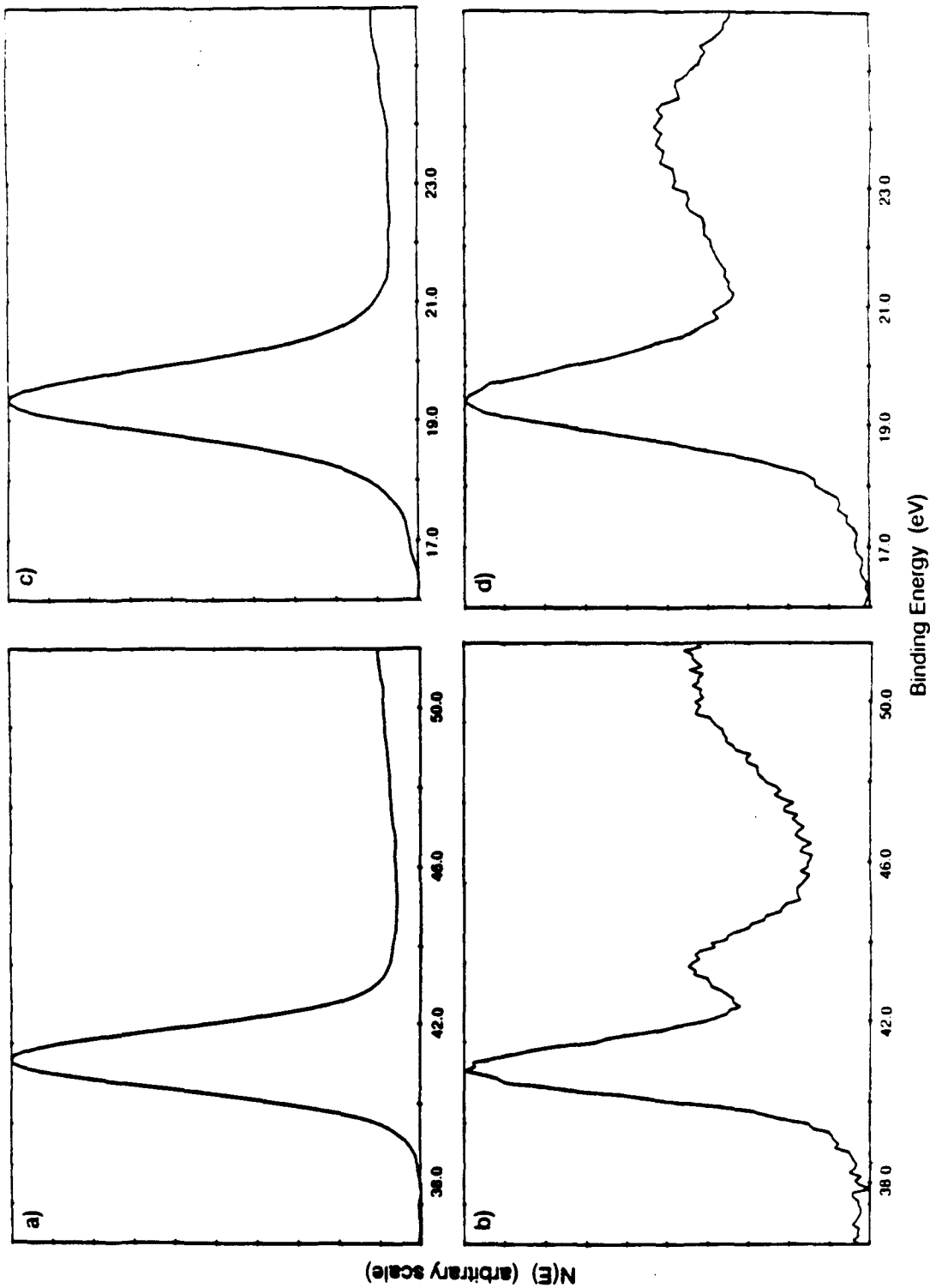


Figure 3: XPS of anaerobically-handled (100)-oriented n-GaAs substrates. The raw data are displayed after being corrected for binding energy relative to C 1s. (a) As 3d region of 4:1:1 (con. H₂SO₄: 30% H₂O₂: H₂O) etched, base (1.0 M KOH) exposed sample. Sample-normal to detector angle 65°. (b) As 3d region of an etched substrate subsequently exposed to 0.010 [Co(III)(NH₃)₆]³⁺ complex at pH = 12. The new peak at *ca.* 44 BeV is due to As₂O₃. Sample-normal to detector angle 15°. (c) Ga 3d region of same substrate as in a. (d) Ga 3d region of same substrate as in b. The presence of Ga₂O₃ (20.7 BeV) has resulted in a broadening of the substrate line towards higher binding energies. Interference from O 2s line can be seen as a broad peak centered about 24 BeV.



The reduction of Co(III) to Co(II) in 0.010 M KOH solution implies that oxidation of the GaAs should also occur. For exposure to $[\text{Co(III)(NH}_3)_6]^{3+}$, this was confirmed by the presence of an arsenic oxide (As_2O_3) line at 43.6 BeV (As 3d region) and a gallium oxide line at 20.7 BeV (Ga 3d region) (Figure 3). Oxidized Ga and As were also observed after exposure of GaAs to $[\text{Co(III)(bipy)}_3]^{3+}$, but no detectable ($\leq 2 \times 10^{-10}$ mol cm^{-2}) oxide was observed after exposure to $[\text{Co(II)(bipy)}_3]^{2+}$, or to $[\text{Co(II)(NH}_3)_6]^{2+}$ stabilized in aqueous NH_3 (Table III). Oxidation of GaAs thus takes place with a variety of Co(III)-based reagents and is detectable both by XPS and by chemical analysis for the resulting Co(II) (*vide infra*).

The lack of detectable Co XPS signal from $[\text{Co(III/II)(bipy)}_3]^{3+/2+}$ exposure at $1 < \text{pH} < 12.0$ (Table II, III) demonstrates that a simple electrostatic binding interaction between Co complex ion and GaAs surface is insufficient to explain the chemisorption process. This is the case even for $\text{pH} > 11$, where surface oxides might be expected to generate a substantial concentration of ionized hydroxide-like species. The observed oxidation of the GaAs substrate in the presence of basic solutions of $[\text{Co(III)(bipy)}_3]^{3+}$ does, however, support the involvement of electron transfer steps in the chemisorption mechanism (Table III).

The chemisorption process also was found to depend on the pH of the aqueous solution. In contrast to the facile chemisorption of $[\text{Co(III)(NH}_3)_5\text{X}]^{n+}$ ($\text{X} = \text{N}_3^-$, Br^- , OH^- , NH_3) in 0.010 M KOH, no bound Co or the oxidation of GaAs was observed when using Co(III) ammine complexes at $\text{pH} = 1 - 2$ (Table II, III). This is in accord with chemical studies indicating that $[\text{Co(III)(NH}_3)_6]^{3+}$ is not sufficiently oxidizing to react with GaAs in acidic media (*vide infra*). Notably, the solubility product³⁴ of *roseo*- Co(OH)_2 is $K_{\text{sp}} = 1.99 \times 10^{-15}$, indicating that if a Co(OH)_2 species is produced, it would be expected to dissolve at low pH values. However, by XPS, negligible oxidation of the

Table III: Surface Coverage (Γ)^a of Reacted (100) GaAs Surfaces

Sample and Reaction Conditions	GaAs Substrate					
	θ^b	Ga 3d		As 3d		As ^c Ga
		peak ^c	intensity ^d	peak	intensity	
4:1:1 etched GaAs + 1.0 M KOH T \approx 180 K ¹	0 55	18.9 19.0	3,897 3,727	40.8 41.0	3,468 3,438	0.89 0.92
4:1:1 etched GaAs + KClO ₄ pH = 11.0 room temp. (R.T.)	0 55	19.8 19.9	2,288 1,815	41.7 41.8	2,000 1,743	0.87 0.96
GaAs + [Co(III)(NH ₃) ₆] ³⁺ 0.010 M KOH T \approx 180 K	10 30 55 70	19.0 n n 19.1	1,933 ---- ---- 910	41.1 41.0 41.1 41.1	1,654 1,472 753 882	0.86 ---- ---- 0.97
GaAs + [Co(III)(NH ₃) ₆] ³⁺ 0.010 M KOH R.T.	15 35 50 65	19.0 19.0 18.6 18.5	p p p p	41.0 40.9 40.6 40.4	991 889 808 391	---- ---- ---- ----
GaAs + [Co(III)(NH ₃) ₆] ³⁺ ; pH = 12.9 (sat'd NH ₃) T \approx 180 K	30	19.4	3,164	41.4	2,937	0.93
GaAs + [Co(III)(NH ₃) ₅ (OH)] ²⁺ 0.010 M KOH, R.T.	30	19.5	3,114	41.5	2,517	0.81
GaAs + [Co(III)(NH ₃) ₅ (OH ₂)] ³⁺ 0.10 M HCl, R.T.	30	19.5	14,664	41.5	13,659	0.93
GaAs + [Co(III)(NH ₃) ₅ N ₃] ²⁺ pH = 6.2 (MES buffer) ^s T \approx 180 K	65	19.3	2,628	41.2	1,815	0.69

Table III (continued)

Sample and Reaction Conditions	GaAs Substrate					
	θ^b	Ga 3d		As 3d		As ^e Ga
		peak ^c	intensity ^d	peak	intensity	
GaAs + [Co(III)(NH ₃) ₅ Br] ²⁺ ; 0.010 M KOH, R.T.	30	19.4	p	41.4	272	----
GaAs + [Co(III)(NH ₃) ₅ Br] ²⁺ ; 0.10 M HCl, R.T.	30	19.7	11,673	41.7	10,869	0.93
GaAs + [Co(III)(bipy) ₃] ³⁺ pH = 11.3, R.T. ^s	30 50 60 65	19.1 19.0 19.1 19.0	2,361 1,905 1,491 1,148	41.2 41.2 41.3 41.3	2,980 2,495 1,810 1,654	1.26 1.31 1.21 1.44
GaAs + [Co(III)(bipy) ₃] ³⁺ ; 0.10 M HCl, R.T. ^s	30	19.5	10,108	41.5	10,649	1.05
GaAs + Co(II) _(aq) ²⁺ ; 0.010 M KOH, R.T.	30	19.2	7,684	41.2	6,790	0.88
GaAs + Co(II) _(aq) ²⁺ ; pH = 12.9 (sat'd NH ₃) T≈180 K	30	19.4	3,164	41.4	2,937	0.93
GaAs + Co(II) _(aq) ²⁺ ; 0.10 M HCl, R.T.	30	19.3	11,451	41.3	10,271	0.90
GaAs + [Co(II)(bipy) ₃] ²⁺ ; pH = 12.0, R.T. ^s	65	19.1	3,901	41.3	7,315	1.88
GaAs + [Co(II)(bipy) ₃] ²⁺ ; 0.10 M HCl, R.T. ^s	30	19.4	11,330	41.4	10,723	0.95
GaAs + [Co(III)(NH ₃) ₆] ³⁺ (0.010 M KOH) + KOH-Se ⁻²⁻ , T≈180 K	0 70	19.1 19.2	1,436 724	41.2 41.2	1,071 595	0.75 0.82

Table III (continued)

Sample and Reaction Conditions	Substrate Oxides						
	θ^b	<u>As₂O₃ (As 3d)</u>			<u>Ga₂O₃ (Ga 3d)</u>		
		peak ^c	intensity ^d	Γ (As ₂ O ₃)	peak	intensity	Γ (Ga ₂ O ₃)
4:1:1 etched GaAs + 1.0 M KOH T \approx 180 K ^l	0	m	----	----	m	----	----
	55	m	----	----	m	----	----
4:1:1 etched GaAs + KClO ₄ pH = 11.0 room temp. (R.T.)	0	m	----	----	m	----	----
	55	m	----	----	m	----	----
GaAs + [Co(III)(NH ₃) ₆] ³⁺ 0.010 M KOH T \approx 180 K	10	43.7	130	5 x 10 ⁻¹⁰	20.6	36	2 x 10 ⁻¹⁰
	30	43.6	180	7 x 10 ⁻¹⁰	n	----	----
	55	43.7	105	5 x 10 ⁻¹⁰	n	----	----
	70	43.7	124	3 x 10 ⁻¹⁰	20.8	25	1 x 10 ⁻¹⁰
GaAs + [Co(III)(NH ₃) ₆] ³⁺ 0.010 M KOH R.T.	15	43.6	282	1.6 x 10 ⁻⁹	p	----	----
	35	43.5	261	1.4 x 10 ⁻⁹	p	----	----
	50	43.5	330	1.5 x 10 ⁻⁹	p	----	----
	65	43.5	220	1.3 x 10 ⁻⁹	p	----	----
GaAs + [Co(III)(NH ₃) ₆] ³⁺ ; pH = 12.9 (sat'd NH ₃) T \approx 180 K	30	44.0	104	2 x 10 ⁻¹⁰	20.7	91	3 x 10 ⁻¹⁰
GaAs + [Co(III)(NH ₃) ₅ (OH)] ²⁺ 0.010 M KOH, R.T.	30	44.7	328	7 x 10 ⁻¹⁰	21.3	110	3 x 10 ⁻¹⁰
GaAs + [Co(III)(NH ₃) ₅ (OH ₂)] ³⁺ 0.10 M HCl, R.T.	30	43.6	188	< 2 x 10 ⁻¹⁰	21.2	226	< 2 x 10 ⁻¹⁰
GaAs + [Co(III)(NH ₃) ₅ N ₃] ²⁺ pH = 6.2 (MES buffer) ^s T \approx 180 K	65	43.5	306	5 x 10 ⁻¹⁰	21.0	98	1 x 10 ⁻¹⁰

Table III (continued)

Sample and Reaction Conditions	Substrate Oxides						
	θ^b	<u>As₂O₃ (As 3d)</u>			<u>Ga₂O₃ (Ga 3d)</u>		
		peak ^c	intensity ^d	Γ (As ₂ O ₃)	peak	intensity	Γ (Ga ₂ O ₃)
GaAs + [Co(III)(NH ₃) ₅ Br] ²⁺ ; 0.010 M KOH, R.T.	30	44.5	99	1.9×10^{-9}	p	----	----
GaAs + [Co(III)(NH ₃) ₅ Br] ²⁺ ; 0.10 M HCl, R.T.	30	43.5	150	$< 2 \times 10^{-10}$	21.3	119	$< 2 \times 10^{-10}$
GaAs + [Co(III)(bipy) ₃] ³⁺ pH = 11.3, R.T. ^s	30	43.7	315	6×10^{-10}	21.0	o	----
	50	43.7	295	5×10^{-10}	21.0	o	----
	60	43.9	300	5×10^{-10}	21.1	o	----
	65	44.0	288	5×10^{-10}	21.1	o	----
GaAs + [Co(III)(bipy) ₃] ³⁺ ; 0.10 M HCl, R.T. ^s	30	43.5	73	$< 2 \times 10^{-10}$	m	----	----
GaAs + Co(II) _(aq) ²⁺ ; 0.010 M KOH, R.T.	30	43.3	191	$< 2 \times 10^{-10}$	m	----	----
GaAs + Co(II) _(aq) ²⁺ ; pH = 12.9 (sat'd NH ₃) T \approx 180 K	30	44.0	104	$\leq 2 \times 10^{-10}$	20.7	91	2×10^{-10}
GaAs + Co(II) _(aq) ²⁺ ; 0.10 M HCl, R.T.	30	43.1	215	$< 2 \times 10^{-10}$	m	----	----
GaAs + [Co(II)(bipy) ₃] ²⁺ ; pH = 12.0, R.T. ^s	65	m	----	----	m	----	----
GaAs + [Co(II)(bipy) ₃] ²⁺ ; 0.10 M HCl, R.T. ^s	30	42.9	224	$< 2 \times 10^{-10}$	m	---	----
GaAs + [Co(III)(NH ₃) ₆] ³⁺ (0.010 M KOH) + KOH-Se ⁻²⁻ , T \approx 180 K	0	44.1	197	1.2×10^{-9}	20.3	124	1.0×10^{-9}
	70	43.7	198	7×10^{-10}	20.5	50	7×10^{-10}

Table III (continued)

Sample and Reaction		Adsorbate Layers							
Conditions	θ^b	Co(OH)_2 (Co 2p _{3/2})			Raw O 1s		O^i	C 1s	
		peak ^c	intensity ^d	$\Gamma_{\text{Co(OH)}_2}$	peak	intensity	Co	intensity	Γ_{CHO}^k
4:1:1 etched GaAs	0	m	----	----	532.3	11,660	----	o	----
+ 1.0 M KOH	55	m	----	----	532.4	11,420	----	3,561	2.2×10^{-9}
T \approx 180 K ^l									
4:1:1 etched GaAs	0	n	----	----	532.8	7,961	----	6,186	7.5×10^{-9}
+ KClO ₄	55	n	----	----	532.6	9,340	----	7,842	5.2×10^{-9}
pH = 11.0; room temp. (R.T.)									
GaAs +	10	781.3	1,387	4.4×10^{-9}	531.5	13,934	2.00	5,444	5.1×10^{-9}
[Co(III)(NH ₃) ₆] ³⁺	30	781.1	1,715	4.4×10^{-9}	n	----	----	n	----
0.010 M KOH	55	781.3	1,557	4.3×10^{-9}	n	----	----	n	----
T \approx 180 K	70	781.3	1,696	2.4×10^{-9}	531.6	13,326	2.44	n	----
GaAs +	15	780.5	12,481	1.7×10^{-8}	530.8	47,682	1.87	o	----
[Co(III)(NH ₃) ₆] ³⁺	35	780.5	12,098	1.4×10^{-8}	530.8	47,354	1.92	o	----
0.010 M KOH	50	780.8	14,404	1.2×10^{-8}	530.9	56,474	1.92	o	----
R.T.	65	781.9	12,295	9.3×10^{-9}	532.0	58,688	2.34	o	----
GaAs +	30	(781) ^q	< 100 ^r	$< 2 \times 10^{-10}$	533.3	9,939	m	2,000	2.3×10^{-9}
[Co(III)(NH ₃) ₆] ³⁺ ; pH = 12.9 (sat'd NH ₃)									
T \approx 180 K									
GaAs +	30	780.8	8,114	8.2×10^{-9}	532.4	50,950	2.16	4,452	2.6×10^{-9}
[Co(III)(NH ₃) ₅ (OH)] ²⁺									
0.010 M KOH, R.T.									
GaAs +	30	m	----	----	532.0	12,070	----	1,748	6×10^{-10}
[Co(III)(NH ₃) ₅ (OH ₂)] ³⁺									
0.10 M HCl, R.T.									
GaAs +	65	m	----	----	531.9	13,790	----	8,137	3.5×10^{-9}
[Co(III)(NH ₃) ₅ N ₃] ²⁺									
pH = 6.2 (MES buffer) ^s									
T \approx 180 K									

Table III (continued)

Sample and Reaction		Adsorbate Layers							
		<u>Co(OH)₂ (Co 2p_{3/2})</u>		<u>Raw O 1s</u>		<u>Oⁱ</u>		<u>C 1s</u>	
Conditions	θ ^b	peak ^c	intensity ^d	Γ _{Co(OH)₂}	peak	intensity	Co	intensity	Γ _{CHO^k}
GaAs + [Co(III)(NH ₃) ₅ Br] ²⁺ ; 0.010 M KOH, R.T.	30	782.1	18,218	2.4 x 10 ⁻⁸	532.1	18,247	2.04	887	2 x 10 ⁻¹⁰
GaAs + [Co(III)(NH ₃) ₅ Br] ²⁺ ; 0.10 M HCl, R.T.	30	m	----	----	532.5	13,060	m	7,574	2.4 x 10 ⁻⁹
GaAs + [Co(III)(bipy) ₃] ³⁺	30	m	----	----	531.8	19,817	----	12,389	7.4 x 10 ⁻⁹
pH = 11.3, R.T. ^s	50	m	----	----	531.8	20,060	----	12,500	6.0 x 10 ⁻⁹
	60	m	----	----	531.8	19,858	----	11,440	5.1 x 10 ⁻⁹
	65	m	----	----	531.8	21,416	----	o	----
GaAs + [Co(III)(bipy) ₃] ³⁺ ; 0.10 M HCl, R.T. ^s	30	m	----	----	532.4	13,670	----	8,009	2.7 x 10 ⁻⁹
GaAs + Co(II) _(aq) ²⁺ ; 0.010 M KOH, R.T.	30	781.3	6,383	3.9 x 10 ⁻⁹	531.5	34,565	2.02	2,591	1.2 x 10 ⁻⁹
GaAs + Co(II) _(aq) ²⁺ ; pH = 12.9 (sat'd NH ₃) T≈180 K	30	(782) ^q	< 300 ^r	< 6 x 10 ⁻¹⁰	533.3	9,939	----	2,000	2.3 x 10 ⁻⁹
GaAs + Co(II) _(aq) ²⁺ ; 0.10 M HCl, R.T.	30	m	----	----	532.2	14,050	----	8,556	2.8 x 10 ⁻⁹
GaAs + [Co(II)(bipy) ₃] ²⁺ ; pH = 12.0, R.T. ^s	65	(781) ^q	< 200 ^r	< 2 x 10 ⁻¹⁰	531.8	16,377	----	9,438	1.9 x 10 ⁻⁹
GaAs + [Co(II)(bipy) ₃] ²⁺ ; 0.10 M HCl, R.T. ^s	30	m	----	----	532.3	9,119	----	7,748	2.5 x 10 ⁻⁹
GaAs + [Co(III)(NH ₃) ₆] ³⁺ (0.010 M KOH) + KOH-Se ⁻²⁻ , T≈180 K	0	59.0 ^t	376 ^u	1.6 x 10 ⁻⁹	1.79	531.2	7,427	54.4	675
	70	59.0 ^t	381 ^u	1.5 x 10 ⁻⁹	1.80	531.1	o	54.0	687

Table III (continued)

Notes to Table III

- a. Coverage is presented as the total moles per cm squared (Γ) projected area GaAs.
- b. Angle between surface normal and photoelectron detector axis.
- c. All peak positions are reported in binding electron volts (BeV) and are referenced against adventitious carbon defined to be at C 1s = 284.6 BeV.
- d. Intensities (counts per second per eV) normalized with respect to the relevant photoelectron cross-section, escape depth, and atomic number density, except for O 1s, which is given as the raw intensity (counts per eV) normalized by the scan duration.
- e. Ratio of normalized peak intensities.
- f. Coverage calculated assuming the density of vitreous As₂O₃.
- g. Coverage calculated based on the average of the densities for α and β Ga₂O₃.
- h. Coverage calculated based on the density of *roseo*-Co(OH)₂.
- i. Corrected O 1s intensity derived from total O 1s signal by subtraction of counts due to substrate oxides and H₂O, and then normalized as in note d.
- j. Coverage assuming the density of trogtalyte, CoSe₂; Cobalt intensity based on Co 3p lines.
- k. Coverage calculated assuming an average hydrocarbon density. See experimental for details.
- l. Approximate (± 10 K) temperature of sample during analysis.
- m. No peak observed above background.
- n. Region not analyzed.
- o. Peak position determined, area not deconvoluted.
- p. Peak position obscured by O 2s line.
- q. Edge of poorly defined peak barely discernible above background.
- r. Estimate of upper limit of intensity. No N 1s signal above background; no signal above background due to counter ions.
- s. No N 1s signal above background; no signal above background due to counterions.
- t. Co 3p peak position.
- u. Normalized Co 3p peak intensity.

substrate GaAs was observed in 0.10 M HCl in the presence of $[\text{Co(III)(NH}_3)_5\text{X}]^{n+}$ ($\text{X} = \text{OH}_2, \text{Br}^-$) or at $\text{pH} = 2.0$ in the presence of $[\text{Co(III)(NH}_3)_6]^{3+}$. It is therefore concluded that no reaction between GaAs and $[\text{Co(III)(NH}_3)_5\text{X}]^{n+}$ ($\text{X} = \text{NH}_3, \text{OH}_2, \text{Br}^-$) occurred at $\text{pH} = 1 - 2$.

The proposed redox mechanism places no limit on the number of equivalent monolayers of Co(III) that may be reduced. Quantitative coverage information obtained from an analysis of the XPS peak intensities is summarized in Table III. Four separate experiments using single crystal (100) n-GaAs surfaces with Co(III) ammine complexes ($11.3 < \text{pH} < 12$) yielded Co coverages between $(2.4 \pm 1.0) \times 10^{-9}$ and $(24.0 \pm 3.2) \times 10^{-9}$ mol (Co) cm^2 (GaAs). This corresponds to approximately 2 - 18 monolayers of Co(OH)_2 . After corrections for O 1s intensity due to water, substrate oxides, and adventitious oxides of carbon, the expected $\text{O}_{\text{corr}}/\text{Co}$ ratio for Co(OH)_2 should be 2.0. This is in excellent agreement with the average experimental value of $\text{O}_{\text{corr}}/\text{Co} = 2.1 \pm 0.2$ (Table III). Arsenic oxide coverages ranged between $(5 \pm 2) \times 10^{-10}$ and $(1.9 \pm 0.1) \times 10^{-9}$ mol cm^2 (GaAs), with $\text{As}_2\text{O}_3/\text{Co}$ mole ratios of 0.12 ± 0.04 . For a 6-electron oxidation of GaAs (*vide infra*),³⁷ the expected $\text{As}_2\text{O}_3/\text{Co}$ mole ratio is 0.083; this however assumes that no As_2O_3 or Co(II) dissolves into the electrolyte during exposure of GaAs surface to the electrolyte. Wet chemical studies of Co loaded GaAs powder (*vide infra*) have demonstrated that, if the pH of the rinse water is sufficiently low ($1.0 < \text{pH} < 7.0$), surface bound Co(OH)_2 will dissolve, thus implying that the surface composition will not accurately reflect the reaction stoichiometry at this pH. On substrates that contained substantial amounts of oxide, it was difficult to monitor the Ga 3d line due to interference from the O 2s line. On those samples where it was possible to monitor gallium oxide peaks, $\text{Ga}_2\text{O}_3/\text{As}_2\text{O}_3$ mole ratios of 0.37 ± 0.05 were observed.

Further information on the stoichiometry and morphology of the surface phase was obtained from angle-resolved XPS experiments on single crystal n-GaAs surfaces

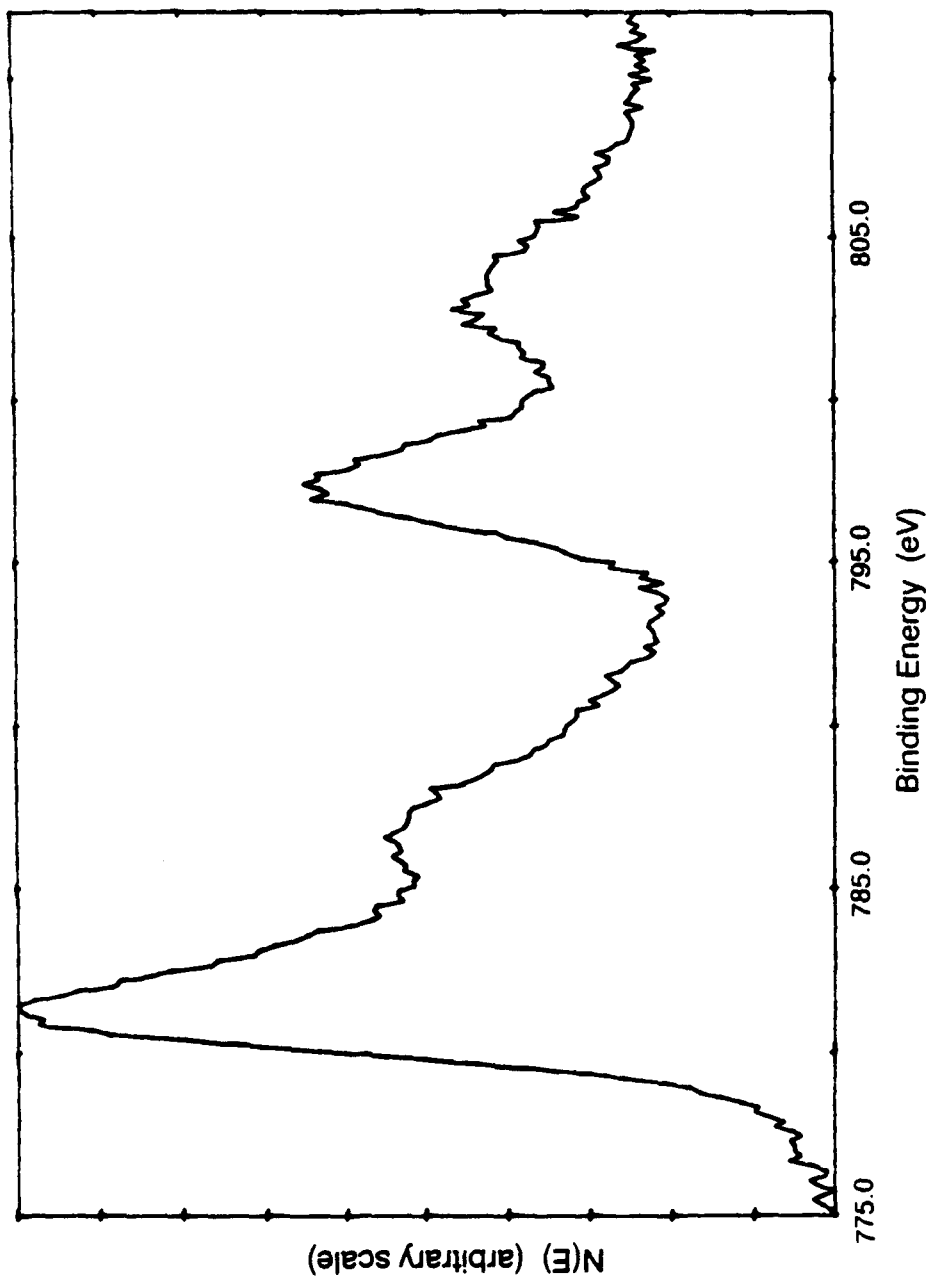
(Table III). For a given GaAs sample treated with a basic Co(III) ammine complex, the angular dependence of the XP peak intensity deviated from that expected for a homogeneous, fixed thickness, overlayer. The systematic variations in the overlayer/substrate intensity ratios of thin adlayers were consistent with that of a rough, coarse interface. The ratio variations of thicker oxo-layers were similar, and could be viewed as due to a porous oxide layer. Additionally, at increasingly surface sensitive take-off angles, the O/Co ratio also increased. This trend in the O/Co ratio indicated a surface phase that was more oxygen rich at the overlayer/vacuum interface than at the substrate/overlayer interface. The presence of hydrated outermost layers of the cobalt-oxo phase would be consistent with the observed angular dependence of the O/Co ratio. Support for this assignment was obtained from an observed increase in the intensity of the high binding energy side (BeV \approx 534) of the O 1s XP peak at increasingly surface sensitive take-off angles. This binding energy is typical of surface-bound H₂O.³⁸

B. Co(II) Complexes: XPS Studies of Co Chemisorption on GaAs.

Cobalt was also observed to adsorb on GaAs that had been exposed to basic aqueous solutions of [Co(II)(OH₂)₆]²⁺. XP spectra of single crystal and powdered GaAs samples yielded Co 2p lines at 780.8 and 796.9 BeV and satellite structure at 786.0 and 802.5 BeV, shown in Figure 4. To within 0.2 eV, the primary Co 2p XPS peak positions and splittings observed for GaAs surfaces exposed to [Co(II)(OH₂)₆]²⁺ (0.010 M KOH) or [Co(III)(NH₃)₆]³⁺ were identical. Additionally, the parent Co 2p peak positions and splitting for Co(II) treated GaAs were within 0.2 eV of signals obtained from pure *roseo*-Co(OH)₂.

Solutions of Co(II) ions made basic by the addition of hydroxide ion quickly formed precipitates of Co(OH)₂, and in the presence of GaAs, apparently some of this precipitate nucleated on the GaAs surface. In 0.010 M KOH solutions, weaker (relative to

Figure 4: Co 2p region XPS of an etched (100)-oriented n-GaAs substrate exposed to a basic (pH = 12) 0.010 M $[\text{Co}(\text{II})(\text{OH}_2)_6](\text{Cl})_2$ solution. The raw data are displayed after being corrected for binding energy relative to C 1s.



substrate GaAs signals) Co 2p and O 1s signal intensities were observed from [Co(II)(H₂O)₆]²⁺ treated GaAs samples than from Co(III) ammine treated GaAs (Tables II, III). XPS performed on (100) n-GaAs substrates exposed to 0.010 M KOH solutions of [Co(II)(OH)₂]²⁺ showed no evidence of substrate oxidation above background levels ($\leq 2 \times 10^{-10}$ mol cm⁻²). Consistently, total coverages of cobalt were in the low end of the range obtained from exposure of GaAs to Co(III) ammine complexes.

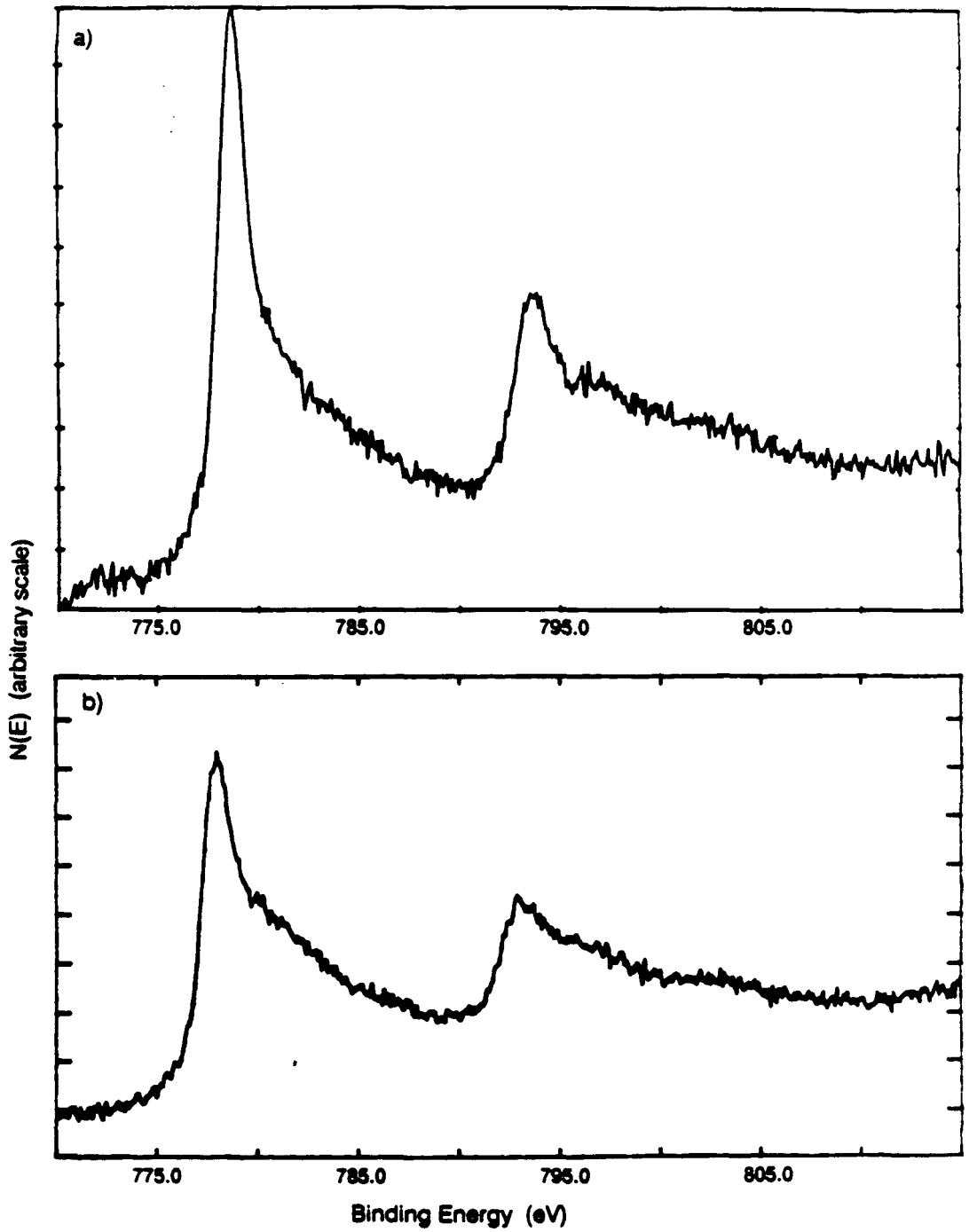
As was found for the Co(III) ammine complexes, GaAs surfaces exposed to [Co(II)(H₂O)₆]²⁺ solutions of 0.10 M HCl displayed no detectable Co XPS signals. Furthermore, GaAs surfaces laden with a Co(OH)₂ precipitate and then exposed to ammonia solutions (14.8 M NH₃, pH = 12.9) showed no signals due to Co(II) remaining in the XP spectra. Consistently, GaAs samples that had been exposed to Co(II) solutions in concentrated aqueous ammonia also yielded no resolvable Co 2p XPS signals above background. NH₃ stabilizes Co(II) as [Co(II)(NH₃)₆]²⁺ relative to Co(OH)₂;³⁶ thus, this complexation reaction effectively competes with the deposition of Co(OH)₂ onto GaAs surfaces.

2. XPS Studies of Co Chemisorption on GaAs:

Properties After Exposure to Aqueous KOH-K₂Se-K₂Se₂ Solutions.

XPS data were also obtained for GaAs samples that had been exposed to aqueous solutions of 1.0 M KOH-0.8 M K₂Se-0.1 M K₂Se₂ after chemisorption of Co.⁸ Both (100)-oriented n-type single crystals and powdered GaAs samples displayed Co 2p XPS peaks at 778.4 and 793.3 BeV (Figure 5a). In contrast to Figure 1, these spectra showed no satellite structure. A wide (0-1100 BeV) XP scan showed only the presence of signals from As, Ga, C, Se, O, and Co (Table II). Identical Co 2p spectra were obtained from GaAs that had been exposed to [Co(III)(NH₃)₅X]ⁿ⁺ (X = NH₃, OH⁻, Br⁻)

Figure 5: Co 2p region XPS; the raw data are displayed after being corrected for binding energy relative to C 1s. (a) Etched (100)-oriented n-GaAs substrate exposed to basic (pH = 12) 0.010 M $[\text{Co(III)(NH}_3)_6]^{3+}$ complex and subsequently immersed in 1.0 M KOH-0.8 M K_2Se -0.2 M K_2Se_2 electrolyte. (b) Ar^+ ion sputtered sample of CoSe set in In foil.



(0.010 M KOH) or to $[\text{Co(II)(OH}_2)_6]^{2+}$ complexes (0.010 M KOH), and then immersed in the KOH- Se^{-2-} solution. Low (*ca.* 1/2 monolayer) to no detectable ($< 1/4$ monolayer by XPS) Se 3d peak intensity has been observed on etched GaAs samples exposed only to Se^{-2-} electrolyte. Large intensity (> 2 monolayer) persistent Se 3d signals were observed only on GaAs substrates that also possessed surface bound Co(II).

A comparison of Figures 1 and 5a clearly shows that the adsorbed Co has undergone a chemical reaction with the KOH- Se^{-2-} electrolyte. In contrast to the $[\text{Co(III)(NH}_3)_6]^{3+}$ or Co(OH)_2 spectra of Figure 2, the Co 2p features in Figure 5a are comparable to those reported previously for the low spin ($S = 1/2$) cobalt chalcogenides³⁹ and to spectra obtained in this work from an argon ion sputtered sample of authentic CoSe (Figure 5b). The presence of Se in the overlayer, the lack of any observable Co 2p satellite structure, and the absence of counter ions such as K^+ , strongly suggest that Se^{2-} has reacted with the Co(II) sites and has been introduced into the inner sphere of surface-bound Co.

The stoichiometry of the resulting surface phase was estimated to be $\text{Co}_{1.0}\text{Se}_{1.8}$. A raw intensity ratio $\text{Co}(2p)/\text{O}(1s) \approx 3$ is, however, observed in the surface bound film, and therefore implies the possibility of a mixed seleno-oxo inner sphere for cobalt. An argument against this scenario comes from the fact that oxo and hydroxo ions are relatively weak field ligands, and would be expected to lead to high spin ($S = 3/2$) Co(II), and hence satellite lines in the Co 2p XPS, which is not observed. Nonetheless, an estimate of the Co:O:Se stoichiometry based on the detected Co 2p, O 1s, and Se 3d peak intensities will prove useful in comparison to the identity of the Co inner-shell scatterers found from EXAFS data summarized in section 3.B. Assuming an atomic density of $4.7 \times 10^{-2} \text{ mol cm}^{-3}$ (which is the average of the atomic densities for Co(OH)_2 and CoSe_2), the Co/O/Se intensity ratios (normalized to Co) would, at the upper limit of

complete oxygen incorporation into the inner sphere of Co(II), be represented by the composition $\text{Co}_{1.0}\text{Se}_{0.7}\text{O}_{1.3}$.

Analysis of the angle-resolved XPS data showed that after exposure to the KOH- Se^{-2} electrolyte, the Co(II)-containing surface layer was inhomogeneous. Additionally, the Co-Se coverages were not substantially reduced compared to the amount of Co adsorbed from the aqueous Co(III) or Co(II) solutions. Table III summarizes the Co and Se coverage data. In general, Se^{-2} exposure of surface bound Co-ion always resulted in the transformation of the Co 2p peaks from a high spin Co(II) state to a low spin Co(II) state, as well as the appearance of Se signals in the XPS.

3. X-Ray Absorption and Fluorescence Spectra: Properties in Vacuo and in Aqueous Solution.

The work represented in this section, the extended x-ray absorption fine structure (EXAFS) experiments and analyses performed on GaAs powders exposed to Co(III) and Co(II) complexes, represents the pooled efforts of over ten researchers. Even though the focus of the EXAFS experiments was directed at key problems pertaining to this thesis work and the author was heavily involved in this endeavor, EXAFS research is, by nature, a group effort. The results of the EXAFS work are, therefore, group intellectual property; in keeping with this spirit, special mention and credit are due to Sharon R. Lunt, Dr. Ian L. Abrahams, and Patrick G. Santangelo for their outstanding contribution to this activity. A full accounting of this work, with proper acknowledgement of all personnel, is available from a published paper.^{8c}

A. GaAs Exposed to Aqueous Co(III) Complexes.

In order to obtain further information on the coordination environment of the GaAs-bound Co, x-ray absorption and fluorescence studies were performed. Amplitude

and phase parameters for specific absorber-scatterer pairs were obtained from EXAFS data for the model compounds Co(OH)_2 , CoSe_2 , $[\text{Co(II)(OH)}_2]_6(\text{ClO}_4)_2$, CoO(OH) , and CoAs_3 . Potential first shell (O, Se, N) and second shell (Co, As, Ga) absorber-scatterer interactions were isolated by application of Fourier filtering techniques on κ^3 weighted data.^{30c-f}

Figure 6 displays the Co K edge spectra, Co-based EXAFS (taken in fluorescence mode), and Fourier transform of the EXAFS for GaAs powder treated with $[\text{Co(III)(NH}_3)_5(\text{OH})]^{2+}$. For comparison, Figure 7 displays the x-ray absorption spectra and Fourier transformed EXAFS for two model compounds, Co(II)(OH)_2 and Co(III)O(OH) .

The position of the Co K edge in Figure 6a verifies that the GaAs-bound Co is in the Co(II) oxidation state. Edge position data taken at 77 K for $[\text{Co(II)(OH)}_2]_6(\text{ClO}_4)_2$, and CoO(OH) (Table IV), and for other Co(II) and Co(III) model complexes, are consistent with this assignment. This assignment is also consistent with the oxidation state deduced from the Co 2p binding energy, peak splittings, and satellite structure observed in the XPS spectra (*vide supra*).

A summary of the EXAFS data analysis is presented in Table IV. For the Co/GaAs sample, the first shell around Co was found to consist of (6 ± 1) second row atoms (most likely N or O) at $(2.08 \pm 0.05) \text{ \AA}$, and the second shell consisted of (6 ± 1) third row scatterers at $(3.13 \pm 0.05) \text{ \AA}$. The XPS analysis of these samples strongly indicated that the light element was O, because no N (above background) was found to support the required Co:N mass balance (Table II). The 2.08 \AA first shell bond distance is in excellent accord with that found by EXAFS and x-ray diffraction for the first shell Co-O distance in *roseo*- Co(OH)_2 ($d_{\text{Co-O}} = 2.097 \text{ \AA}$).⁴⁰ It also is longer than typically observed for Co(III)-O distances in compounds with all octahedral sites occupied by oxygen, such as

Figure 6: Co k-edge x-ray fluorescence spectrum. Data for GaAs powder treated with pH = 12 (KOH) solution of 0.010 M $[\text{Co(III)(NH}_3)_5(\text{OH})]^{2+}$, collected at room temperature on an unfocussed beam line at 10^{-6} torr. (a) Raw x-ray fluorescence data. (b) κ^3 weighted EXAFS extracted from spectrum a. Superimposed on the raw data is the fit (dashed curve) obtained from the summation of individual fits to the first shell (Co-O) and second shell (Co-Co) scattering contributions. (c) Fourier transform of the EXAFS in b.

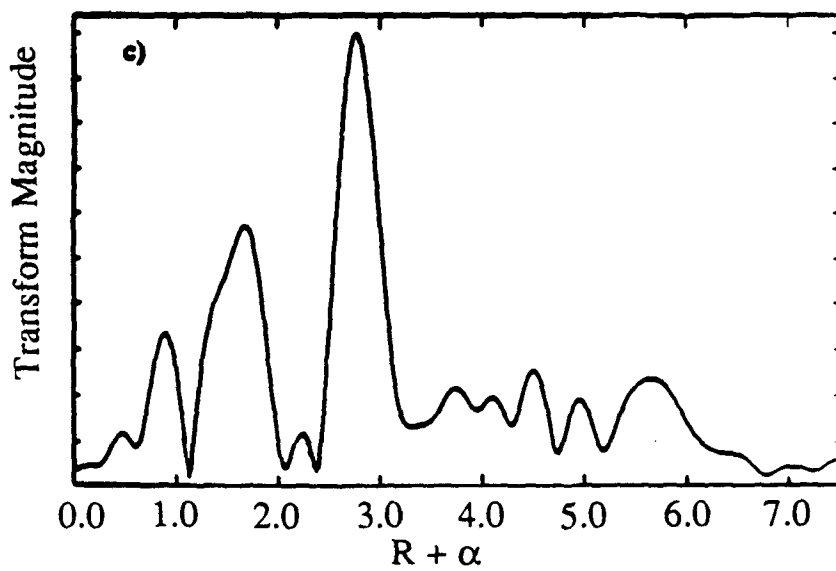
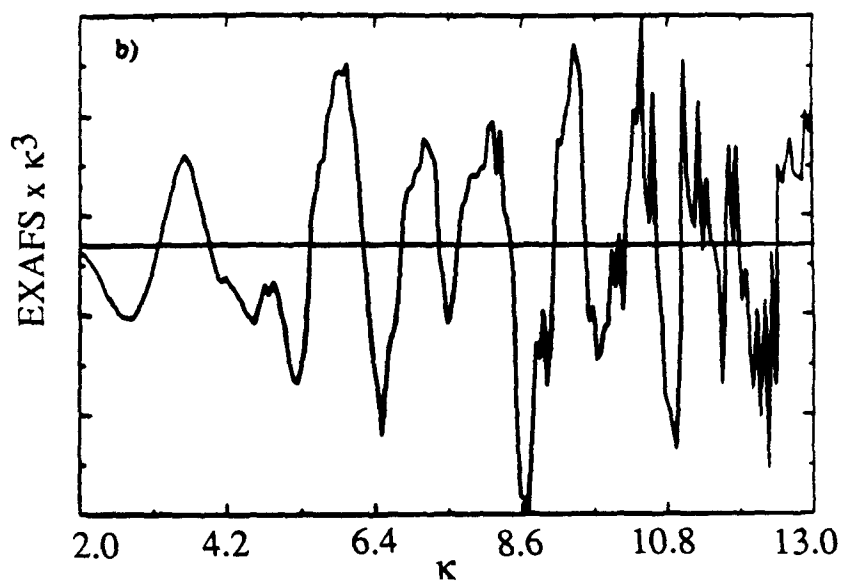
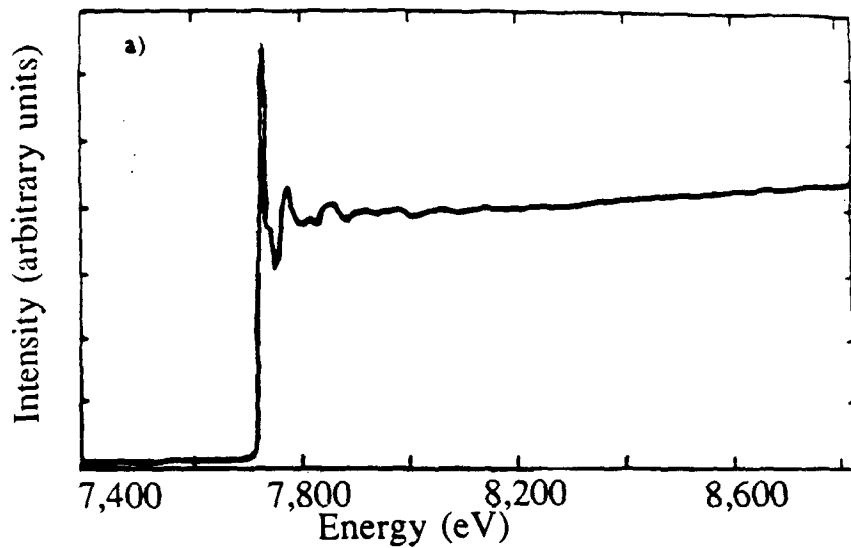


Figure 7: κ^3 weighted EXAFS and Fourier transform data for model compounds *roseo*-Co(II)(OH)₂ and Co(III)O(OH). Spectra were collected in transmission mode at 77 K on a focussed beam line at 10⁻⁶ torr. (a) Co k-edge EXAFS of *roseo*-Co(OH)₂. (b) Co k-edge EXAFS of CoO(OH). (c) Fourier transform of the EXAFS in a. (d) Fourier transform of the EXAFS in b.

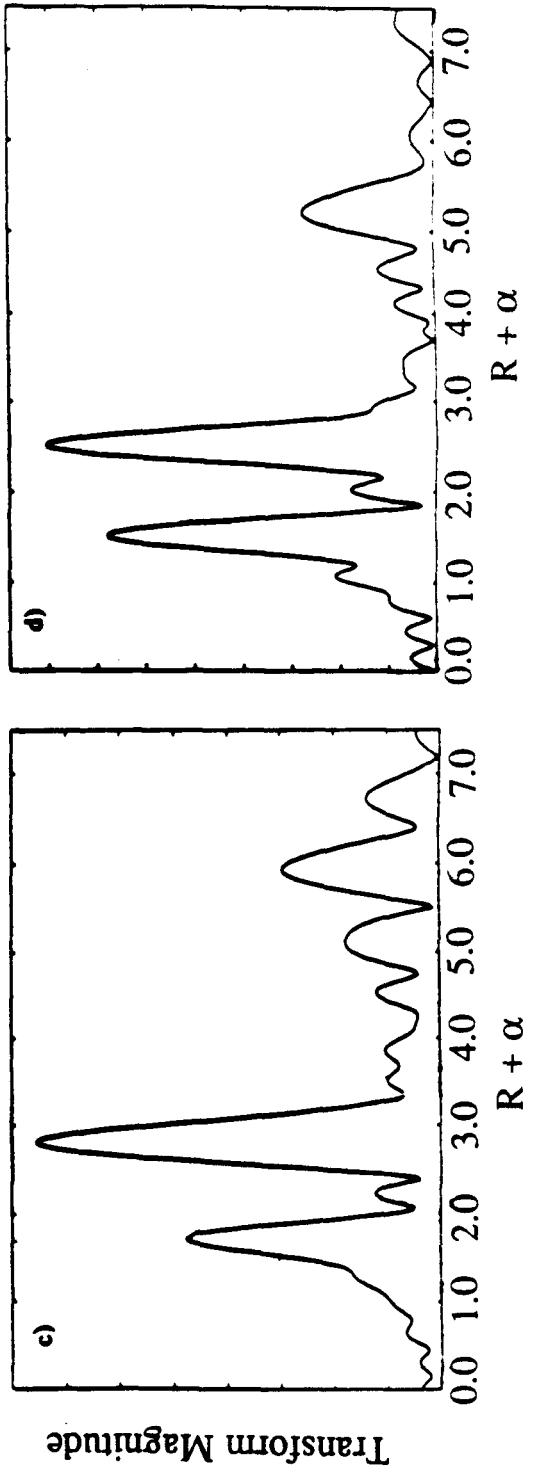
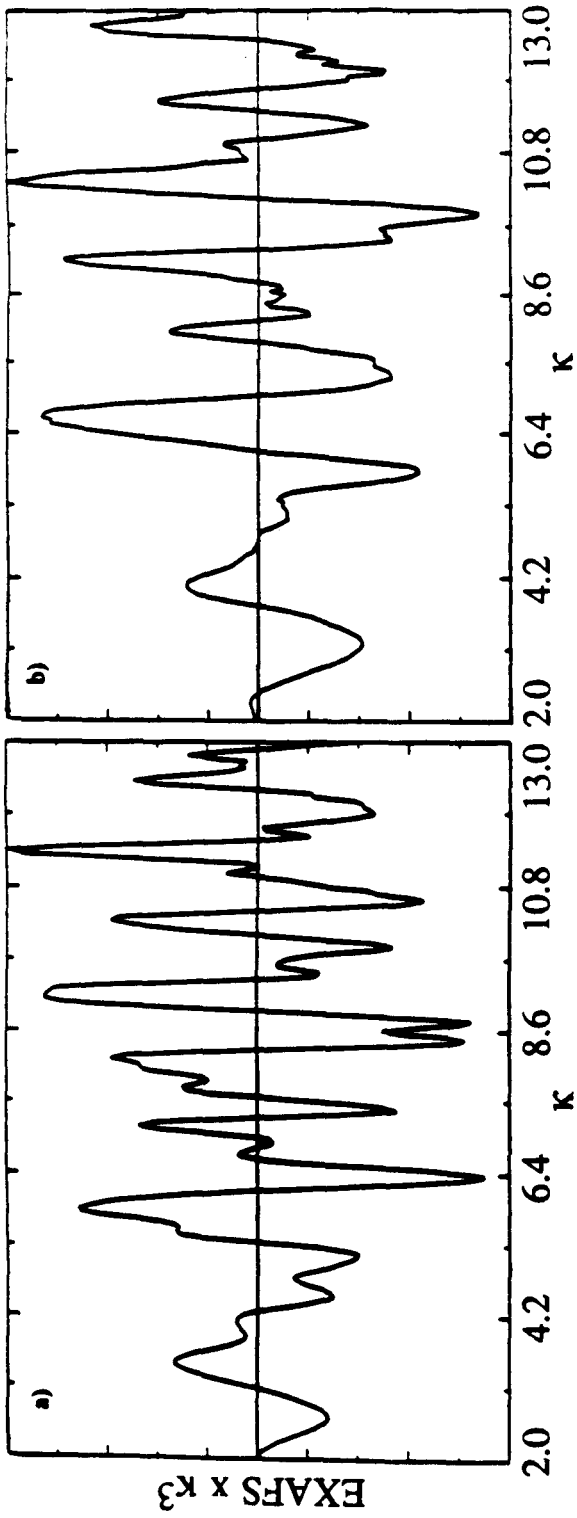


Table IV:**EXAFS Derived Nearest Neighbor Distances and Coordination Numbers**

Experiment ^a	1st Shell		2nd Shell		Absorption Edge (eV) ^b
	d _{Co-O} (Å)	N _O	d _{Co-Co} (Å)	N _{Co}	
<i>roseo</i> -Co(OH) ₂ ^c					
T=77 K ^d	2.097	6.0	3.17	6.0	7,719.7
[Co(II)(OH ₂) ₆](ClO ₄) ₂ ^e					
T=77 K	2.085	6.0	---	---	7,720.1
CoO(OH) ^f					
T=77 K	1.90g	6.0	---	---	7,721.3
	2.69h	4.0	---	---	
GaAs + [Co(III)(NH ₃) ₅ (OH)] ²⁺ ; 0.010 M KOH					
T=10 K	2.08 ± 0.05	7 ± 1 ⁱ	3.13 ± 0.05	7 ± 1 ⁱ	7,720.7
T=77K	2.08 ± 0.05	8 ± 1 ⁱ	3.13 ± 0.05	8 ± 1 ⁱ	7,720.3
T=298K	2.08 ± 0.05	7 ± 1 ⁱ	3.14 ± 0.05	7 ± 1 ⁱ	7,720.8
GaAs + [Co(III)(NH ₃) ₅ (OH)] ²⁺ ; 0.010 M KOH slurry					
T=298 K	2.09 ± 0.05	6 ± 1	3.13 ± 0.05	7 ± 1 ⁱ	7,720.7
GaAs + Co(II) _(aq) ²⁺ ; 0.010 M KOH					
T=10 K	2.08 ± 0.05	6 ± 1	3.13 ± 0.05	8 ± 1	7,720.3
CoSe ₂ ^j	d _{Co-Se} (Å)	N _{Se}			
	2.42	6.0	---	---	7,716.2
GaAs + [Co(III)(NH ₃) ₆] ³⁺ ; (0.010 M KOH) + KOH-Se ⁻²⁻					
T=77 K	2.36 ± 0.05	5.3 ± 1.0	---	---	7,717.1
GaAs + [Co(III)(NH ₃) ₅ (OH)] ²⁺ ; (0.010 M KOH) + KOH-Se ⁻²⁻					
T=10 K	2.34 ± 0.05	4.6 ± 1.0	---	---	7,719.0

Table IV (continued)

Notes to Table IV

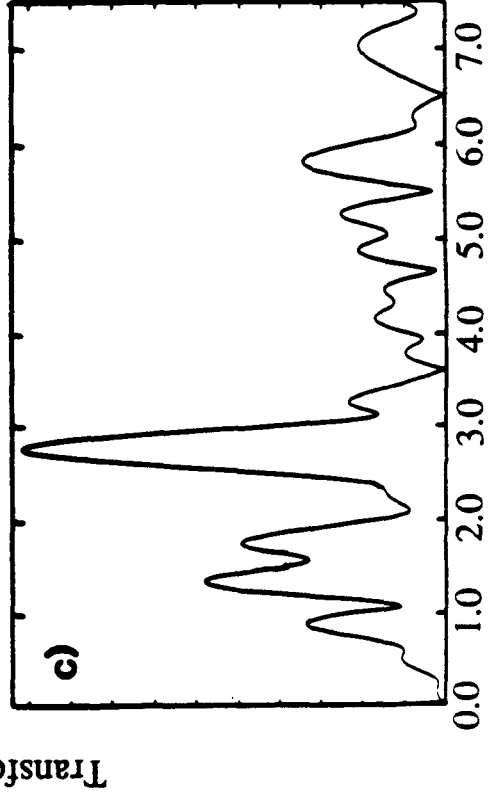
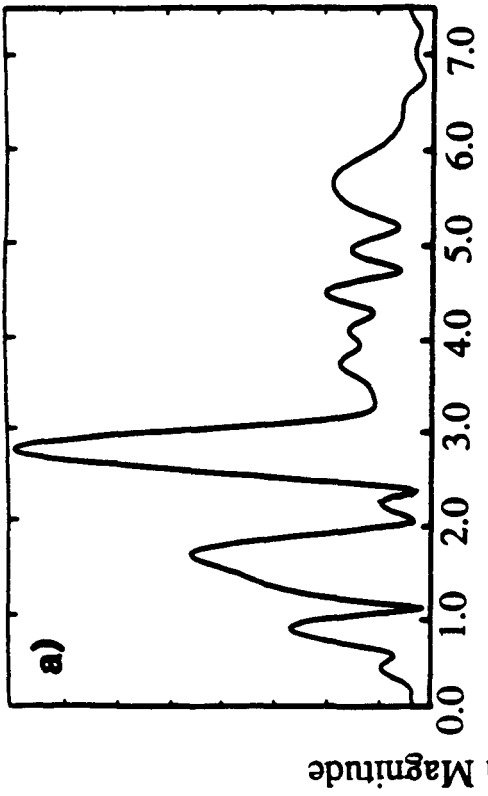
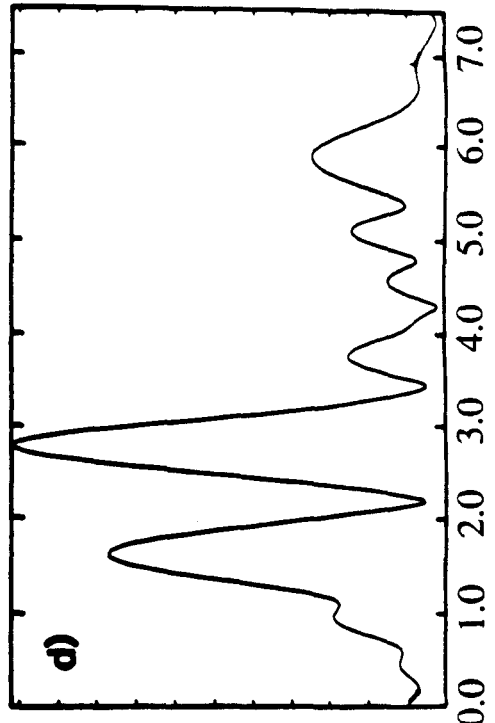
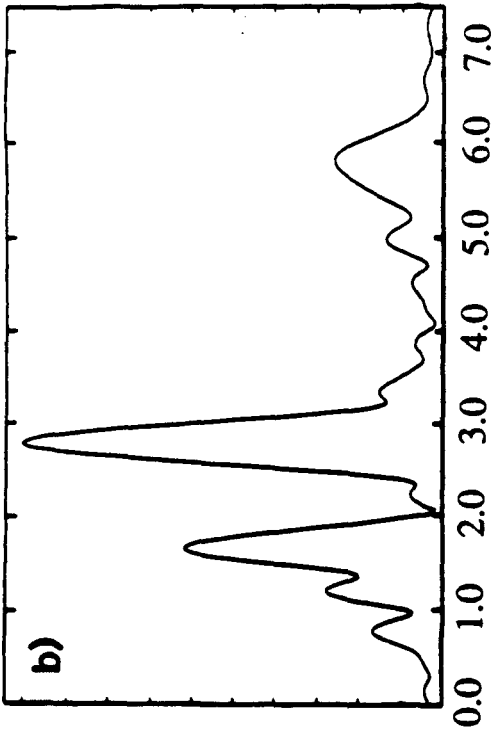
- a. Range of κ and R-space values used in all fits: κ (\AA^{-1})={3.2-12.75},
R(\AA)={0.00-7.50}; R interval=0.025.
- b. Taken as the energy of the half-height of the absorption edge.
- c. From reference 40.
- d. T at which EXAFS data collected.
- e. From reference 31.
- f. From reference 15b.
- g. $d_{\text{Co-O}}$ distance.
- h. $d_{\text{Co-OH}}$ distance.
- i. Coordination numbers higher than expected due to Cu fluorescence interference from the sample mount.
- j. From reference 16b, c.

trisacetylacetonatocobalt(III) (average $d_{\text{Co-O}} = 1.888 \text{ \AA}$),⁴¹ which further confirms the oxidation state assignment as Co(II).

The relatively high coverage (up to $2.4 \times 10^{-8} \text{ mol cm}^{-2}$) of Co from the XPS and radioisotope data (*vide infra*) supports the assignment of the predominant second shell scatterer to Co. The second shell distance for the GaAs-bound Co is within 0.017 \AA of the Co-Co distance in Co(OH)_2 ,⁴⁰ and this is consistent with the existence of a disordered network solid that would be expected from the redox deposition mechanism of Co onto GaAs.⁴² Angle resolved XPS analysis (*vide supra*) of these samples yielded an upper limit on the $\text{As}_2\text{O}_3/\text{Co}$ mole ratio of 0.16 and an upper limit on the $\text{Ga}_2\text{O}_3/\text{Co}$ mole ratio of 0.05. These observations strongly suggest that most of the second shell EXAFS scattering is due to Co-Co backscattering. Thus, the combined EXAFS and XPS data yield a structure for the adsorbed Co which is closely analogous to that of bulk Co(OH)_2 . At present, the relatively high Co coverages, combined with the similar scattering properties of the third row elements Co, Ga, and As, have precluded direct observation of the Co-Ga or Co-As surface bonding in this system. However, by comparison of fits to the data displayed in Figure 6 with model EXAFS data obtained from CoAs_3 , direct Co-As first shell coordination can be confidently ruled out as the predominant mode of Co chemisorption onto GaAs powders.

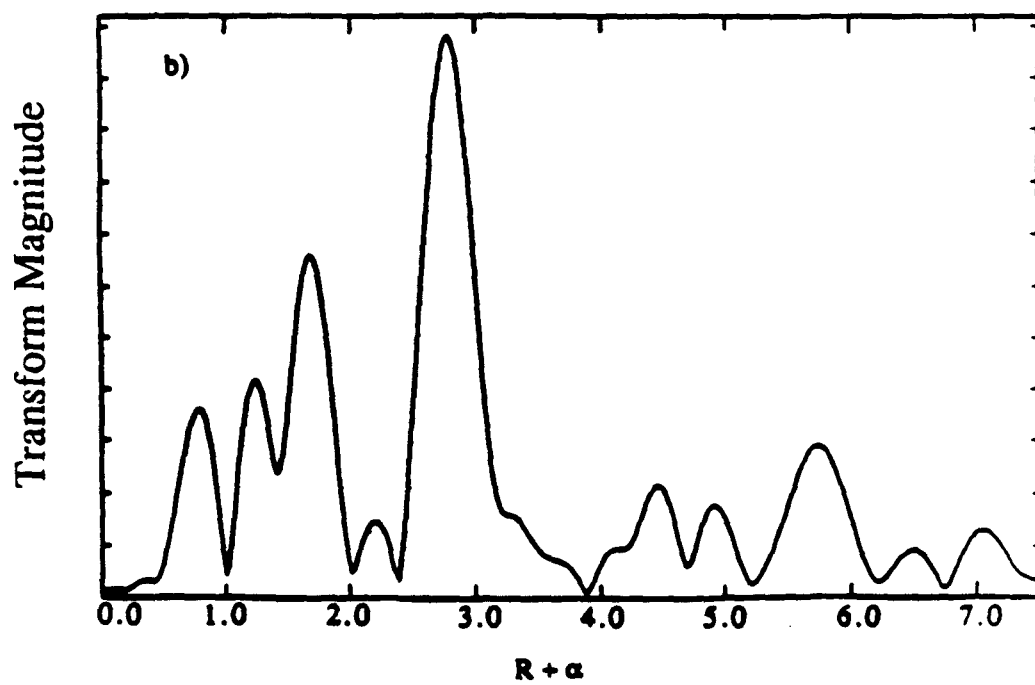
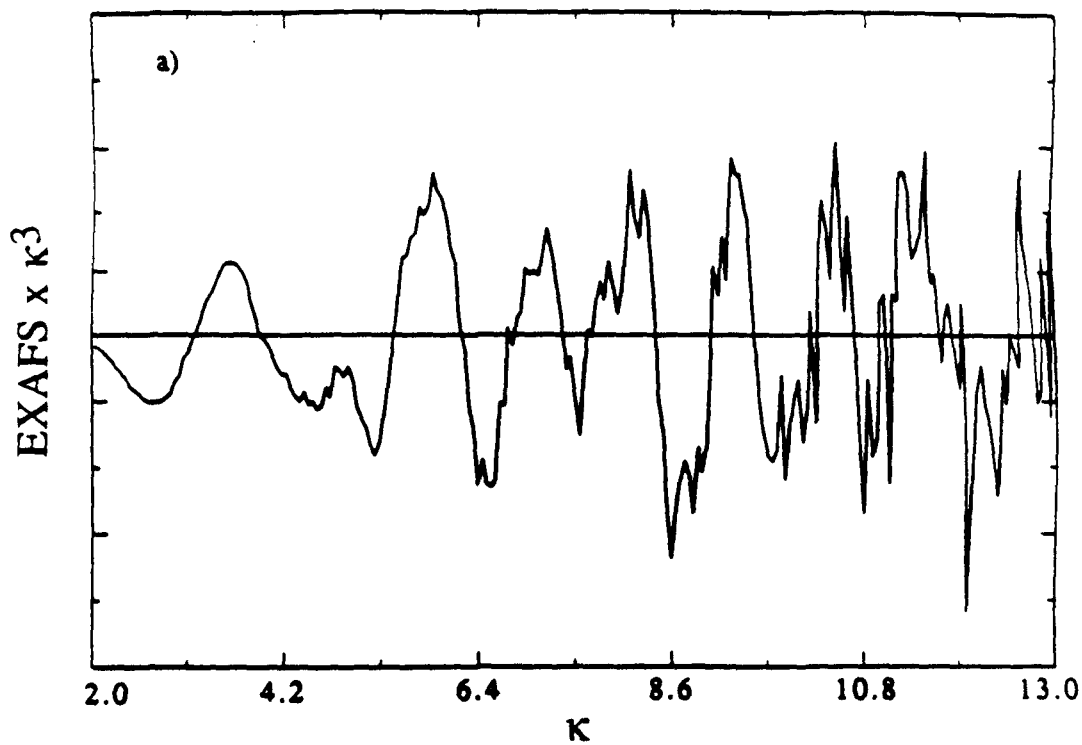
Figure 8 displays the Fourier transformed EXAFS data for a $[\text{Co(III)(NH}_3)_5(\text{OH})]^{2+}$ treated GaAs sample that had been evacuated and held sequentially at 10 K, 77 K and 298 K. The data from the aqueous slurry of GaAs powder at 298 K, also depicted in Figure 8, were very similar to that for the cooled and evacuated samples, except for the minor differences expected from a reduction in Debye-Waller factors at the lower temperatures. Hence, the analysis of the low temperature data sets, summarized in Table IV, may be taken to be good representations of the coordination structure for the

Figure 8: *In vacuo* and *in situ* comparison of Fourier transformed Co k-edge EXAFS of GaAs powder treated with a pH = 12 (KOH) solution of 0.010 M $[\text{Co(III)(NH}_3)_5(\text{OH})]^{2+}$. Data collected in fluorescence mode. Each panel displays a different temperature and contacting environment for the Co-complex treated powder. (a) T = ambient, p = 10^{-6} torr. (b) T = 77 K, p = 10^{-6} torr. (c) T = 10 K, p = 10^{-6} torr. (d) Powder in contact with pH = 12 (KOH) aqueous solution at ambient temperature and pressure (N_2).



$R + \alpha$

Figure 9: κ^3 weighted EXAFS and Fourier transform of GaAs powder treated with pH = 12 (KOH) solution of 0.010 M $[\text{Co(II)(H}_2\text{O)}_6](\text{SO}_4)$. X-ray fluorescence data collected on a focussed beam line at 77 K and 10^{-6} torr. (a) Fluorescence EXAFS. Superimposed on the raw data is the fit (dashed curve) obtained from the summation of individual fits to the first shell (Co-O) and second shell (Co-Co) scattering contributions. (b) Fourier transform of a.



adsorbed Co while in contact with the aqueous electrolyte.

Exposure of GaAs powder to a basic solution of $[\text{Co(II)(OH}_2)_6]^{2+}$ ions gave Co K edge and EXAFS data (Figure 9) that were extremely similar to that obtained from Co(OH)_2 (Figure 7). The results of the EXAFS fits to this data are also summarized in Table IV.

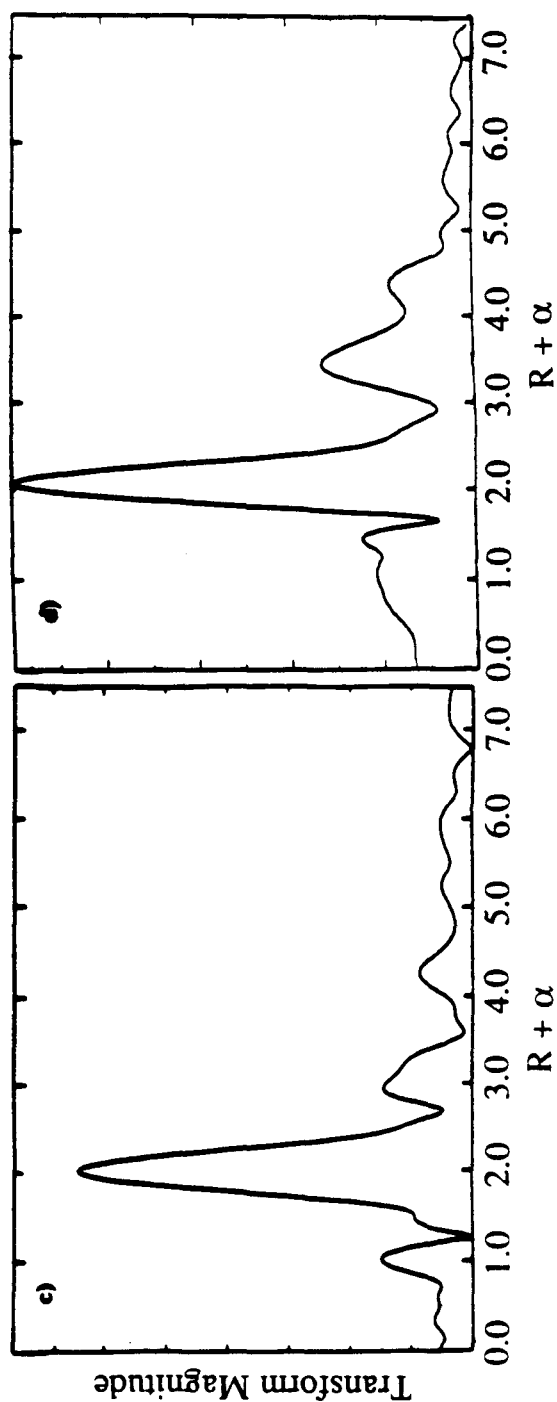
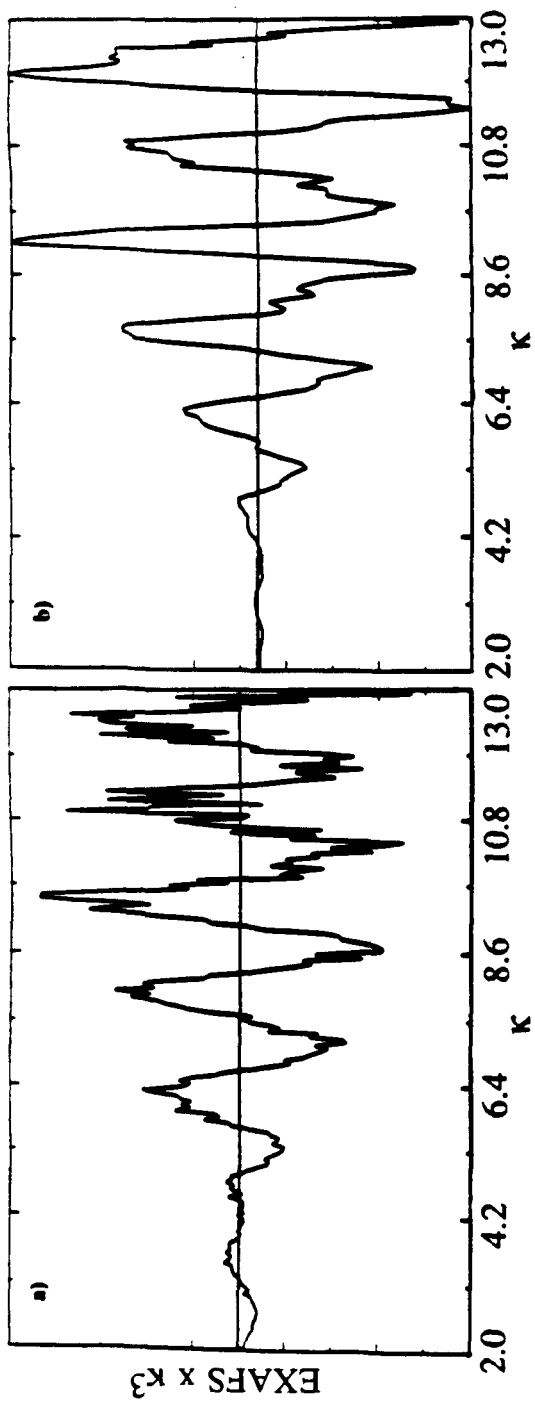
B. GaAs Exposed to Aqueous Co(III) Complexes and KOH-Se^{-1/2}-Electrolyte.

Figure 10 shows the Co EXAFS and Fourier transformed EXAFS amplitude of GaAs powders that had been exposed to $[\text{Co(III)(NH}_3)_5(\text{OH})]^{2+}$ or $[\text{Co(III)(NH}_3)_6]^{3+}$ ions and then exposed to 1.0 M KOH-0.8 M K_2Se -0.1 M K_2Se_2 solutions. The scattering amplitude and phase factor for the Co-Se absorber-scatterer pair were obtained from an EXAFS experiment performed on pure single phase CoSe_2 (synthetic Trogtalite). The best fits to the EXAFS data are presented in Table IV.

A comparison of Figure 10 to Figure 6 shows that the Co coordination sphere was substantially altered as a result of exposure to the KOH-Se^{-1/2}-electrolyte. These results are consistent with changes in the XPS spectra between the two samples (Figures 1 and 5). Fits to the EXAFS indicated a Co inner shell composition of 5 ± 1 Se. This EXAFS fit represents a composition close to CoSe_2 , which is in reasonable agreement with the composition deduced from XPS data.

Attempts to fit the EXAFS data with parameters for both selenium and oxygen in cobalt's inner shell led to unphysical results. While reasonable first shell scattering distances ($d_{\text{Co-X}}$) could be obtained, these two-component fits were always accompanied by unrealistic values for the number (> 10) of nearest neighbor scatterers about Co. Similarly, fits attempted using only oxygen shell parameters never gave good values for the

Figure 10: κ^3 weighted EXAFS and Fourier transform data of CoSe₂ model compound and GaAs powder initially treated with pH = 12 (KOH) solution of 0.010 M [Co(III)(NH₃)₆]³⁺ and subsequently exposed to 1.0 M KOH-0.8 M K₂Se-0.1 M K₂Se₂ electrolyte. Model compound data collected in x-ray transmission mode, GaAs powder data collected in fluorescence mode; both sets obtained on a focussed beam line at 77 K and 10⁻⁶ torr. (a) Fluorescence EXAFS of KOH (aq)-Se⁻²⁻ exposed Co-treated GaAs powder. Superimposed on the raw data is the fit (dashed curve) obtained from the first shell (Co-Se) scattering contribution. (b) Transmission EXAFS of CoSe₂ model compound. (c) Fourier transform of a. (d) Fourier transform of b.



nearest neighbor distances or for the number of scatterers. Only the use of selenium scattering parameters led to good fits to the EXAFS data. Taken together with evidence from XP spectra on identically treated surfaces, the EXAFS data support the hypothesis that oxygen is no longer bound to Co(II) following reaction in basic selenide electrolyte.

4. Quantitative Analyses of Co Chemisorption on GaAs: pH dependence and ^{57}Co Radiotracer Experiments.

A. Wet Chemical Studies

An interesting feature of the GaAs/Co(III) chemisorption process is the lack of detectable Co in either the XPS or x-ray absorption spectra for GaAs exposed to Co(III) in acidic media. To ascertain the pH dependence and overall stoichiometry of the Co(III)-GaAs chemisorption reaction, GaAs powder was treated with aqueous solutions containing $[\text{Co(III)(NH}_3)_6]^{3+}$ or $[\text{Co(III)(bipy)}_3]^{3+}$ and the resulting solutions were subjected to analysis by wet chemical and x-ray fluorescence methods, or to UV-VIS spectrophotometry.

In HEPES buffer (pH = 7.4) or 14.8 M NH_4OH (pH = 12.9), the quantitative reduction of $[\text{Co(III)(NH}_3)_6]^{3+}$ to Co(II) by GaAs powder was observed (Table V). The resulting solutions also contained increased concentrations of soluble As and Ga species, which were analyzed by XRF methods. This yielded relative ratios of [As]:[Ga]:[Co], normalized to the As concentration, of 1.0 ± 0.2 : 1.0 ± 0.2 : 6.0 ± 0.6 . These data clearly indicate a six electron transfer process in the oxidation of one equivalent of GaAs. Additional evidence for electron transfer between GaAs and Co(III) complexes at high pH was obtained by UV-VIS spectrophotometric methods. Solutions (pH = 11.7) of $[\text{Co(III)(bipy)}_3]^{3+}$ in contact with GaAs powder were observed to undergo quantitative reduction to $[\text{Co(II)(bipy)}_3]^{2+}$. These processes are consistent with the Co(II) oxidation

Table V: Distribution of Product Ions by XRF Analysis

Experiment	Raw Counts ^a				Concentration, mM ^b		
	As	Ga	M ^c	Br ^d	[As]	[Ga]	[M] ^e
GaAs + [Co(III)(NH ₃) ₆] ³⁺ ; sat'd NH ₃ , pH = 12.9							
	4,836.4	2,728.9	2,120.4	1,304.4	1.11	1.05	6.19
	3,980.5	2,461.4	2,170.6	1,358.9	0.88	0.91	6.08
	4,561.4	2,752.8	1,978.0	1,137.3	1.20	1.22	6.62
	<u>average of concentrations:</u>				1.1 ± 0.2	1.1 ± 0.2	6.3 ± 0.3 ^e
	<u>ratio of average concentrations, relative to [As]:</u>				1.0 ± 0.2	1.0 ± 0.2	5.9 ± 0.3
GaAs + [Co(III)(NH ₃) ₆] ³⁺ ; CAPS buffer, pH = 10.6							
	f	f	f				
GaAs + [Co(III)(NH ₃) ₆] ³⁺ ; HEPES buffer, pH = 7.4							
	889.2	605.8	547.5	765.5	0.20	0.19	1.19
	<u>ratio of concentrations, relative to [As]:</u>				1.00	0.93	5.98
GaAs + [Co(III)(NH ₃) ₆] ³⁺ ; 0.1 M HCl, pH = 1.0							
	g	g	g				
GaAs + Fe(III)Cl ₃ (aq); 0.1 M HCl, pH = 1.0							
	577.5	376.8	455.1	3287.7	0.30	0.27	1.82
	<u>ratio of concentrations, relative to [As]:</u>				1.00	0.90	6.06

a. Acquisition times: at pH = 12.9, 500 sec; all others 300 sec.

b. Raw counts converted to concentrations by the use of empirically determined cross-sections, σ , relative to $\sigma_{Br} = 1$, and the equation: $[X] = CTS_X \cdot \sigma \cdot [Br] / CTS_{Br}$.

Cross-sections were found to be solution composition dependent. At pH = 12.9:

$\sigma_{Co} = 12.82$; $\sigma_{As} = 1.011$; $\sigma_{Ga} = 1.694$. At pH = 7.4: $\sigma_{Co} = 16.47$; $\sigma_{As} = 1.698$;

$\sigma_{Ga} = 2.308$. At pH = 1.0: $\sigma_{Fe} = 14.05$; $\sigma_{As} = 1.698$; $\sigma_{Ga} = 2.308$.

c. M = Co or Fe, see Experiment column.

d. Counts obtained from the KBr internal standard. At pH = 12.9, [Br] = 0.297 mM; at pH = 7.4, [Br] = 0.101 mM; at pH = 1, [Br] = 1.01 mM.

e. Increase in [Co] over initial value of 5.00 mM was found to be due to a decrease in the solution volume from loss of NH₃(g). An independent check by UV-VIS at the end of the reaction period gave [Co(II)] = 5.80 mM. Further losses in air account for the final state concentration.

f. Not possible to measure at this pH. See text for discussion.

g. No detectable reaction for this system at this pH.

state obtained from the XPS and x-ray absorption data analysis of GaAs samples exposed to basic 0.010 M $[\text{Co(III)(NH}_3)_5\text{X}]^{n+}$ ($\text{X} = \text{NH}_3, \text{N}_3^-, \text{OH}^-, \text{Br}^-$) solutions.

In 0.10 M HCl, only low levels ($< 300 \mu\text{M}$) of Co(II) were found spectrophotometrically in the reaction solution, and only small amounts of $[\text{Co(III)(NH}_3)_6]^{3+}$ were observed (by UV-VIS spectroscopy) to react with GaAs. The concentrations of soluble As and Ga species detected by XRF were also low, and were near that of the background levels found when GaAs powder was treated with 0.10 M HCl. Furthermore, pH = 1.7 solutions of $[\text{Co(III)(bipy)}_3]^{3+}$ in contact with GaAs powder were not observed spectrophotometrically to produce $[\text{Co(II)(bipy)}_3]^{2+}$, or to deplete the absorbance of $[\text{Co(III)(bipy)}_3]^{3+}$ due to adsorption of Co onto the GaAs. In 0.10 M HCl, both Co(II) aquo ions and oxides of the GaAs are soluble, making it unlikely that the reaction would be impeded by an insoluble oxide layer on the GaAs. It may therefore be concluded that the Co(III) species investigated are not reactive with GaAs in 0.10 M HCl on the timescale of the experiment.

To assess the reactivity of GaAs in 0.10 M HCl with suitable oxidants, GaAs powders were exposed to $[\text{Fe(III)(H}_2\text{O)}_6]^{3+}$. X-ray fluorescence analysis of GaAs solutions exposed to Fe^{3+} in 0.10 M HCl showed that six electrons per GaAs equivalent were consumed in the reaction (Table V). This result demonstrates that, given a sufficiently powerful oxidant, GaAs will react by a net six electron redox pathway in 0.10 M HCl.³⁷ This strongly suggests that the lack of reactivity of GaAs with $[\text{Co(III)(NH}_3)_5\text{X}]^{n+}$ ($\text{X} = \text{Br}^-, \text{OH}_2$) (0.10 M HCl) and $[\text{Co(III)(bipy)}_3]^{3+}$ (pH = 1.7) arises from thermodynamic considerations as opposed to oxide dissolution limitations.

The pH stability of Co(OH)_2 bound to GaAs was assessed by exposing GaAs powder that had been previously reacted with $[\text{Co(III)(NH}_3)_6]^{3+}$ in 0.010 M KOH to solutions of 0.10 M HCl, phosphate buffer (pH = 7.0), or 0.010 M KOH, and analyzing

the resulting solution for Co(II) spectrophotometrically.³² In 0.010 M KOH, no Co(II) was detected in the rinse solution. However, in 0.10 M HCl, or phosphate buffer (pH = 7.0), all of the Co(III) that had reacted with the GaAs was liberated as Co(II) and was detected as the soluble Co(II) thiocyanate complex. These results verify that, if GaAs had reacted with Co(III) at 0.10 M HCl, the reaction products would have been detected in the solution phase. They also confirm that XPS analysis of the GaAs surface composition in 0.010 M KOH should yield an accurate measure of the amount of Co(OH)₂ formed due to the reactions of interest.

B. ⁵⁷Co(III)ammine Studies of Co Chemisorption on GaAs.

As a check on the Co coverages obtained from the XPS data analysis, (100) oriented n-GaAs single crystals were treated with 34.0 $\mu\text{Ci ml}^{-1}$ [⁵⁷Co(III)(NH₃)₆]³⁺ in 3.46 mM total [Co(III)(NH₃)₆]³⁺ solution in base (pH = 12.0, KOH_(aq)). The samples were then removed from the γ -active Co solution, and the GaAs surface was etched to remove approximately 0.5 μm of GaAs. The Co in the etch effluent and the remaining GaAs were then separately analyzed for γ -activity. No radioactivity above background was observed for treated and etched GaAs samples, while the effluent displayed γ -ray counts consistent with 5-8 Co(OH)₂-equivalent monolayers (one monolayer of Co(OH)₂ in terms of mole per area is $\Gamma_{\text{Co(OH)}_2} = 1.4 \times 10^{-9} \text{ mol cm}^{-2}$) adsorbed onto (100) GaAs.

The pH dependence of the Co chemisorption was also investigated by these radiotracer methods. GaAs crystals exposed to [⁵⁷Co(III)(NH₃)₆]³⁺ solutions at pH = 1.0 yielded no γ -ray counts above background (Table VI). Additionally, GaAs substrates that were initially exposed to pH = 12.0 [⁵⁷Co(III)(NH₃)₆]³⁺ solutions and then immersed in pH = 1.0 HCl for 30 sec passed all ⁵⁷Co to the acidic rinse solution. The subsequent γ -activity of the acid rinse solutions represented 5-6 Co(OH)₂-equivalent

Table VI: ^{57}Co Coverage on Single Crystal GaAs

Experiment ^a	CPM ^b	Surface Coverage ^c
H ₂ O background ^d	50 ± 2	----
Pt background, from pH = 12.0 (KOH)	1,123 ± 342 ^e	----
Pt background, pH = 1.0 (HCl) ^f	148 ± 15	----
GaAs + [$^{57}\text{Co(III)(NH}_3)_6$] ³⁺ pH = 12.0 (KOH)	104,933 73,612 81,864 <u>Average:</u> 86,803 ± 16,234	1.09 x 10 ⁻⁸ 7.6 x 10 ⁻⁹ 8.5 x 10 ⁻⁹ (9.0 ± 1.7) x 10 ⁻⁹
GaAs + [$^{57}\text{Co(III)(NH}_3)_6$] ³⁺ pH = 12.0 (KOH), then immerse pH = 1.0 (HCl) 30 sec ^g	75,808 75,163 68,041 <u>Average:</u> 73,004 ± 4,310	7.9 x 10 ⁻⁹ 7.8 x 10 ⁻⁹ 7.1 x 10 ⁻⁹ (7.6 ± 0.4) x 10 ⁻⁹
GaAs + [$^{57}\text{Co(III)(NH}_3)_6$] ³⁺ pH = 1.0 (HCl)	(-27 ± 23) ^h (-2 ± 24) ^h (-38 ± 22) ^h <u>Average:</u> (-22 ± 23) ^h	i i i i

a. 1 min exposure to 3.46 mM radiolabeled (^{57}Co) [$\text{Co(III)(NH}_3)_6$](Cl)₃ solution at the pH indicated.

b. Counts per minute, foreground-background for all entries except backgrounds; error limits are ± 1 standard deviation. Calibration curve gives 9.16 x 10⁻¹⁴ mol (Co) cpm⁻¹.

c. mole (Co) cm⁻² (GaAs), GaAs area = 0.884 cm.

d. Background obtained from deionized water.

e. GaAs samples were immersed in radiolabeled and etch solutions in a basket made from thin Pt wire. Counts observed from etched and rinsed Pt thread basket after immersion in pH = 12.0 ^{57}Co ammine solution.

f. Counts observed from etched and rinsed Pt thread basket after immersion in pH = 1.0 ^{57}Co ammine solution.

g. Counts observed in acid immersion solution.

h. Foreground-background including ± 1 standard deviation.

i. Negative cpm indicates Co coverage, if any, well below detectability limit. Foreground count rate places an upper limit < 1 x 10⁻¹¹ mol (Co) cm⁻² on GaAs, *i.e.* < 1/100th of a monolayer.

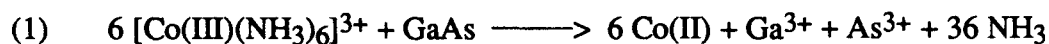
monolayers. These experiments offer estimates of Co chemisorption onto GaAs surfaces consistent with, and independent of, XPS measurements. They also confirm the XRF analyses regarding the pH stability of surface-bound Co(OH)_2 on GaAs.

Discussion

The above data allow one of three possible pathways for the chemisorption of Co(III) onto GaAs to be distinguished: electrostatic binding of the complex ion to oppositely charged sites on the semiconductor surface,⁴³ substitution of a ligand site in the inner sphere of a Co(III) complex by a surface-attached ligand group, and a redox reaction to produce a labile Co(II) oxidation state. The absence of detectable chemisorption for $[\text{Co(III)(bipy)}_3]^{3+}$ or $[\text{Co(II)(bipy)}_3]^{2+}$ over a range of pH values implies that electrostatic forces alone are not sufficient to explain the observed reactions with the $[\text{Co(III)(NH}_3)_5\text{X}]^{n+}$ ($\text{X} = \text{NH}_3, \text{OH}_2, \text{Br}^-, \text{N}_3^-, \text{OH}^-$) complexes. Ligand substitution on $[\text{Co(III)(NH}_3)_5\text{X}]^{n+}$ ($\text{X} = \text{NH}_3, \text{OH}_2, \text{Br}^-, \text{N}_3^-, \text{OH}^-$) complexes is far too slow to account for the observed Co chemisorption: at $\text{pH} = 1.0$ and 0.01 M $[\text{Co(III)(NH}_3)_5\text{X}]^{n+}$ ($\text{X} = \text{Br}^-, \text{OH}_2$), the half-life of surface ligands should be from 10^7 to 10^{11} sec, while at $\text{pH} = 10$ it should be *ca.* 10^{10} sec.³⁶ In contrast, $^{57}\text{Co(III)}$ ammine experiments reveal that *ca.* $1.1 \times 10^{-8} \text{ mol cm}^{-2}$ of Co can be adsorbed onto GaAs in ≤ 60 sec. Furthermore, anation on a Co(III) site should result in signals attributable to the remaining NH_3 groups being observed in an XPS experiment, and should also result in Co 2p XPS signals and x-ray absorption edge features that are characteristic of $[\text{Co(III)(NH}_3)_5\text{X}]^{n+}$ ($\text{X} = \text{NH}_3, \text{OH}_2, \text{Br}^-, \text{N}_3^-, \text{OH}^-$) complexes. The absence of such signals in the XPS and EXAFS data demonstrate that a Co(III) substitutional pathway cannot be a dominant process in the chemisorption of Co onto GaAs. Additionally, the observation of identical surface chemical behavior from experiments performed on GaAs surfaces in the dark (*vide supra*) indicates that the reaction is thermal in nature and is not initiated by photochemical

events on either the substrate or the metal complex. This data therefore strongly suggests that a redox process to yield Co(II) is the dominant binding pathway.

Quantitative chemical analysis of solutions of GaAs and Co(III) ammines provides excellent evidence for a redox dominated chemisorption pathway. In 14.8 M NH₄OH (pH = 12.9), complete reduction of [Co(III)(NH₃)₆]³⁺ by GaAs was observed spectroscopically, and a stoichiometric amount of Co(II) was produced. To within experimental error, the relative concentrations of [As]:[Ga]:[Co] as determined by x-ray fluorescence studies are consistent with the consumption of six electrons in the oxidation of one equivalent of GaAs by Co(III):



This reaction has precedence in the electrochemical dissolution studies of GaAs reported by Gerischer and Memming,³⁷ and is consistent with the previous estimate of the redox potential of GaAs obtained from Born-Haber cycles and rotating disk corrosion studies.⁴⁴ It also is consistent with the XPS and EXAFS data obtained in this work for the reaction of [Co(III)(NH₃)₅X]ⁿ⁺ (X = NH₃, OH₂, Br⁻, N₃⁻, OH⁻) with GaAs single crystals and with GaAs powders.

The lack of reaction in 0.10 M HCl for both [Co(III)(NH₃)₅X]ⁿ⁺ (X = Br⁻, OH₂) and [Co(III)(bipy)₃]³⁺ species indicates that the reduction potential of GaAs is a function of pH. This is expected from the Pourbaix diagrams for Ga and As.³³ Due to the irreversibility of the proposed reaction (1) above, a full set of binding vs. pH data have not collected to quantitatively estimate the formal redox potential for GaAs. However, it is clear that metal ions with reduction potentials positive of those for [Co(III)(NH₃)₅X]ⁿ⁺ (X = NH₃, Br⁻, N₃⁻, OH⁻) and [Co(III)(bipy)₃]³⁺ (*i.e.*, E^o > +0.2 V vs. SCE) can be expected to be reduced by GaAs at pH > 10. Furthermore, more oxidizing species, such as Fe³⁺, will be reduced by GaAs at lower pH values, as was observed in this work.

The measurable binding of Co(OH)_2 from aqueous 0.010 M KOH solutions of Co^{2+} is consistent with the formation of an arrested precipitate of the insoluble Co(OH)_2 on the GaAs surface.⁴² The surface accumulation of Co(OH)_2 is expected to be far greater when it is formed at $\text{pH} > 10$ (where Co(OH)_2 is insoluble) from the reduction of Co(III) ammines by the GaAs surface since, in this case, reduction results in a large effective surface concentration of Co(II) ; this is confirmed by the quantitative coverage data presented above. Although the overlayer obtained either from reactions of Co(II) or $[\text{Co(III)(NH}_3)_5\text{X}]^{n+}$ ($\text{X} = \text{NH}_3, \text{Br}^-, \text{N}_3^-, \text{OH}^-$) with GaAs was found to contain Ga, As, and Co, the close similarity of the first and second shell EXAFS data to that of Co(OH)_2 strongly suggests that the predominant adsorbed Co from these precursors has the Co(OH)_2 structure and stoichiometry.

One of the key issues in surface passivation studies is the chemical nature of electrical trap sites.⁴⁵ Prior work with Ru^{3+} chemisorption has described reductions in the GaAs surface recombination velocity at air interfaces,⁴⁶ as well as improvements in current-voltage behavior at semiconductor/liquid junctions.^{4,47} Due to the relatively high coverage of Co (3-10 monolayers) and the similarity in x-ray scattering factors between Co, Ga, and As, these studies have been unable to identify the GaAs surface moiety that is directly responsible for binding Co(II) . However, as demonstrated in chapter two, recent electrochemical studies have shown that the predominant effect of metal ion binding on GaAs is to increase the interfacial charge transfer rate in the $\text{KOH-Se}^{-/2-}$ electrolyte^{8b,9,18bc}, as opposed to decreasing the surface recombination rate. Therefore chemical studies of the variation in the electrical trap levels at the GaAs surface are not expected to have direct relevance to the reported photoelectrochemical properties of the GaAs/ $\text{KOH-Se}^{-/2-}$ interface. An outstanding question of general interest remains as the identification of the various important ligation properties of the GaAs surface towards various metal ions.

The studies in this work also show that metal ion binding alone may not be sufficient to improve the electrical behavior of a semiconductor/liquid interface. The XPS and EXAFS studies of Co chemisorption clearly indicate that reactions of the surface-bound metal ion with the KOH-Se⁻²⁻ electrolyte yield the species of photoelectrochemical interest. It has previously been shown that treatment of GaAs with [Co(III)(NH₃)₅X]ⁿ⁺ (X = NH₃, Br⁻, N₃⁻, OH⁻) complexes does not result in a substantial reduction of the surface recombination velocity at air interfaces,^{8a} yet the chemical change in the KOH-Se⁻²⁻ electrolyte does result in an improved current-voltage characteristic of the n-GaAs/KOH-Se⁻²⁻ junction.^{8a,18} Thus, correlations between reactivity and electrical properties must account for possible chemical reactions which can create the surface species of electrical interest. An important consequence of the redox activity of the GaAs semiconductor surface is that the dissolved metal ions used for surface treatment might serve merely as precursors for the oxidation state that is actually bound on the semiconductor surface. This appears to be relevant to previous studies of metal ion binding on GaAs,^{2,4,8a,9,18} and should also be considered in explaining the pH dependence of metal ion binding for ions at GaAs surfaces. Similar considerations have been noted in studies of the behavior of gold ion adsorption on the natural mineral semiconductors PbS and FeS₁₋₂.⁴⁸ This would also seem to be relevant to efforts to characterize the photoelectrochemical effect of Ru³⁺ on GaAs by investigating changes in the interface trap density of GaAs that has been exposed to Ru⁰ in ultra-high vacuum,⁴⁹ and to the general usefulness of the Ru³⁺ ion as a surface passivant when in contact with air,⁴⁶ aqueous I⁻/I₃⁻,⁵⁰ and other potentially reactive interfaces.⁵¹

In summary, the interfacial reactions of Co(III) and Co(II) complexes with GaAs surfaces have been identified, and the structure of the surface-bound species has been identified by a combination of methods. Other metal ions may employ different modes of binding to chemisorb on GaAs surfaces, and a complete set of spectroscopic studies would

be needed in order to elucidate the chemical state of the various other surface treatments that have been identified in the literature. Such studies would be especially important for ions that can drastically change the rate of surface recombination under high level injection conditions (implying a reduction in surface state trapping rates as opposed to a chemisorption-induced shift in surface potential), although no such metal ion systems have yet been identified in the literature. It has also been shown that the initial metal binding state need not be representative of the species relevant to the electrical behavior of semiconductor electrodes, and that *in situ* characterization methods are required in order to address these issues.

References

1. Wrighton, M. S. *Accts. Chem. Res.* **1979**, *12*, 303.
2. Heller, A. In *Photoeffects at Semiconductor-Electrolyte Interfaces*; Nozik, A., Ed.; ACS Symposium Series 146; American Chemical Society: Washington D.C., 1981; pp 57-77.
3. (a) Parce, J. W.; Owicki, J. C.; Kercso, K. M.; Sigal, G. B.; Wada, H. G.; Muir, V. C.; Bousse, L. J.; Ross, K. L.; Sikic, B. I.; McConnell, H. M. *Science (Washington, D.C.)* **1989**, *246*, 243. (b) Lisensky, G. C.; Meyer, G. J.; Ellis, A. B. *Anal. Chem.* **1988**, *60*, 2531. (c) Madou, M. J.; Morrison, S. R. *Chemical Sensing with Solid State Devices*; Academic Press: San Diego, 1989.
4. Parkinson, B. A.; Heller, A.; Miller, B. *J. Electrochem. Soc.* **1979**, *126*, 954.
5. (a) Meyer, G. J.; Leung, L. K.; Yu, J. C.; Lisensky, G. C.; Ellis, A. B. *J. Am. Chem. Soc.* **1989**, *111*, 5146. (b) Meyer, G. J.; Lisensky, G. C.; Ellis, A. B. *J. Am. Chem. Soc.* **1988**, *110*, 4914. (c) Dannhauser, T.; O'Neil, M.; Johansson, K.; Whitten, D.; McLendon, G. *J. Phys. Chem.* **1986**, *90*, 6074.
6. (a) Sandroff, C. J.; Nottenburg, R. N.; Bischoff, J.-C.; Bhat, R. *Appl. Phys. Lett.* **1987**, *51*, 33. (b) Yablonovitch, E.; Sandroff, C. J.; Bhat, R.; Gmitter, T. G. *Appl. Phys. Lett.* **1987**, *51*, 439. (c) Sandroff, C. J.; Hegde, M. S.; Farrow, L. A.; Chang, C. C.; Harbison, J. P. *Appl. Phys. Lett.* **1989**, *54*, 362.
7. Parkinson, B. A.; Furtak, T. E.; Canfield, D.; Kam, K.-K.; Kline, G. *Faraday Discuss. Chem. Soc.* **1981**, *70*, 234.

8. (a) Abrahams, I. L.; Tufts, B. J.; Lewis, N. S. *J. Am. Chem. Soc.* **1987**, *109*, 3472. (b) Abrahams, I. L.; Casagrande, L. G.; Rosenblum, M. D.; Rosenbluth, M. L.; Santangelo, P. G.; Tufts, B. J.; Lewis, N. S. *Nouv. J. Chim.* **1987**, *11*, 157. (c) Tufts, B. J.; Abrahams, I. L.; Caley, C. E.; Lunt, S. R.; Miskelly, G. M.; Sailor, M. J.; Santangelo, P. G.; Lewis, N. S.; Roe, A. L.; Hodgson, K. O. *J. Am. Chem. Soc.* **1990**, *112*, 5123.
9. Tufts, B. J.; Abrahams, I. L.; Santangelo, P. G.; Ryba, G. N.; Casagrande, L. G.; Lewis, N. S. *Nature (London)* **1987**, *326*, 861.
10. Literature preparation of $[\text{Co(III)(NH}_3)_6](\text{Cl})_3$: Bjerrum, J.; McReynolds, J. P. *Inorg. Synth.* **1946**, *2*, 217.
11. Literature preparation of: (a) $[\text{Co(III)(NH}_3)_5\text{Cl}](\text{Cl})_2$: Schlessinger, G. *Inorg. Synth.* **1967**, *9*, 160. (b) $[\text{Co(III)(NH}_3)_5\text{Br}](\text{Br})_2$ and $[\text{Co(III)(NH}_3)_5(\text{OH}_2)](\text{Br})_3$: Diehl, H.; Clark, H.; Willard, H. H. *Ibid.* **1939**, *1*, 186. (c) $[\text{Co(III)(NH}_3)_5(\text{N}_3)](\text{Cl})_2$: Linhard, M.; Flygare, H. Z. *Anorg. Chem.* **1950**, *262*, 328.
12. (a) Blau, F. *Monatsh. Chem.* **1889**, *10*, 372. (b) Blau, F. *Monatsh. Chem.* **1898**, *19*, 647. (c) Burstal, F. M.; Nyholm, R. S. *J. Chem. Soc.* **1952**, 3570.
13. (a) Blau, F. *Monatsh. Chem.* **1898**, *19*, 669. (b) Shilts, A. A. *J. Am. Chem. Soc.* **1960**, *82*, 3000.
14. Brauer, G. *Handbook of Preparative Inorganic Chemistry*; 2nd ed. Academic Press: New York, 1965; Vol. 2; p 1521.

15. (a) Feitknecht, W.; Bédert, W. *Helv. Chim. Acta* **1941**, *24*, 683.
(b) Delaplane, R. G.; Ibers, J. A.; Ferraro, J. R.; Rush, J. J. *J. Chem. Phys.* **1969**, *50*, 1920.
16. (a) Heide, H. van der; Hemmel, R.; Bruggen, C. F. van; Haas, C. *J. Solid State Chem.* **1980**, *33*, 17. (b) Ramdohr, P.; Schmitt, M. *Neues Jahrb. Mineral. Monatsh.* **1955**, *6*, 133. (c) Bohm, F.; Gronvold, F.; Haraldsen, H.; Prydz, H. *Acta Chem. Scand.* **1955**, *9*, 1510.
17. Mandel, N.; Donohue, J. *Acta Crystallog. Sect B: Struct. Sci.* **1971**, *B27*, 2288.
18. (a) Gronet, C. M.; Lewis, N. S. *J. Phys. Chem.* **1984**, *88*, 1310. (b) Tufts, B. J.; Abrahams, I. L.; Casagrande, L. G.; Lewis, N. S. *J. Phys. Chem.* **1989**, *93*, 3260. (c) Lunt, S. R.; Casagrande, L. G.; Tufts, B. J.; Lewis, N. S. *J. Phys. Chem.* **1988**, *92*, 5766.
19. Seah, M. P.; Dench, W. A. *Surf. Interface Anal.* **1979**, *1*, 2.
20. Scofield, J. H. *J. Electron Spectrosc. Relat. Phenom.* **1976**, *8*, 129.
21. Feldman, L. C.; Mayer, J. W. *Fundamentals of Surface and Thin Film Analysis*; North-Holland: New York, 1986.
22. The molar density was calculated from the formula weight and mass density as reported in: Weast, R. C., Astle, M. J., Eds. *CRC Handbook of Chemistry and Physics*; Chemical Rubber Co.: Boca Raton, 1980; Vol. 60, p B-73. The atomic number density of an atom in a compound is given by the mass density of the compound multiplied by the stoichiometric coefficient for the atom.

23. Weast, R. C., Astle, M. J., Eds. *CRC Handbook of Chemistry and Physics*; Chemical Rubber Co.: Boca Raton, 1980; Vol. 60, p B-57.
24. Weast, R. C., Astle, M. J., Eds. *CRC Handbook of Chemistry and Physics*; Chemical Rubber Co.: Boca Raton, 1980; Vol. 60, p B-80.
25. Bain, C. D.; Whitesides, G. M. *J. Phys. Chem.* **1989**, *93*, 1670.
26. The sample-detector angle was varied over the range $\theta = 0-70^\circ$. See Table III.
27. Fadley, C. S. *Prog. Solid State Chem.* **1976**, *11*, 265.
28. Phillips, L. V.; Salvati, L.; Carter, W. J.; Hercules, D. M. In *Quantitative Surface Analysis of Materials*; McIntyre, N. S., Ed.; ASTM Special Technical Publication 643, American Society for Testing and Materials: Philadelphia, 1978; pp 47-63.
29. Kim, K. S. *Phys. Rev. B* **1975**, *11*, 2177.
30. (a) Stern, E. A.; Heald, S. M. *Rev. Sci. Instr.* **1979**, *50*, 1579. (b) Lytle, F. W.; Greigor, R. B.; Sandstrom, D. R.; Marques, E. C.; Wong, J.; Spiro, C. L.; Huffman, G. P.; Huggins, F. E. *Nucl. Instr. Meth.* **1984**, *226*, 542. (c) Cramer, S. P.; Hodgson, K. O.; Stiefel, E. I.; Newton, W. E. *J. Am. Chem. Soc.* **1978**, *100*, 2748. (d) Cramer, S. P.; Hodgson, K. O. *Prog. Inorg. Chem.* **1979**, *15*, 1. (e) Scott, R. A.; Hahn, J. E.; Doniach, S.; Freeman, H. C.; Hodgson, K. O. *J. Am. Chem. Soc.* **1982**, *104*, 5364. (f) Scott, R. A. *Methods Enzymol.* **1985**, *117*, 414.
31. (a) Prelesnik, B. V.; Gabela, F.; Ribár, B.; Krstanovic, I. *Cryst. Struct. Comm.* **1973**, *2*, 581. (b) Chastain, R. V.; Natt, J. J.; Witkowska, A. M.; Lingafelter, E. C. *Acta Cryst.* **1967**, *22*, 775. (c) Ray, S.; Zalkin, A.; Templeton, D. H. *Acta Crystallog. Sect. B: Struct. Sci.* **1973**, *B29*, 2741.

32. Brown, W. B.; Steinbach, J. F. *Anal. Chem.* **1959**, *31*, 1805.
33. Pourbaix, M. *Atlas of Electrochemical Equilibria in Aqueous Solution*; Pergamon: New York, 1966.
34. Feitknecht, W.; Schindler, P. *Pure Appl. Chem.* **1963**, *6*, 130.
35. (a) Frost, D. C.; McDowell, C. A.; Woolsey, I. S. *Chem. Phys. Lett.* **1972**, *17*, 320. (b) Frost, D. C.; McDowell, C. A.; Woolsey, I. S. *Mol. Phys.* **1974**, *27*, 1473. (c) Haraguchi, H.; Fujiwara, K.; Fuwa, K. *Chem. Lett.* **1975**, 409.
36. Basolo, F.; Pearson, R. G. *Mechanisms of Inorganic Reactions*; 2nd ed.; Wiley: New York, 1967.
37. (a) Gerischer, H. *J. Vac. Sci. Technol.* **1979**, *15*, 1422. (b) Memming, R. *J. Electrochem. Soc.* **1978**, *125*, 117.
38. Augustynski, J.; Koudelka, M.; Sanchez, J.; Conway, B. E. *J. Electroanal. Chem.* **1984**, *160*, 233.
39. Mandle, A. B.; Badrinarayanan, S.; Date, S. K.; Sinha, A. P. B. *J. Electron Spectrosc. Relat. Phenom.* **1984**, *33*, 61.
40. Lotmar, W.; Feitknecht, W. *Z. Kristallogr.* **1936**, *93*, 368.
41. Kruger, G. J.; Reynhardt, E. C. *Acta Crystallogr. Sect. B: Struct. Sci.* **1974**, *B30*, 822.
42. (a) Dillard, J. G.; Schenk, C. V. In *Geochemical Processes at Mineral Surfaces*; Davis, J. A., Hayes K. F., Eds.; ACS Symposium Series 323; American Chemical Society: Washington, D.C., 1986; pp 503-522. (b) Parks, G. A. *Chem. Rev.* **1965**,

- 65, 177. (c) Benjamin, M. M.; Leckie, J. O. *J. Colloid Interface Sci.* **1981**, *79*, 209.
- (d) Benjamin, M. M.; Leckie, J. O. *J. Colloid Interf. Sci.* **1981**, *83*, 410. (e) Benjamin, M. M.; Leckie, J. O. *Environ. Sci. Technol.* **1982**, *16*, 162.
43. (a) Tschapek, M.; Wasowski, C.; Torres Sanchez, R. M. *J. Electroanal. Chem.* **1976**, *74*, 167. (b) Uchida, I.; Akahoshi, H.; Toshima, S. *J. Electroanal. Chem.* **1978**, *88*, 79.
44. (a) Frese, K. W., Jr.; Madou, M.; Morrison, S. R. *J. Phys. Chem.* **1980**, *84*, 3172. (b) Frese, K. W., Jr.; Madou, M.; Morrison, S. *J. Electrochem. Soc.* **1981**, *128*, 1527. (c) Frese, K. W., Jr.; Madou, M.; Morrison, S. *J. Electrochem. Soc.* **1981**, *128*, 1939.
45. Many, A.; Goldstein, Y.; Grover, N. B. *Semiconductor Surfaces*; North Holland: Amsterdam, 1965.
46. Nelson, R. J.; Williams, J. S.; Leamy, H. J.; Miller, B.; Parkinson, B. A.; Heller, A. *Appl. Phys. Lett.* **1980**, *36*, 76.
47. (a) Heller, A. *Acc. Chem. Res.* **1981**, *14*, 154. (b) Hodes, G.; Fonash, S. J.; Heller, A.; Miller, B. *Adv. Electrochem. Electrochem. Eng.* **1984**, *13*, 113.
48. Jean, G. E.; Bancroft, G. M. *Geochim. Cosmochim. Acta* **1985**, *49*, 979.
49. Ludwig, M.; Heymann, G.; Janietz, P. *J. Vac. Sci. Technol.* **1986**, *B4*, 485.
50. Allongue, P.; Cachet, H.; Clechet, P.; Froment, M.; Martin, J. R.; Verney, E. *J. Electrochem. Soc.* **1986**, *209*, 219.
51. Mandel, K. C.; Basu, S.; Bose, D. N. *J. Phys. Chem.* **1987**, *91*, 4011.

Chapter 3

Correlations Between the Interfacial Chemistry and Current-Voltage Behavior of n-GaAs/Liquid Junctions

Abstract: Correlations between the surface chemistry of etched, (100)-oriented n-GaAs electrodes and their subsequent photoelectrochemical behavior have been probed by high-resolution x-ray photoelectron spectroscopy. GaAs photoanodes were chemically treated to prepare either an oxide-free near stoichiometric surface, a surface enriched in zero-valent arsenic (As^0), or a substrate-oxide terminated surface. The current-voltage (I - V) behavior of each surface-type was subsequently monitored in contact with an acetonitrile-90.0 mM ferrocene-0.5 mM ferrocenium hexafluorophosphate-0.7 M lithium perchlorate electrolyte. Additionally, the I - V behavior of the GaAs surfaces in contact with aqueous 1.0 M KOH-0.8 M K_2Se -0.1 M K_2Se_2 electrolytes and in contact with Au Schottky barriers has been monitored and correlated with the surface chemistry.

Introduction

Attempts to expand the materials base of electronic devices beyond silicon (Si) have revealed fundamental shortcomings in our understanding of the physics and chemistry of recombination processes at semiconductor interfaces.¹ Gallium arsenide (GaAs) serves as a case in point. Based on considerations of high carrier mobility, GaAs based circuits are expected to be much faster than similar circuits made of Si.² In practice, however, the superior bulk properties of such GaAs devices are not realized due to the very high surface recombination velocities ($S \geq 10^6 \text{ cm s}^{-1}$) observed at GaAs-metal or GaAs-insulator contacts.³ (In contrast, Si-SiO₂ interfaces are routinely fabricated with $S < 100 \text{ cm s}^{-1}$.)⁴ High surface recombination rates are a problem at most semiconductor interfaces; therefore, the elucidation of factors controlling interfacial recombination rates remains a major focus of research in the semiconductor materials community.

The chemical nature of recombination sites at GaAs surfaces and GaAs/metal junctions has attracted attention from numerous research groups.⁵⁻⁹ Recombination models invoking the presence of interfacial defects,⁷ excess elemental arsenic (As⁰),⁵ or metal-induced gap states⁸ have been proposed to rationalize the behavior of these junctions. To date, none of these models has been tested by a combination of experimental methods that both characterize the chemical composition of a prepared GaAs junction and collect current-voltage data for that specific interface. The work presented in this chapter satisfies precisely this experimental arrangement. By choice of specific chemical treatments, n-GaAs electrodes have been etched to yield initially either an interface with minimal amounts of oxides, an interface rich in As⁰, or an oxide-covered surface. Each of these surfaces was then immersed into each of two electrolytes to form n-GaAs/liquid^{10,11} contacts in order to monitor changes in current-voltage (*I-V*) behavior in response to changes in interfacial chemistry. In all cases in order to determine the surface composition,

each of the prepared n-GaAs surfaces was characterized, before and after exposure to electrolyte, by high resolution x-ray photoelectron spectroscopy (XPS). These studies have provided valuable correlations between junction transport behavior and GaAs surface composition.

Experimental

A. Chemicals.

All solvents and etches used were either J. T. Baker MOS grade or Mallinckrodt Transistar stock. Anhydrous non-denatured ethanol was obtained from the Quantum Chemical Corporation (Punctilious label). A Barnstead NANOpure water purifier provided 18M Ω deionized water. All solutions were deaerated by sparging with a stream of dry N₂ gas for at least 15 minutes.

Ferrocene (FeCp₂) was obtained from Aldrich and purified by vacuum sublimation prior to use. Ferrocenium hexafluorophosphate was prepared by the oxidation of purified ferrocene with an equivalent of benzoquinone in methanol, isolated by the addition of hexafluorophosphoric acid, and purified by fractional recrystallization from hot methanol solution. The isolated ferrocenium salt was then placed in a warmed schlenk tube (60 - 70 °C) and dried by pumping under active vacuum for several days. Lithium perchlorate was made anhydrous by melting the salt (Aldrich) in a quartz schlenk tube at 300 °C held under active vacuum for eight hours. Aluminum selenide (Al₂Se₃) and potassium hydroxide (KOH), for use in the preparation of the KOH-K₂Se-K₂Se₂ electrolyte, were purchased from Alfa and J. T. Baker, respectively.

Acetonitrile and carbon disulfide were purified by distillation, under N₂, from phosphorous pentoxide (Aldrich) and stored in sealed round-bottom flasks over activated 3A molecular sieves (Linde). All non-protic, non-aqueous solvents and all molecular

solids were maintained in the anhydrous anaerobic atmosphere of a Vac Atmosphere's dry box prior to use.

High purity gold wire (0.010 in, % 99.999), for use in the formation of Au/GaAs Schottky contacts was purchased from the Materials Research Corporation. Silver wire (0.127 mm, % 99.99+) for forming contacts to the finished Schottky junction, was purchased from Aldrich. Silver print conductive paint, used to contact the silver wire to the gold surface layer, was purchased from G. C. Electronics.

For use in XPS experiments, transport of chemicals from the Vac Atmosphere dry box to the import/export load lock of the x-ray photoelectron spectrometer's primary glove box was effected by use of sealed schlenk glassware backfilled with N₂. The spectrometer's glove box system consists of an import/export load lock to the primary glove box, a load lock connecting the primary box to the secondary box, and a final load lock connecting the secondary box directly to the high vacuum storage chamber of the x-ray photoelectron spectrometer. The atmosphere in the spectrometer glove boxes was constantly refreshed (*ca.* 3 m³ min⁻¹) by the direct blow off of a high purity liquified N₂ (O₂ ≈ 2 ppm) source.

B. GaAs Surfaces and Electrodes.

Preparation of the n-GaAs electrodes and the 1.0 M KOH - 0.8 M K₂Se - 0.1 M K₂Se₂ electrolyte, the aqueous based electrochemical cells, and the equipment used to record current-voltage behavior have been described in chapter one.

The non-aqueous based acetonitrile (CH₃CN) - 0.20 M FeCp₂ - 0.5 mM FeCp₂PF₆ - 0.7 M LiClO₄ electrolyte was prepared in the primary spectrometer glove box in stages, in order to maintain optimally dry solution conditions. Typically, a 0.20 M solution of FeCp₂ in CH₃CN was first stored over activated 3A molecular sieves

for at least two days. A 10 to 15 mL aliquot of this solution was then added to another flask containing sufficient proportions of LiClO_4 and FeCp_2PF_6 to make up the final electrolyte. This solution was then stirred for a few minutes and subsequently filtered through a $0.45\ \mu\text{m}$ disk filter (Uniflo, Schleicher and Schuell) by precision plastic syringe (Becton Dickinson) into the electrochemical cell, which was then sealed with glass or rubber stoppers.

Single crystals of (100)-oriented n-GaAs were grown either by organometallic vapor phase epitaxy (OMVPE) to yield $N_D = 2 \times 10^{17}\ \text{cm}^{-3}$ Se doped epilayers or were Czochralski grown to yield $N_D = 1 - 4 \times 10^{17}\ \text{cm}^{-3}$ Si doped samples. The general method of electrode preparation has been previously described in chapter two. However, electrodes made for the experiments conducted in this chapter were not sealed with Hysol epoxy, but rather with a high vacuum compatible epoxy called Torr Seal (Varian Vacuum). There is essentially no difference in the curing processes required for setting each epoxy resin. The components used in Torr Seal epoxy have exceptionally low vapor pressures, allowing use of small amounts of the cured resin in vacuum environments lower than 10^{-9} torr. A slight modification to each electrode body was made to accommodate measurements in the XP spectrometer. All electrodes were constructed in the side-on fashion and had two strips of cut microscope slide epoxied to the glass tubing supporting each electrode such that the face of each electrode lay parallel to the XPS support platen.

Finished GaAs electrodes were etched, in the secondary spectrometer glove box, by three different etch procedures that yielded, reproducibly, three chemically distinct interfaces; the latter two etches are based on the first etch:

(i) Etch A, based on a protocol for producing atomically abrupt near-stoichiometric GaAs interfaces developed by Aspnes and Stocker,¹² involves sequential and repeated exposure of an electrode to an aqueous 1.0 M KOH solution followed by immersion into

a mildly oxidizing 0.05 % (vol) Br₂/MeOH solution. In a typical example, an electrode is initially introduced into a KOH solution, with stirring, for 15 seconds. The electrode is then removed from solution, rinsed with a steady stream (*ca.* 10 mL) of H₂O, then MeOH, and blown dry with a stream of high purity (oxygen, water, and oil free) fluorochlorocarbon gas from a "duster" aerosol can. The electrode is next immersed into a Br₂/MeOH solution, with stirring, for 15 seconds. It is then removed, and rinsed with MeOH and then H₂O, and then blown dry, as before. This procedure is repeated three more times. Finally, the electrode is immersed in 1.0 M KOH solution, with stirring, for 30 seconds, rinsed with H₂O and then MeOH, and then blown dry, as above.

(ii) Etch B produces a layer of excess elemental arsenic (As⁰) on the electrode surface. An electrode is initially treated to Etch A and then immersed into a 1:1:100 (vol) solution of con. H₂SO₄:30 % H₂O₂:H₂O, with stirring, for 60 seconds, rinsed with H₂O and blown dry, as above.

(iii) Etch C yields a highly oxidized surface layer. An electrode, following Etch B, is exposed to a stirred 30 % H₂O₂ solution for 60 seconds, rinsed with H₂O and blown dry, as above.

Following any given procedure, an etched electrode was placed either in the primary box-to-secondary box load lock for transport to a photoelectrochemical cell residing in the primary box, or into the vacuum load lock of the x-ray photoelectron spectrometer. Occasionally, the blow dry step was omitted from the routine, and instead electrodes were dried by wicking away rinse solvent with the corner of a clean room cloth. The drying method produced no discernible effect on the electrode's surface composition.

Gold Schottky barriers were formed on n-GaAs electrodes that had been etched in air. Immediately following etching, an electrode was placed in a filament evaporator (Consolidated Vacuum Corporation, LCI-14B), pumped down to $\leq 10^{-6}$ torr, and coated

by filament evaporation with *ca.* 100 Å of gold. The deposition rate and thickness were followed by use of an oscillating quartz crystal acoustic impedance thickness monitor (R. D. Mathis, TM-100).

C. Photoelectrochemistry.

A description of the potentiostat set-up and illumination source used in collecting current-voltage curves was given in chapter two. All photoelectrochemistry was performed in the primary spectrometer glove box, isolated from any moisture or oxidizing gases evolved from the etches by means of the primary box-to-secondary box load lock. Electrical contacts to the working, auxiliary, and reference electrodes were made through the back wall of the primary glove box to the control electronics by means of a gas-tight multiple pin electrical feedthrough socket. The temperature of the cell was monitored by means of a thermometer immersed in the electrolyte. Immediately following solution exposure or photoelectrochemical cycling, the electrodes were removed from solution, rinsed with either CH₃CN (for electrodes cycled in the FeCp₂⁺⁰ based cells), or H₂O (for electrodes cycled in Se⁻²⁻ based cells), blown dry and loaded into the primary box-to-secondary box load lock, passed through the secondary glove box and into the spectrometer load lock and placed under high vacuum. Prior (*ca.* 10 - 20 minutes) to passage through the secondary glove box, all etches, solvents, and solutions in that box had been sealed, and therefore potential oxidants (*e.g.*, O₂ or Br₂) or contaminants (*i.e.*, H₂O) in the atmosphere of the secondary box had been swept out of the box before the electrode was passed through it to the spectrometer load lock.

Contacts to the gold layer of the n-GaAs/Au Schottky barriers were made by wrapping a silver wire around the glass stem of the electrode and touching the silver wire (connected to the working lead of a potentiostat) and the gold surface layer with a film of silver print conductive paint. The back contact of the electrode was connected to both the

reference and auxillary leads of the potentiostat. Current-voltage curves were collected in the air under illumination from ELH (Kodak) W-halogen bulbs in a two-electrode configuration.

D. X-ray Photoelectron Spectroscopy.

I. Procedures. X-ray photoelectron spectra were obtained on a custom modified Surface Science Instruments SSX 100 "top hat" small spot x-ray photoelectron spectrometer attached to a custom modified vacuum system. All spectra were acquired at a base pressure of $< 5 \times 10^{-9}$ torr using monochromatic Al $K_{\alpha 1,2}$ ($h\nu = 1486.6$ eV) irradiation. The x-ray beam formed a variable sized elliptical spot (semimajor axis/semiminor axis ≈ 3) on the sample, having a maximum size of $1000 \mu\text{m}$ (semimajor axis). Typically, samples were irradiated with spot sizes (semimajor axis) of $600 \mu\text{m}$ (survey scans) or $300 \mu\text{m}$ (single region scans). The detector was operated at 25 eV pass energy (resolution 3) during survey scans, and at 12.5 eV pass energy (resolution 2) during single region scans. The focussed x-ray source operated at 10 kV and at variable current levels dependent upon the spot size: 20 mA ($1000 \mu\text{m}$), 15 mA ($600 \mu\text{m}$), and 10 mA ($300 \mu\text{m}$).

All samples were chemically and photoelectrochemically manipulated in the N_2 atmosphere of the spectrometer glove boxes. GaAs treated by Etch A displayed lattice As $3d_{5/2}$ at (41.27 ± 0.09) BeV and lattice Ga $3d_{5/2}$ at (19.41 ± 0.09) BeV, and had oxide region peak intensities consistent with $< 5 \times 10^{-10}$ mol cm^{-2} (*i.e.*, $< 1/2$ monolayer) of arsenic oxides and of gallium oxides (Figure 3). These low background values required careful anaerobic handling of the GaAs through all etching steps and subsequent solution manipulations; however, under these conditions, changes in XPS signals reliably indicated changes in surface composition, and hence the effect of solution exposure or photoelectrochemical treatments on the initial electrode surface composition.

II. Data Analysis. The choice of energy reference level was determined by the nature of the samples. All of the samples used in this work were n-GaAs electrodes with good back ohmic contacts. Each electrode was grounded to the spectrometer by means of a second mounting clip in contact with the wire forming the electrode's back contact. The Fermi level of any given electrode was therefore at the Fermi level of the spectrometer, and no offset of measured binding energy due to charging processes was possible (or observed). Changes in the observed peak position for the same material will be due, then, to the relative drift in the work functions of an electrode surface and the photoelectron detector surfaces. Hence, for a conducting inert substrate of constant work function, the drift in the observed energy of a peak defined to be at a particular value over the course of the experiments follows the drift in detector work function and also sets the drift in the value of the raw peak positions of all other peaks. Because no charging problem exists for these samples, it is not necessary to use the C 1s level of "adventitious" carbon as a reference point, and a well defined material may be used for this purpose instead. A polycrystalline gold overlayer filament evaporated onto a stainless steel mounting clip and kept in the analysis chamber of the spectrometer, was used for this purpose. The instrumental linewidth was observed (300 μm spot; resolution 2) to be 0.88 eV at the full-width at half-maximum of the Au 4f_{7/2} line *defined* to be at 84.00 binding electron volts (BeV). Corrections to raw peak positions were made by applying the difference between the observed and defined values of the Au 4f_{7/2} line to each observed peak. The position of the Au 4f_{7/2} line was monitored at least daily. Over the course of all of these experiments, spectrometer drift never exceeded 0.14 eV.

Peak deconvolutions were performed using standard software routines provided by Surface Science Instruments. Signals derived from substrate Ga or As, or from elemental As, were typically fit by constraining the ratio of the 3d_{5/2} peak to the 3d_{3/2} peak to be 1.50, in keeping with intensity expectations arising from quantum mechanics. The

separation between the As 3d doublet levels was further constrained to the spin-orbit splitting value of 0.70 eV (As); the 3d doublet separation for Ga was not constrained. (Generally, the area ratio constraint was sufficient alone to give substrate GaAs or As⁰ peak deconvolutions with doublet splittings to within ± 0.03 eV of the stated spin-orbit splitting values: lattice As = 0.71 ± 0.03 eV; As⁰ = 0.69 ± 0.01 eV; lattice Ga = 0.49 ± 0.02 eV.) No constraints were placed on the relative position or area of any individual 3d doublet pair (*i.e.*, no constraints on As⁰ relative to lattice As). All other peaks (those attributable to substrate oxides, selenides, elemental gallium, and carbonaceous material in the As 3d, Ga 3d, C 1s, Se 3d, and O 1s regions) were fit with a single line. All peaks were fit using a symmetric Voigt line shape that was weighted 70 % Gaussian and 30 % Lorentzian.

Estimates of the photoelectron escape depths (λ) of substrate GaAs, As⁰, Ga⁰, Se⁰, and substrate based oxides were obtained using the method of Seah and Dench,¹³ with photoelectron differential cross-sections as given by Scofield.¹⁴ GaAs electrodes exposed to Etch A never gave signal intensity due to As⁰, and only very small amounts of substrate oxide (*vide infra*). In contrast, GaAs electrodes exposed to Etch B always displayed signal intensity due to As⁰, observed at (As 3d_{5/2} = 42.12 ± 0.16) BeV. The bulk molar density of 7.64×10^{-2} g-atom cm⁻³ was assumed for As⁰ at the electrode surface.¹⁵ This yielded a value of $\lambda_{As03d} = 23$ Å. Those GaAs electrodes exposed to Etch C consistently displayed signals due to substrate oxides. Sources of As 3d signal attributable to As₂O₃ were assumed to have a molar density equivalent to that of vitreous arsenic oxide ($\rho = 1.89 \times 10^{-2}$ mol cm⁻³)¹⁵; the corresponding value of the photoelectron escape depth is $\lambda_{As3d} = 36$ Å. Sources of Ga 3d signal due to gallium oxide (Ga₂O₃) were occasionally obscured by a broad peak due to the O 2s core level. The density of surface Ga₂O₃ was taken as the average of the molar densities of the α and the β phases, $\rho = 3.30 \times 10^{-2}$ mol cm⁻³;¹⁶ this yielded an escape depth of $\lambda_{Ga3d} = 28$ Å. XPS

signals from the C 1s region showed that more than one type of hydrocarbon was in the surface overlayer. The value of the hydrocarbon molar density was estimated as $\rho = 1.5 \times 10^{-2} \text{ mol (C) cm}^{-3}$ and the carbon atomic number density was estimated as $\rho = 3.3 \times 10^{-2} \text{ gram-atom cm}^{-3}$. In determining the amount of carbonaceous material at each surface, the experimentally determined value¹⁷ of $\lambda_{C1s} = 35 \text{ \AA}$ for the mean free path of the photoelectrons in an organic film was used.

Employing the simple homogeneous overlayer model of photoelectron attenuation,¹⁸ the surface coverage was then determined with respect to the intensity, photoelectron escape depth ($\lambda_{As3d} = 25 \text{ \AA}$), and molar density ($n_{As} = 3.68 \times 10^{-2} \text{ mol cm}^{-3}$)¹⁹ for As in the substrate GaAs, the integrated peak intensity of the surface species in question (As^0 , substrate oxides, and contributions from carbonaceous material) and its atomic number density (# g-atom cm^{-3} of the element in the surface species in question), and the known value of the sample-detector angle ($\theta = 38.8^\circ$). The simple XPS substrate/overlayer intensity model of Fadley²⁰ was applied. Using this model, it is assumed that after etching, elemental arsenic will be closest to the GaAs interface, followed by substrate oxides, and finally an adventitious hydrocarbon layer.

For those GaAs samples subsequently exposed to Se^{-2} - electrolyte, estimates of $Se^{0/2-}$, As_2Se_3 , and Ga^0 coverage were based on the integrated Se 3d, As 3d (As_2Se_3) and Ga (Ga^0) 3d intensities, respectively. Following the procedure described above, using the atomic density of Se^0 ($\rho = 6.07 \times 10^{-2} \text{ gram-atom cm}^{-3}$),²¹ As_2Se_3 ($\rho = 1.23 \times 10^{-2} \text{ mole cm}^{-3}$),¹⁵ and of Ga^0 ($\rho = 8.47 \times 10^{-2} \text{ gram-atom cm}^{-3}$),²² the photoelectron escape depths for $Se^{0/2-}$, As_2Se_3 , and Ga^0 were estimated as $\lambda_{Se3d} = 26 \text{ \AA}$, $\lambda_{As2Se3} = 25 \text{ \AA}$, and $\lambda_{Ga03d} = 23 \text{ \AA}$, respectively. Table I summarizes all of the estimated and calculated parameters used in the determination of surface coverages and surface chemical compositions.

Table I:**X-ray Photoelectron Spectroscopy: Surface Analysis Materials Parameters**

Compound	line ^a	n (g-atom cm ⁻³) ^b	$\sigma_{\text{Scofield}}^c$	λ (Å) ^d	Γ (mole cm ⁻²) ^e	d (Å) ^e
GaAs (lattice)	As 3d	3.68×10^{-2}	$\Sigma^f = 1.821$	25	1.31×10^{-9}	----
	Ga3d	3.68×10^{-2}	$\Sigma = 1.085$	25		
As ⁰	As 3d	7.64×10^{-2}	$\Sigma = 1.821$	23	2.1×10^{-9}	2.8
Ga ⁰	Ga 3d	8.47×10^{-2}	$\Sigma = 1.085$	23	2.3×10^{-9}	2.7
As ₂ O ₃ (vitreous)	As 3d	3.78×10^{-2}	$\Sigma = 1.821$	36	8.4×10^{-10}	4.4
	O 1s	5.67×10^{-2}	2.93	29		
Ga ₂ O ₃ ($\alpha + \beta$) ^g	Ga 3d	6.59×10^{-2}	$\Sigma = 1.085$	28	1.2×10^{-9}	3.7
	O 1s	9.89×10^{-2}	2.93	22		
As ₂ Se ₃	As 3d	2.46×10^{-2}	$\Sigma = 1.821$	25	6.3×10^{-10}	5.1
Se ⁰	Se 3d	6.07×10^{-2}	$\Sigma = 2.294$	26	1.8×10^{-9}	3.0
C _x H _y O _z ^h	C 1s	3.3×10^{-2}	1.000	35	7.3×10^{-10}	4.8
	O 1s	2.8×10^{-2}	2.93	37		

a. Detected line due to photoemission from the relevant core level.

b. Elemental equivalent in a cubic centimeter of solid compound.

c. Core level differential photoelectron cross section, as calculated by Scofield.²⁰

d. Photoelectron escape depth at the given core line energy in the compound material.

e. Mole equivalent in a monolayer thick film and idealized thickness for the compound material.

f. Σ is used when lines from core levels with net spin overlap, and indicates the sum of the pertinent Scofield differential photoelectron cross sections.

g. Average of $\alpha + \beta$ phases of Ga₂O₃.

h. Generic oxygen containing carbonaceous material.

Results

1. Current-Voltage Behavior of Etched n-GaAs/Liquid Junctions.

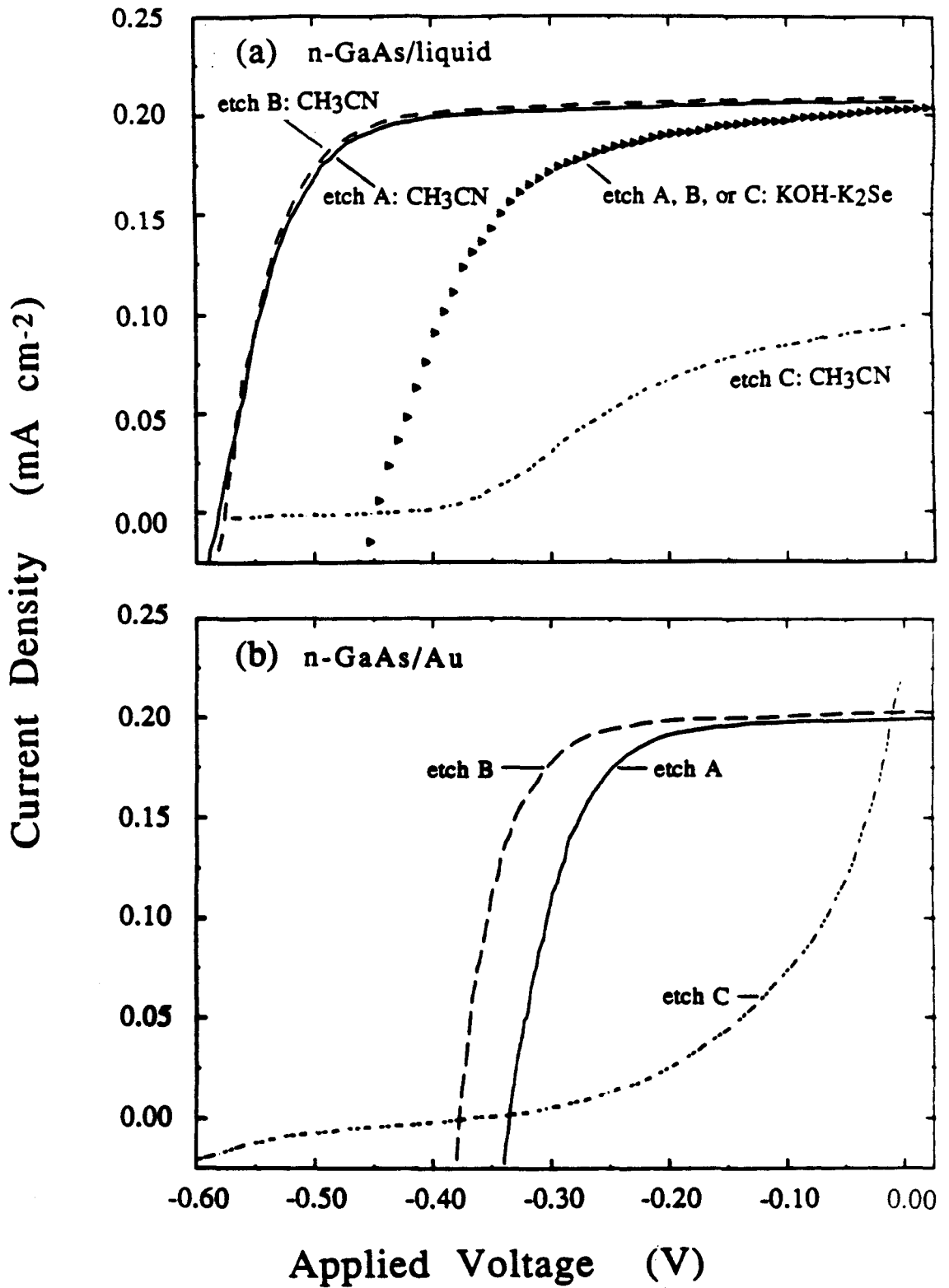
A. Response in $\text{FeCp}_2^{+/0} - \text{LiClO}_4 - \text{CH}_3\text{CN}$ Electrolyte.

Figure 1a displays the effect of various surface treatments on the photoelectrochemical I - V behavior of the n-GaAs/acetonitrile (CH_3CN)-90.0 mM ferrocene (FeCp_2)-0.5 mM ferrocenium hexafluorophosphate (FeCp_2PF_6)-0.7 M lithium perchlorate (LiClO_4) junction.¹¹ The initial, etched surface was prepared by exposure of the GaAs to etch A (see Experimental for the details of each etch).¹² Use of etch A consistently yielded a surface free of elemental arsenic (As^0), having a slightly gallium rich substrate composition, and having sub-monolayer amounts of substrate oxides (*vide infra*). In the n-GaAs/ CH_3CN - $\text{FeCp}_2^{+/0}$ cell, this surface produced an open circuit voltage (V_{oc}) of (568 ± 10) mV at a short circuit photocurrent density (J_{sc}) of 0.21 mA cm^{-2} (Figure 1a). Open circuit voltages of this value at the reported light intensities are in keeping with the highest V_{oc} 's observed for the n-GaAs/ CH_3CN - $\text{FeCp}_2^{+/0}$ cell.¹¹

Previous work¹² has shown that an As^0 -rich GaAs surface can be obtained by applying Etch B to GaAs. No measurable difference ($V_{\text{oc}} = 568 \pm 10$ mV at $J_{\text{sc}} = 0.21 \text{ mA cm}^{-2}$) in I - V properties was observed for such an As^0 -rich n-GaAs surface in contact with the CH_3CN - $\text{FeCp}_2^{+/0}$ electrolyte (Figure 1a), as compared to a n-GaAs electrode treated to Etch A.

In contrast, an oxide-covered surface (prepared by exposing an n-GaAs electrode to etch C)¹² yielded a V_{oc} of 425 mV at $J_{\text{sc}} = 0.09 \text{ mA cm}^{-2}$, and displayed low fill factors in contact with the CH_3CN - $\text{FeCp}_2^{+/0}$ electrolyte (Figure 1a).

Figure 1: (a) Potentiostatic I - V curves (scan from negative to positive voltages, 50 mV s^{-1}) of various n-GaAs/liquid interfaces. The solid, dashed, and dashed-dotted curves were obtained in contact with the CH_3CN -90.0 mM ferrocene (FeCp_2)-0.5 mM FeCp_2PF_6 -0.7 M LiClO_4 electrolyte. (Solid line): n-GaAs etched by method A. (Dashed line): n-GaAs exposed to etch B. (Dashed-dotted line): n-GaAs etched exposed to etch C. (Triangles): Representative I - V curve obtained for n-GaAs, in contact with aqueous 1.0 M KOH -0.8 M K_2Se -0.1 M K_2Se_2 electrolyte, etched by any of the above procedures. All etches, electrochemistry, and sample manipulations were carried out using deaerated solutions in a flowing N_2 atmosphere ($\text{ppm O}_2 \approx 1\text{-}2$) glove box. The residual overpotentials (solid line and dashed line) are largely due to concentration overpotentials and series resistance losses in the potentiostatic 3-electrode cell configuration. (b) Two-electrode I - V measurements (in air) of thin (100-150 Å) Au Schottky barriers formed on n-GaAs electrodes etched as in Figure 1a (solid line-etch A, dashed line-etch B, and dashed-dotted line-etch C).



B. Response in $\text{Se}^{-/2-}$ – KOH Electrolyte.

Additional I - V data were obtained for these GaAs surfaces in contact with an aqueous 1.0 M KOH-0.8 M K_2Se -0.1 M K_2Se_2 electrolyte.¹¹ The KOH- $\text{Se}^{-/2-}$ (aq) system was chosen for study because it has been shown to provide effective kinetic competition with aqueous-based photocorrosion processes.¹⁰ At the concentrations and light intensities used in this study, oxidation of Se^{2-} by photogenerated holes is fast enough to beat out, by several orders of magnitude, oxidation of the GaAs lattice itself.^{10,11} In contact with the KOH- $\text{Se}^{-/2-}$ (aq) medium, n-GaAs surfaces exposed to all three etching treatments produced essentially identical I - V characteristics ($V_{\text{oc}} = 436$ mV; $J_{\text{sc}} = 0.20$ mA cm⁻²) that were distinct from the current-voltage characteristics obtained in the non-aqueous $\text{FeCp}_2^{+/0}$ – LiClO_4 electrolyte (Figure 1a).

2. Current-Voltage Behavior of Etched n-GaAs/Au Schottky Junctions.

n-GaAs/Au Schottky barriers (Figure 1b) showed slight differences in V_{oc} from the near-stoichiometric surface, etch A ($V_{\text{oc}} = 333$ mV at $J_{\text{sc}} = 0.20$ mA cm⁻²), to the As⁰-rich surface, etch B ($V_{\text{oc}} = 374$ mV at $J_{\text{sc}} = 0.20$ mA cm⁻²), whereas the oxidized n-GaAs surface, etch C, yielded low fill factors (< 0.25) and a V_{oc} of 470 mV at $J_{\text{sc}} = 0.20$ mA cm⁻².

3. X-ray Photoelectron Spectra of Etched and Photoelectrochemically Cycled n-GaAs Electrodes.

The ability to resolve the x-ray photoelectron (XP) signal intensity of lattice As from elemental As⁰ is critical to the correlation of the XPS data with the I - V data in this study. Figure 2 displays examples of line fits to the As 3d region of two GaAs electrodes, one etched by method A (clean substrate), the other by method B (As⁰-rich interface). In the absence of interfacial elemental arsenic, the As 3d region displays a characteristic lower

shoulder on the higher binding energy side of the As substrate signal.²³ The observed peak is shown deconvoluted as two main peaks which comprise the As 3d_{5/2} (larger of the two) and As 3d_{3/2} contributions to the overall signal (Figure 2a). In contrast, Figure 2b shows a reversal of the sloping shoulder of the XP signal to the lower binding energy side of the spectrum, a clear signature of the presence of elemental arsenic.²³ The deconvolution of this XP signal clearly shows both the 3d_{5/2} and 3d_{3/2} contributions from lattice As, and appearing at higher binding energy, the contributions of the 3d_{5/2} and 3d_{3/2} components of As⁰. Note that the signal from the 3d_{5/2} component of As⁰ falls nearly directly under the 3d_{3/2} component of the signal from lattice As, hence the need for very high resolution in the XPS. Both spectra show a sub-monolayer contribution due to arsenic sub-oxides on the high binding energy side of the foot of the main signal.

Analysis of XP spectra confirms expectations (*vide supra*) as to the surface chemical character of n-GaAs electrodes prepared by Etch A, B, or C. Surfaces etched by method A were slightly gallium rich (As/Ga = 0.89 ± 0.01), and supported less than a monolayer of lattice oxides. Etch B produced a near stoichiometric lattice surface (As/Ga = 1.02 ± 0.04), less than a monolayer of lattice oxides, and (90 ± 30) % of a monolayer of As⁰. Etch C gave a near stoichiometric surface free of As⁰, but was covered with 3 to 4 monolayers of lattice oxides. Each etched surface averaged about 3 to 7 monolayers of carbonaceous adsorbates. Figure 3 displays representative As 3d and Ga 3d XPS signals for each GaAs etch treatment before and after photoelectrochemical cycling in contact with CH₃CN-FeCp₂⁺⁰ or KOH-Se⁻²-(aq) electrolytes. Wide scans for samples in Figure 3 a-c consistently displayed XPS signals only from As, Ga, O, Se, and C sources; samples shown in 3 d-e gave signals only for As, Ga, O, and C sources. No signal intensity was observed, on any of the samples, for S, Br, K, Fe, F, or P sources. Table II lists the peak positions and intensities observed, and Table III summarizes the analysis of the various surface species found on each sample.

Figure 2: X-ray photoelectron spectra of the As 3d regions of etched n-GaAs surfaces.

(a) n-GaAs electrode etched by method A. The solid line shows both the raw data and the fit to the peak shape, which are superimposable on one another. The two major dashed curves show the contributions of the lattice As 3d_{5/2} (lower binding energy) and As 3d_{3/2} (higher binding energy) components, in the expected spin-orbit ratio of 3:2 integrated signal intensity, to the overall peak shape. A trace of sub-oxide is visible at the higher binding energy foot of the observed peak. (b) n-GaAs electrode etched by method B. The solid line shows both the raw data and the fit to the peak shape, which are superimposable on one another. The pair of short-dashed curves represents the spin-orbit contribution from lattice As to the overall peak shape. The pair of long-dashed curves gives the spin-orbit contribution from elemental As⁰ to the overall peak shape. This substrate shows $\Gamma_{As^0} = 2.5 \times 10^{-9}$ mole cm⁻² (3.4 Å; 1.2 monolayer coverage) on the surface. Both spin-orbit pairs reflect the expected 3:2 ratio of integrated signal intensity. A small amount of sub-oxide is visible at the higher binding energy foot of the observed peak.

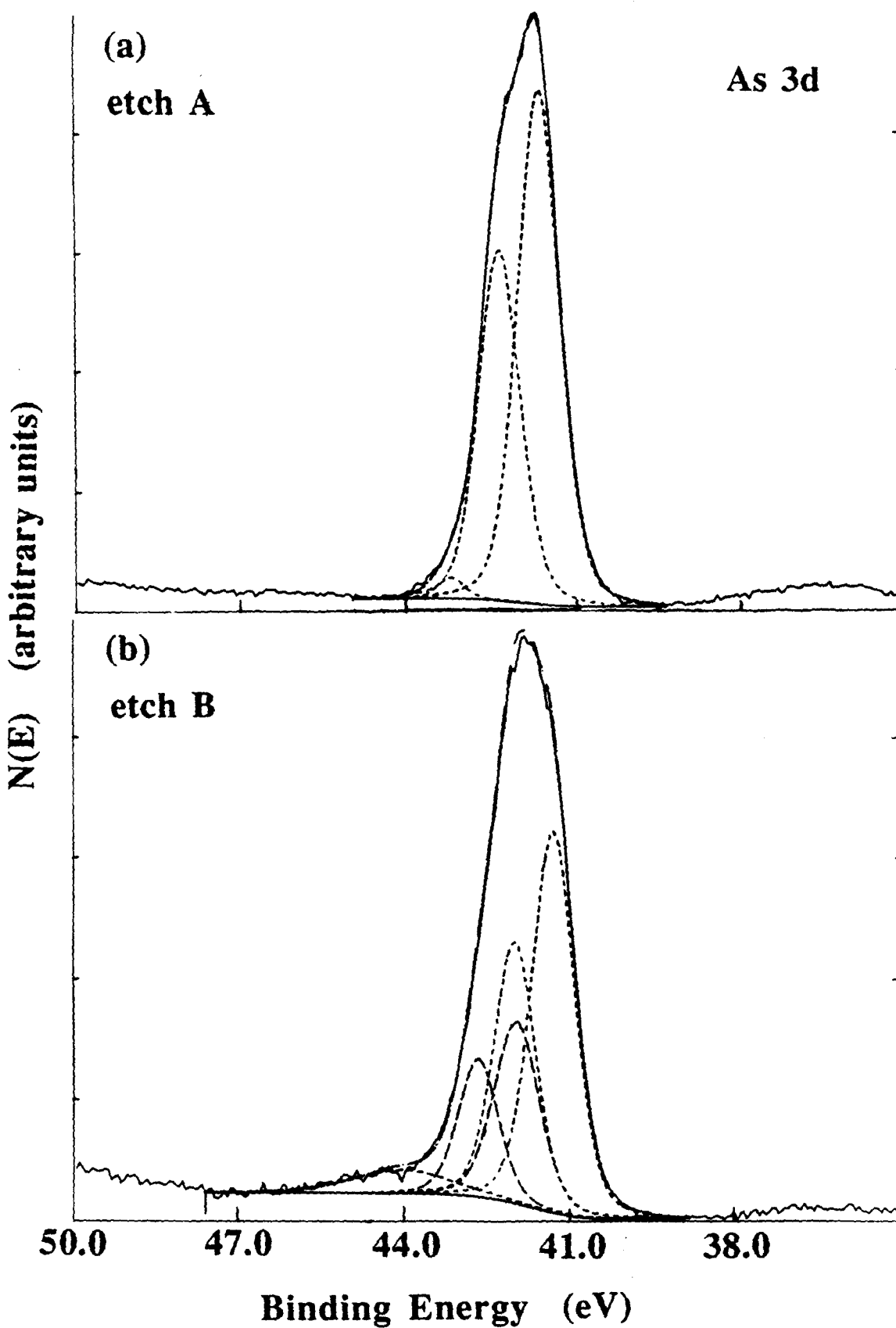


Figure 3: X-ray photoelectron spectra of As 3d and Ga 3d regions of etched and photoelectrochemically cycled n-GaAs surfaces. The overlaid spectra in each panel were scaled such that their relative intensities due to lattice As 3d and Ga 3d contributions from each peak matched to within $\pm 2\%$. (a) (Solid line): n-GaAs etched by exposure to Etch A. (Dashed line): Identical electrode subsequently photoelectrochemically cycled in KOH(aq)-Se⁻²⁻ electrolyte. Note the 3:2 area ratio of the As 3d doublet peaks, which is in excellent agreement with the lineshape for substrate As with negligible contributions from As⁰. (b) (Solid line): n-GaAs etched by exposure to Etch B. The As 3d doublet peaks now clearly show a contribution from As⁰. (Dashed line): Identical electrode subsequently photoelectrochemically cycled in KOH(aq)-Se⁻²⁻ electrolyte. Loss of As⁰ from the surface was clearly indicated by changes in the line shape of the As 3d doublet. (c) (solid line): n-GaAs etched by exposure to Etch C. The As 3d doublet shows a 3:2 area ratio (negligible As⁰), but the peaks at *ca.* 44 eV, 46 eV, and 21 eV indicate As₂O₃, As₂O₅, and Ga₂O₃, respectively. Photoemission from oxygen 2s core levels gives rise to the peak partially shown at *ca.* 25 eV. (Dashed line): Identical electrode subsequently photoelectrochemically cycled in KOH(aq)-Se⁻²⁻ electrolyte. Note that the 3:2 area ratio of the As 3d doublet is unperturbed and that the surface oxides have been completely stripped from the interface. (d) (Solid line): n-GaAs exposed to etch A. (Dashed line): Identical electrode following photoelectrochemical cycling in CH₃CN-FeCp₂⁺⁰ electrolyte. Note the 3:2 area ratio of the As 3d doublet peaks, which is in excellent agreement with the lineshape for substrate As with negligible contributions from As⁰. (e) (Solid line): n-GaAs exposed to etch B. The As 3d doublet peaks now clearly show a contribution from As⁰. (Dashed line): Identical electrode following photoelectrochemical cycling in CH₃CN-FeCp₂⁺⁰ electrolyte. The As 3d doublet peaks still indicate the presence of As⁰.

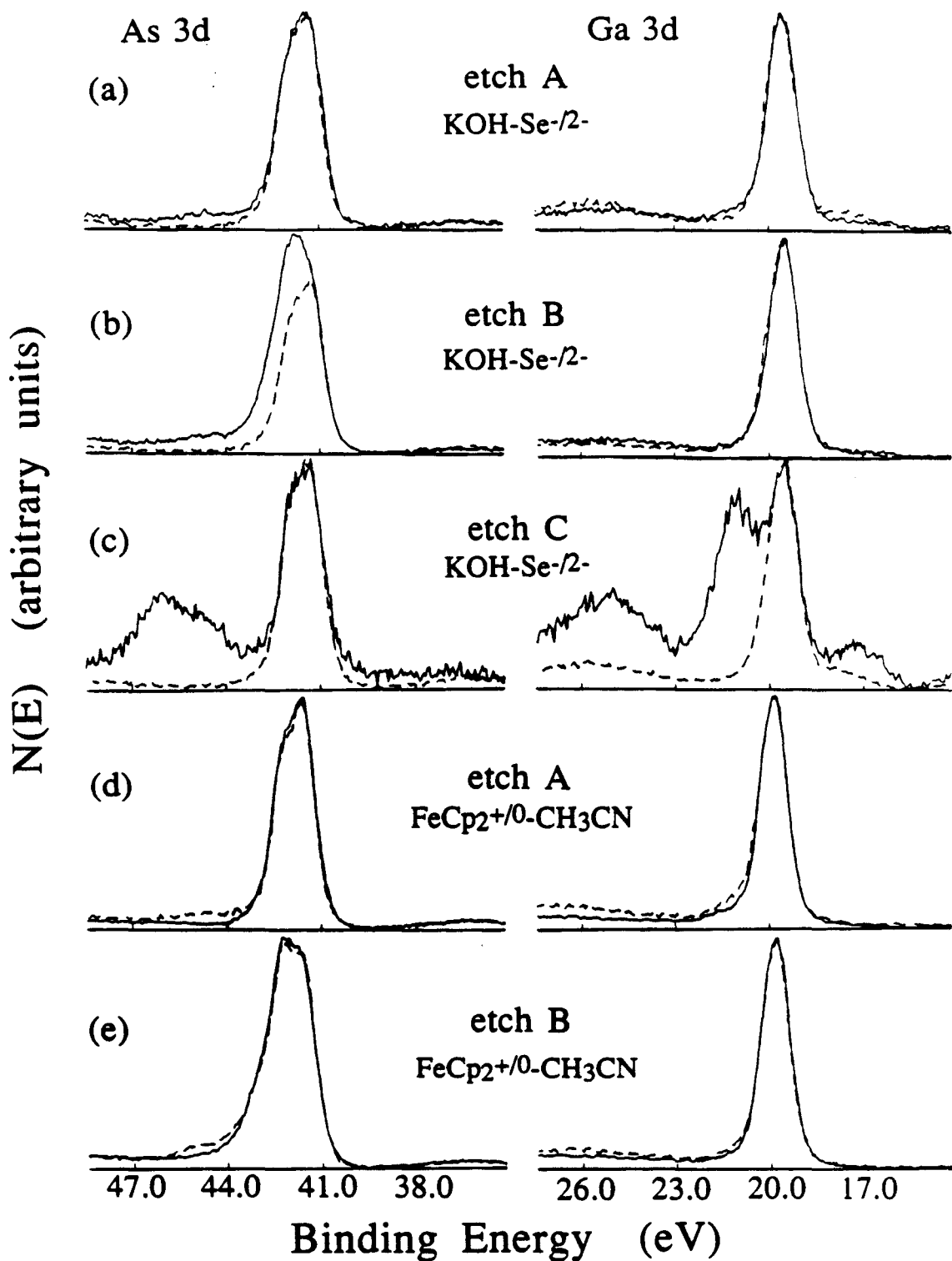


Table II: XPS Peak Positions^a and Intensities^b of Etched and Photoelectrochemically Cycled (100) n-GaAs Electrodes

Experiment	GaAs Substrate				Elemental Arsenic	
	GaAs (As 3d) ^c		GaAs (Ga 3d) ^c		As ⁰ (As 3d)	
	Peak ^d	Intensity	Peak ^d	Intensity	Peak ^d	Intensity
Etch A: Br ₂ -CH ₃ OH/KOH	41.18	1,740	19.32	1,968	e	----
Etch A + photoelectrochemical cycling ^f in KOH(aq)-Se ⁻²⁻	41.20	2,081	19.34	2,495	e	----
Etch B: Br ₂ -CH ₃ OH/KOH + 60 s 1:1:100 solution	41.20	2,669	19.29	2,577	41.95	645
Etch B + photoelectrochemical cycling ^f in KOH(aq)-Se ⁻²⁻	41.29	4,123	19.44	5,273	e	----
Etch C: Br ₂ -CH ₃ OH/KOH + 60 s 1:1:100 solution + 60 s 30% H ₂ O ₂ (aq)	41.19	607	19.31	585	e	----
Etch C + photoelectrochemical cycling ^f in KOH(aq)-Se ⁻²⁻	41.19	2,849	19.36	3,803	e	----
Etch A: Br ₂ -CH ₃ OH/KOH	41.36	8,613	19.50	9,619	e	----
Etch A + photoelectrochemical cycling ^f in FeCp ₂ ⁺⁰ -CH ₃ CN	41.36	4,309	19.57	4,438	e	----
Etch B: Br ₂ -CH ₃ OH/KOH + 60 s 1:1:100 solution	41.37	7,445	19.46	7,483	42.15	1,097
Etch B + photoelectrochemical cycling ^f in FeCp ₂ ⁺⁰ -CH ₃ CN	41.34	5,549	19.50	6,568	42.26	938

Table II (continued)

Experiment	Substrate Oxides				Carbon Sources	
	<u>As₂O₃ (As 3d)</u>		<u>Ga₂O₃ (Ga 3d)</u>		<u>C_xH_yO_z (1 s)</u>	
	Peak ^g	Intensity	Peak ^g	Intensity	Peak ^g	Intensity
Etch A: Br ₂ -CH ₃ OH/KOH	43.66	229	20.53	70	284.71	5,488
Etch A + photoelectrochemical cycling ^f in KOH(aq)-Se ⁻²⁻	h	83	20.44	48	284.93	9,693
Etch B: Br ₂ -CH ₃ OH/KOH + 60 s 1:1:100 solution	43.44	220	20.46	45	284.61	6,258
Etch B + photoelectrochemical cycling ^f in KOH(aq)-Se ⁻²⁻	43.32	191	20.49	74	285.18	7,885
Etch C: Br ₂ -CH ₃ OH/KOH + 60 s 1:1:100 solution + 60 s 30% H ₂ O ₂ (aq)	46.04 ⁱ	249	20.99	366	284.94	8,459
Etch C + photoelectrochemical cycling ^f in KOH(aq)-Se ⁻²⁻	h	----	j	----	285.32	9,210
Etch A: Br ₂ -CH ₃ OH/KOH	42.96	78	21.17	185	284.95	11,227
Etch A + photoelectrochemical cycling ^f in FeCp ₂ ⁺⁰ -CH ₃ CN	42.97 ^k	277	20.36 ^l	360	285.18	18,736
Etch B: Br ₂ -CH ₃ OH/KOH + 60 s 1:1:100 solution	42.98	921	20.43	308	284.81	8,234
Etch B + photoelectrochemical cycling ^f in FeCp ₂ ⁺⁰ -CH ₃ CN	43.15	901	20.73	227	285.06	13,055

Table II (continued)

Experiment	Selenium Sources		Other Substrate Sources				Oxygen Sources	
	Peak ξ	Intensity	Peak ξ	Intensity	Peak ξ	Intensity	Peak ξ	Intensity
Etch A: Br ₂ -CH ₃ OH/KOH	q	----	r	----	s	----	532.24	66,954
Etch A + photoelectrochemical cycling ^f in KOH(aq)-Se ⁻²⁻	54.38	107	42.58	185	17.70	227	532.76	61,642
Etch B: Br ₂ -CH ₃ OH/KOH + 60 s 1:1:100 solution	q	----	r	----	s	----	532.07	83,890
Etch B + photoelectrochemical cycling ^f in KOH(aq)-Se ⁻²⁻	54.51	511	42.56	423	18.32	238	532.68	38,687
Etch C: Br ₂ -CH ₃ OH/KOH + 60 s 1:1:100 solution + 60 s 30% H ₂ O ₂ (aq)	q	----	r	----	s	----	532.60	162,759
Etch C + photoelectrochemical cycling ^f in KOH(aq)-Se ⁻²⁻	54.29	259	42.56	212	17.87	251	532.92	107,512
Etch A: Br ₂ -CH ₃ OH/KOH	q	----	r	----	s	----	532.56	116,450
Etch A + photoelectrochemical cycling ^f in FeCp ₂ ⁺⁰ -CH ₃ CN	q	----	r	----	s	----	533.37	190,203
Etch B: Br ₂ -CH ₃ OH/KOH + 60 s 1:1:100 solution	q	----	r	----	s	----	532.54	74,263
Etch B + photoelectrochemical cycling ^f in FeCp ₂ ⁺⁰ -CH ₃ CN	q	----	r	----	s	----	532.57	176,512

Table II (continued)

Notes to Table II

- a. All peak positions are expressed in binding electron volts (BeV) relative to an observed Au 4f_{7/2} line, defined to be at 84.00 BeV, detected from a polycrystalline gold film on a stainless steel mounting clip grounded to the spectrometer.
- b. Normalized signal intensities given for all measured lines, *except the O 1s line*, were obtained from raw signal intensities normalized by the scan duration, and appropriate photoelectron mean-free path, atomic number density, and photoelectron differential cross-section. X-ray excitation was obtained from a monochromatized Al K_α (1486.6 eV) small spot source.
- c. GaAs and GaAs display As 3d and Ga 3d XPS signal intensity, respectively, contributed from the GaAs crystal substrate.
- d. Peak positions listed are those of the 3d_{5/2} component of the deconvoluted As 3d and Ga 3d line shapes.
- e. No x-ray photoelectron signal intensity was observed that was attributable to As⁰.
- f. Please see Experimental and Results sections for details.
- g. Peak positions listed resulted from a single peak fit to the signal intensities from oxidized substrate, seleno based species, and carbonaceous adsorbates.
- h. No x-ray photoelectron signal intensity was observed that was attributable to arsenic (III or V) oxides.
- i. Main peak observed in the arsenic oxide region, attributed to As₂O₅; a lesser peak (60 % of the integrated signal intensity of the main oxide peak) appeared at 44.58 BeV, attributed to As₂O₃.
- j. No x-ray photoelectron signal intensity was observed that was attributable to gallium oxides.
- k. A very low broad peak (< 70 % of the integrated signal intensity from the main arsenic oxide peak) centered at 44.57 BeV was also observed following photoelectrochemical cycling.
- l. A very low broad peak (< 35 % of the integrated signal intensity from the main gallium oxide peak) centered at 21.28 BeV was also observed following photoelectrochemical cycling.
- m. Attribution of the signal source is ambiguous; Se⁰ and Se²⁻ species are both consistent with the peak position. Intensity given assuming Se⁰.
- n. Attribution of the signal source is ambiguous; As_xSe_y and arsenic sub-oxide species are both consistent with the peak position. Intensity given assuming As₂Se₃.

Table II (continued)

Notes to Table II

- o. Attribution of the signal source is ambiguous; Ga_xSe_y and Ga^0 species are both consistent with the peak position. Intensity given assuming Ga^0 .
- p. Only the raw oxygen 1s intensity is listed, as several possible oxygen containing species contribute to the observed signal.
- q. No x-ray photoelectron signal intensity was observed that was attributable to selenium based sources.
- r. No x-ray photoelectron signal intensity was observed that was attributable to arsenic sub-oxides or arsenic-selenium sources.
- s. No x-ray photoelectron signal intensity was observed that was attributable to gallium-selenium compounds or elemental gallium.

Table III: XPS Surface Composition^a of Etched and Photoelectrochemically Cycled (100) n-GaAs Electrodes

Experiment	\underline{As}^b		Surface Coverage ^c ($\times 10^{10}$ mole cm^{-2})			
	Ga	$\Gamma (As_2O_3)$	$\Gamma (Ga_2O_3)$	$\Gamma (As^0)$	$\Gamma (Se^{0/2-})^d$	$\Gamma (C_xH_yO_z)$
Etch A: Br ₂ -CH ₃ OH/KOH	0.88	5.3	2.2	e	f	43
Etch A + photoelectrochemical cycling ⁱ in KOH(aq)-Se ⁻²⁻	0.83	g	h	e	4.8	53
Etch B: Br ₂ -CH ₃ OH/KOH + 60 s 1:1:100 solution	1.04	2.8	0.8	24	f	34
Etch B + photoelectrochemical cycling ⁱ in KOH(aq)-Se ⁻²⁻	0.78	j	k	e	12	31
Etch C: Br ₂ -CH ₃ OH/KOH + 60 s 1:1:100 solution + 60 s 30% H ₂ O ₂ (aq)	1.04	(12 ± 4) ^l	(24 ± 5) ^l	e	f	69
Etch C + photoelectrochemical cycling ⁱ in KOH(aq)-Se ⁻²⁻	0.75	m	n	e	8.5	43
Etch A: Br ₂ -CH ₃ OH/KOH	0.90	0.4	1.3	e	f	27
Etch A + photoelectrochemical cycling ⁱ in FeCp ₂ ⁺⁰ -CH ₃ CN	0.97	2.7	4.5	e	f	52
Etch B: Br ₂ -CH ₃ OH/KOH + 60 s 1:1:100 solution	0.99	4.4	1.9	15	f	20
Etch B + photoelectrochemical cycling ⁱ in FeCp ₂ ⁺⁰ -CH ₃ CN	0.84	5.5	1.9	17	f	33

Table III (continued)

Notes to Table III

- a. Surface coverage given with respect to the normalized GaAs (As 3d) signal intensity.
- b. Ratio of substrate GaAs to GaAs observed in the detected surface volume.
- c. The surface coverage (Γ) is given in mole cm^{-2} (projected area GaAs).
- d. Attribution of the signal is ambiguous; Se^0 and Se^{2-} species are both consistent with the peak position.
- e. No x-ray photoelectron signal observed that was attributable to As^0 .
- f. No x-ray photoelectron signal observed that was attributable to Se^0 .
- g. Coverage (1.5×10^{-10} mole cm^{-2}) based on an arsenic selenide species at 42.58 BeV.
- h. Coverage (1.1×10^{-10} mole cm^{-2}) based on elemental gallium at 17.70 BeV.
- i. Please see Experimental and Results sections for details.
- j. Coverage (1.7×10^{-10} mole cm^{-2}) based on an arsenic selenide species at 42.56 BeV.
- k. Coverage (0.9×10^{-10} mole cm^{-2}) based on elemental gallium at 18.32 BeV.
- l. Error in the coverage estimate due to uncertainties in the position of the thick oxide layer.
- m. Coverage (1.3×10^{-10} mole cm^{-2}) based on an arsenic selenide species at 42.56 BeV.
- n. Coverage (1.0×10^{-9}) based on elemental gallium at 17.87 BeV.

Photoelectrochemical cycling of n-GaAs (0.05-3.8 C cm⁻² of anodic charge) in contact with the KOH-Se^{-/2-}(aq) electrolyte resulted in nearly identical final GaAs surface compositions after either etch A, B, or C (Figure 3a-c, and Tables II and III). These surfaces were characterized by slightly gallium rich substrates (As/Ga = 0.79 ± 0.04), sub-monolayer (< 1/2) signals attributable to Se⁰ or possibly arsenic selenide or gallium selenide species (based on Se⁰: (8 ± 4) × 10⁻¹⁰ mole cm⁻²), sub-monolayer signals (< 15%) of an arsenic species ascribable to a sub-oxide or an arsenic selenide species (42.57 ± 0.01 BeV and, based on As₂Se₃, (1.5 ± 0.02) × 10⁻¹⁰ mole cm⁻² coverage), and sub-monolayer signals (< 20%) of a gallium species potentially due to elemental gallium or a gallium selenide species (18.0 ± 0.3 BeV and, based on Ga⁰, (4 ± 5) × 10⁻¹⁰ mole cm⁻² coverage). Additionally, only extremely small signals for Ga or As oxide were observed to remain on each surface; this is especially notable for the oxidized surface produced by Etch C (Figure 3c). Electrodes initially exposed to Etch B and subsequently cycled in KOH-Se^{-/2-}(aq) electrolyte showed no evidence of signals due to As⁰ (Figure 3b). At the instrumental limit of detectability, this implies less than 5% of a monolayer as an upper limit on the amount of residual As⁰ that may have remained on the surface. The intensity ratios of the As 3d doublet peaks after photoelectrochemical cycling in KOH-Se^{-/2-}(aq) electrolyte were consistent with that expected for lattice As. Notably, by exposing As⁰ that had been evaporated onto the sidewalls of a large Schlenk vessel to an aliquot of KOH-Se^{-/2-}(aq) electrolyte, it was verified experimentally that both yellow and gray arsenic are soluble in KOH-Se^{-/2-}(aq) solutions, confirming previous suggestions to this effect.²⁴

In contrast, final state surface compositions for etched n-GaAs electrodes photoelectrochemically cycled in CH₃CN-FeCp₂^{+/0} electrolyte (42 mC cm⁻² total anodic current in each case) were nearly identical to their respective initially-prepared surfaces. While changes in the ratio of lattice As to Ga were small and apparently random, each surface experienced a small increase in lattice oxide coverage. Nonetheless, final state

lattice oxide coverage remained below one monolayer in each case. The ratio of the As 3d doublet peaks shown in the XP spectrum of Figure 3e clearly demonstrates that, following exposure to Etch B, the electrode was left with a surface layer of As⁰. The presence of As⁰ and the overall surface composition were not substantially changed after photoelectrochemical cycling in CH₃CN-FeCp₂⁺⁰ electrolyte (Figure 3e, Table III).

Additionally, n-GaAs electrodes etched by method B, when exposed for five minutes to either neat CS₂, neat CH₃CN, and an aliquot of CH₃CN - FeCp₂⁺⁰ electrolyte in the dark, did not show significant differences from the surface compositions found for other n-GaAs electrodes etched in an identical fashion.

Discussion

These results relate to the theories of Schottky barrier formation that are designed to account for the Fermi level position of semiconductor contacts. The advanced unified defect model (AUDM) of Lindau, Spicer, *et al.* assigns the invariance of the Schottky barrier height to the formation of defect levels located at 0.7 eV and 0.9 eV below the conduction band edge.⁷ Within the AUDM, these defects are formed during the act of contact formation with the metal (and/or upon exposure to oxygen). In contrast, the effective work function model of Woodall, Freeouf, *et al.* implicates excess interfacial elemental arsenic as the chemical species that establishes the position of the GaAs surface Fermi level.⁵ In this model, the excess As is formed during contact formation as a result of interfacial alloying between the metal and gallium. Alternatively, the metal-induced gap state (MIGS) model of Tersoff accounts for the barrier height invariance as a result of states formed at mid-gap due to the penetration of metal orbitals from metallic species on the GaAs surface.⁸ (Strictly speaking, no direct evidence as to the metallic or semimetallic nature of As⁰ formed on GaAs surfaces by etch B is available. The direct applicability of the MIGS model is therefore open to debate.)

The liquid junction results are useful in assessing these models. The data indicate that predictions derived from the AUDM do not apply to the n-GaAs/CH₃CN-FeCp₂⁺⁰ interface. Within the AUDM, the maximum potential photovoltage available should not exceed 0.9 V. This is in direct conflict with observations at cooled (220 K) n-GaAs/CH₃CN-FeCp₂⁺⁰ junctions under 10 Suns solar simulated illumination, which yielded V_{oc} values in excess of 1.05 V and activation barriers for minority carrier transport of 1.4 eV. For this case, the observed open-circuit photovoltage exceeds the possible barrier height predicted by the AUDM, thus ruling the defect model out as a viable framework for predicting behavior at the n-GaAs/CH₃CN-FeCp₂⁺⁰ liquid junction. In addition, from the data in this study neither the MIGS model nor the effective work function model can be ruled out as describing the source of Fermi level pinning at semiconductor junctions, because it is expected that acetonitrile contacts may differ substantially from metal contacts both in terms of wavefunction penetration to the underlying GaAs substrate and in terms of the effect of liquids on the apparent work function. However, the MIGS model is substantially weakened as providing a consistent description of the source of Fermi level pinning at semiconductor interfaces. The nearly identical I - V behavior of clean (Etch A) and As⁰-laden (Etch B) n-GaAs surfaces in contact with CH₃CN-FeCp₂⁺⁰ electrolytes indicates that the presence of elemental arsenic at GaAs surfaces is, by itself, an insufficient condition upon which to base predictions of barrier height or dominant recombination processes. This point is supported by reference to Figure 1, where it is seen that, at identical short-circuit current densities, the I - V behavior of the variously etched GaAs surfaces in contact with liquid electrolytes is superior to identically prepared surfaces in contact with Au overlayers. A stronger interplay between theory and experiment would seem to be warranted for this aspect of semiconductor junction physics.

A consistent chemical interpretation of the I - V behavior and XP spectra of etched n-GaAs electrodes in KOH- $\text{Se}^{-/2}$ -(aq) electrolyte (*vide supra*) can be obtained by reference to the solubility properties of oxides of gallium and arsenic, and As^0 . The solubility of Ga oxides and As oxides in aqueous solutions of $\text{pH} > 12$ is well documented.²⁵ Furthermore, the stripping ability of basic selenide solutions toward As^0 was noted above. These properties correlate well with the insensitivity of the GaAs/KOH- $\text{Se}^{-/2}$ -(aq) I - V data to the initial surface preparation condition of the GaAs electrode (Figure 1a). The dominant effect of photoelectrochemically cycling the differently prepared n-GaAs surfaces in KOH- $\text{Se}^{-/2}$ (aq) electrolyte is to strip all lattice oxides and any As^0 initially present from the interface.

While it is interesting to note that the independence of I - V behavior on initial surface preparation in KOH- $\text{Se}^{-/2}$ -(aq) electrolyte results from a common final surface, the results in $\text{CH}_3\text{CN-FeCp}_2^{+/0}$ solution are important precisely because two chemically distinct surfaces displayed identical I - V behavior.

It has been shown that gallium oxide, arsenic oxide, and As^0 are insoluble in CH_3CN or in the $\text{CH}_3\text{CN-FeCp}_2^{+/0}$ electrolyte (*vide supra*). Thus, this nonaqueous solvent system is better suited than the KOH- $\text{Se}^{-/2}$ -(aq) medium for probing the dependence of n-GaAs photoelectrochemical properties on the initial surface composition. The behavior of etched n-GaAs electrodes in $\text{CH}_3\text{CN-FeCp}_2^{+/0}$ electrolyte verifies the assertion above that the I - V curves in this system provide a useful probe of the electrical recombination properties of the various initial surface treatments. Support for this interpretation of the GaAs/ CH_3CN contact chemistry has been obtained from high-resolution x-ray photoelectron spectroscopic (XPS) analysis.²⁶ Notably, the XPS data confirms that the presence of excess As^0 does not necessarily lead to large recombination rates and low open circuit voltages at all GaAs interfaces, as shown by the

I-V properties of the As⁰-rich sample in contact with CH₃CN-FeCp₂⁺⁰ solution (Figure 1a, Etch B).

The lower V_{oc}, decreased fill factor, and the presence of an inflection point^{10,24} for n-GaAs/KOH-Se⁻²-(aq) interfaces, relative to the properties of etched n-GaAs in contact with CH₃CN-FeCp₂⁺⁰ electrolyte, have been previously interpreted in terms of slow hole transfer rates into the KOH-Se⁻²-(aq) solution,^{27,28} and the data are consistent with these conclusions. The lack of substantial differences in the n-GaAs/CH₃CN-FeCp₂⁺⁰ *I-V* characteristics for Br₂-CH₃OH/KOH etched (etch A) and As⁰-rich (etch B) n-GaAs surfaces (Figure 1a), and the relatively large values of V_{oc} for As⁰-rich surfaces (etch B) in contact with CH₃CN-FeCp₂⁺⁰ solution compared to those of n-GaAs/Au contacts (Figure 1b), indicates that the presence of interfacial elemental As⁰ on the GaAs surface is not sufficient to induce low barrier heights and large interfacial electrical recombination currents at all n-GaAs surfaces. This is consistent with the findings of Aspnes and Stocker,^{12b} who observed reductions in the reverse bias dark current for As⁰-rich surfaces on InGaAs mesa diodes, but is not consistent with expectations of high GaAs surface recombination rates associated with the presence of excess interfacial As.²⁴

The near-stoichiometric GaAs surfaces obtained in this work also yield improved photoelectrochemical efficiencies in CH₃CN compared to previous etching procedures.¹¹ Under 88 mW cm⁻² of ELH-type irradiation, V_{oc} values of 0.83 V, short circuit photocurrent densities of 20 ± 0.5 mA cm⁻², fill factors of 0.54-0.64, and efficiencies of 11.0 ± 1.0 % for mirror finished, Br₂-CH₃OH/KOH etched n-GaAs samples (etch A) in contact with 1.0 M LiClO₄-0.20 M FeCp₂-0.5 mM FeCp₂⁺-CH₃CN electrolyte have been previously observed.^{11c} These GaAs/CH₃CN V_{oc} values far exceed those reported for GaAs Schottky barrier systems,^{29,30} and are comparable to the best values reported for any GaAs surface barrier device at these photocurrent densities.³⁰ The bulk recombination/diffusion limited V_{oc} for this material is approximately 1.02 V at

$J_{sc} = 20 \text{ mA cm}^{-2}$,²⁹ implying that even further improvement in I - V properties is possible with additional control over the GaAs surface chemistry.

In conclusion, it has been shown that non-aqueous photoelectrochemical methods (I - V experiments) may be applied to n-GaAs interfaces in order to assess the electrical recombination properties of various surface treatments. It was demonstrated that the presence of interfacial As^0 does not necessarily lead to large recombination rates and poor I - V behavior at all GaAs interfaces. Additionally, it was shown that n-GaAs electrodes with initially different surface compositions (etches A, B, or C) yield a common final state surface composition and I - V characteristic when exposed to the aqueous based $\text{KOH-Se}^{-1/2}$ -electrolyte.

References

1. (a) Many, A.; Goldstein, Y.; Grover, N. B. *Semiconductor Surfaces*; North Holland: Amsterdam, 1965. (b) Morrison, S. R. *The Chemical Physics of Surfaces*; Plenum Press: New York, 1977. (c) Smith, R. A. *Semiconductors*; Cambridge University Press: Cambridge, Great Britain, 1978.
2. Pierret, R. F. *Modern Series on Solid State Devices*; Pierret, R. F., Neudeck, G. W., Eds.; Addison-Wesely: Reading, Massachusetts, 1987; Vol. VI, *Advanced Semiconductor Fundamentals*.
3. (a) Ettenberg, M.; Kressel, H. *J. Appl. Phys.* **1976**, *47*, 1538; (b) Nelson, R. J.; Sobers, R. G. *Appl. Phys. Lett.* **1978**, *32*, 761.
4. Yablonovitch, E.; Swanson, R. M.; Eades, W. D.; Weinberger, B. R. *Appl. Phys. Lett.* **1986**, *48*, 245.
5. (a) Woodall, J. M.; Freeouf, J. L.; *J. Vac. Sci. Technol.* **1981**, *19*, 794. (b) Sharma, B. L. *Metal-Semiconductor Schottky Barrier Junctions and Their Applications*; Plenum: New York, 1984. (c) Freeouf, J. L.; Woodall, J. M. *Appl. Phys. Lett.* **1981**, *39*, 727. (d) Kirchner, P. D.; Warren, A. C.; Woodall, J. M.; Wilmsen, C. W.; Wright, S. L.; Baker, J. M. *J. Electrochem. Soc.* **1988**, *135*, 1822. (e) Wilmsen, C. W.; Kirchner, P. D.; Baker, J. M.; McInturff, D. T.; Pettit, G. D.; Woodall, J. M. *J. Vac. Sci. Technol.* **1988**, *B6*, 1180. (f) Brillson, L. J.; Viturro, R. E.; Mailhot, C.; Shaw, J. L.; Tache, N.; McKinley, J.; Margaritondo, G.; Woodall, J. M.; Kirchner, P. D.; Pettit, G. D.; Wright, S. L. *J. Vac. Sci. Technol.* **1988**, *B6*, 1263.

6. (a) Yablonovitch, E.; Sandroff, C. J.; Bhat, R.; Gmitter, T. *Appl. Phys. Lett.* **1987**, *51*, 439. (b) Yablonovitch, E.; Skromme, B. J.; Bhat, R.; Harbison, J. P.; Gmitter, T. J. *Appl. Phys. Lett.* **1989**, *54*, 555.
7. (a) Spicer, W. E.; Lindau, I.; Skeath, P.; Su, C. Y.; *J. Vac. Sci. Technol.* **1980**, *17*, 1019. (b) Lindau, I.; Chye, P. W.; Garner, C. M.; Pianetta, P.; Su, C. Y.; Spicer, W. E. *J. Vac. Sci. Technol.* **1978**, *15*, 1332. (c) Spicer, W. E.; Liliental-Weber, Z.; Weber, E.; Newman, N.; Kendelewicz, T.; Cao, R.; McCants, C.; Mahowald, P.; Miyano, K.; Lindau, I. *J. Vac. Sci. Technol.* **1988**, *B6*, 1245. (d) Spicer, W. E.; Kendelewicz, T.; Newman, N.; Cao, R.; McCants, C. *Appl. Surf. Sci.* **1988**, *33*, 1009.
8. Tersoff, J. *Phys. Rev. Lett.* **1984**, *52*, 465.
9. (a) Thurmond, C. D.; Schwartz, G. P.; Kammlott, G. W.; Schwartz, B. *J. Electrochem. Soc.* **1980**, *127*, 1366. (b) Kurtin, S.; McGill, T. C.; Mead, C. A. *Phys. Rev. Lett.* **1969**, *22*, 1433. (c) Brillson, L. J. *Phys. Rev. Lett.* **1978**, *40*, 260. (d) Zur, A.; McGill, T. C.; Smith, D. L. *Phys. Rev. B.* **1983**, *28*, 2060.
10. (a) Chang, K. C.; Heller, A.; Schwartz, B.; Menezes, S.; Miller, B. *Science (Washington, D. C.)* **1977**, *196*, 1097. (b) Parkinson, B. A.; Heller, A.; Miller, B. *Appl. Phys. Lett.* **1978**, *33*, 521.
11. (a) Gronet, C. M.; Lewis, N. S. *Appl. Phys. Lett.* **1983**, *43*, 115. (b) Casagrande, L. G.; Lewis, N. S. *J. Am. Chem. Soc.* **1985**, *107*, 7190. (c) Abrahams, I. L.; Casagrande, L. C.; Rosenblum, M. D.; Rosenbluth, M. L.; Santangelo, P. G.; Tufts, B. J.; Lewis, N. S. *Nouv. J. Chim.* **1987**, *11*, 157.

12. (a) Aspnes, D. E.; Studna, A. A. *Appl. Phys. Lett.* **1981**, *39*, 316.
(b) Stocker, H. J.; Aspnes, D. E. *Appl. Phys. Lett.* **1983**, *42*, 85.
13. Seah, M. P.; Dench, W. A. *Surf. Interface Anal.* **1979**, *1*, 2.
14. Scofield, J. H. *J. Electron Spectrosc. Relat. Phenom.* **1976**, *8*, 129.
15. Weast, R. C., Astle, M. J., Eds. *CRC Handbook of Chemistry and Physics*; Chemical Rubber Co.: Boca Raton, 1980; Vol. 60, p B-57.
16. Weast, R. C., Astle, M. J., Eds. *CRC Handbook of Chemistry and Physics*; Chemical Rubber Co.: Boca Raton, 1980; Vol. 60, p B-80.
17. Bain, C. D.; Whitesides, G. M. *J. Phys. Chem.* **1989**, *93*, 1670.
18. Feldman, L. C.; Mayer, J. W. *Fundamentals of Surface and Thin Film Analysis*; North-Holland: New York, 1986.
19. Blakemore, J. J. *J. Appl. Phys.* **1982**, *53*, R123.
20. Fadley, C. S. *Prog. Solid State Chem.* **1976**, *11*, 265.
21. Weast, R. C., Astle, M. J., Eds. *CRC Handbook of Chemistry and Physics*; Chemical Rubber Co.: Boca Raton, 1980; Vol. 60, p B-119.
22. Weast, R. C., Astle, M. J., Eds. *CRC Handbook of Chemistry and Physics*; Chemical Rubber Co.: Boca Raton, 1980; Vol. 60, p B-79.
23. Vasquez, R. P.; Lewis, B. F.; Grunthaner, F. J. *J. Vac. Sci. Technol.* **1983**, *B1*, 791.

24. Heller, A., "Chemical Control of Surface and Grain Boundary Recombination in Semiconductors," In *Photoeffects at Semiconductor-Electrolyte Interfaces*; Nozik, A., Ed.; ACS Symposium Series 146, American Chemical Society: Washington, D. C., 1981; pp 57 - 77.
25. Pourbaix, M. *Atlas of Electrochemical Equilibria in Aqueous Solution*; Pergamon: New York, 1966.
26. (a) Kraut, E. A.; Grant, R. W.; Waldrop, J. R.; Kowalczyk, S. P. *Phys. Rev. B* **1983**, *28*, 1965. (b) Bahl, M. K.; Woodall, R. O.; Watson, R. L.; Irgolic, K. J. *J. Chem. Phys.* **1976**, *64*, 1210.
27. Allongue, P.; Cachet, H. *J. Electrochem. Soc.* **1984**, *131*, 2861.
28. (a) Tufts, B. J.; Abrahams, I. L.; Casagrande, L. G.; Lewis, N. S. *J. Phys. Chem.* **1989**, *93*, 3260. (b) Rosenbluth, M. L.; Casagrande, L. G.; Tufts, B. J.; Lewis, N. S., "Studies of Si and GaAs Semiconductor/Liquid Junction Devices," In *Proceedings, 18th IEEE Photovoltaic Specialists Conference*; IEEE: New York, 1985; pp 1405 - 1408.
29. (a) Fahrenbruch, A. L.; Bube, R. H. *Fundamentals of Solar Cells*; Academic Press: New York, 1983. (b) Sze, S. M. *Physics of Semiconductor Devices*; Wiley: New York, 1981.
30. Stirn, R. J.; Yeh, Y. C. M. *IEEE Trans. Electronic Devices* **1977**, *ED-24*, 476.

Thesis Summary

The body of this thesis work focussed on investigations of interfacial chemistry at n-GaAs electrodes in contact with aqueous 1.0 M KOH - 0.8 M K₂Se- 0.1 M K₂Se₂ and acetonitrile/90.0 mM ferrocene - 0.5 mM ferrocenium hexafluorophosphate - 0.7 M LiClO₄ electrolytes. The principle issues addressed were (i) the kinetic basis for the improvements in current-voltage (*I-V*) behavior observed at transition metal ion treated GaAs electrodes; (ii) the mechanism, stoichiometry, scope, and limitations of the reactions of Co(III) ammine complexes with GaAs surfaces; and (iii) explorations of the surface chemistry and attendant *I-V* properties of specifically prepared n-GaAs surfaces in contact with KOH-Se⁻²⁻(aq) or acetonitrile/LiClO₄-FeCp₂⁺⁰ electrolytes.

With respect to the current-voltage properties of n-GaAs photoanodes in contact with aqueous basic selenide electrolytes, attempts to model the improvements found for transition metal ion-treated electrodes had given rise to two contradictory theories: suppression of surface state recombination by metal/surface state bond formation resulting in a lower density of mid-gap surface states; and reduction in the overpotentials associated with charge transfer to Se⁻²⁻ at the GaAs surface by adsorption of an electrocatalyst. Kinetically, these theories differ in the manner in which metal ion treatment was expected to affect surface recombination and faradaic hole and electron current pathways. A comparison of the *I-V* behavior of illuminated n-type GaAs, unilluminated n⁺-type and p-type GaAs, and 10 % Sn-doped In₂O₃ (ITO) electrodes before and after exposure to transition metal ions revealed that the dominant effect of such treatments was

electrocatalytic in nature. No exception to this observation was found: those metal ion treatments which gave rise to reduced overpotentials for the oxidation and reduction of Se^{-2} species at n^+ -GaAs and ITO electrodes also were observed to give improvements in the current-voltage characteristic at illuminated n -GaAs photoanodes.

Clearly, the improvements observed in the I - V characteristic of transition metal ion-treated GaAs electrodes indicated that the metal complexes were effecting a transformation of some type at the GaAs surface. This hypothesis led naturally to surface sensitive studies of the reactions of transition metal complexes with GaAs interfaces. A technique or combination of techniques, capable of identifying (at the sub-monolayer level) the amount and identity of all surface constituents was required. X-ray photoelectron spectroscopy (XPS) provides data on the amount (to a fraction of a monolayer), oxidation state, and relative composition of all atomic species (except for H) at a given surface. It therefore became the method of choice. An initial XPS survey of GaAs surfaces that had been individually exposed to the metal complexes used in the current-voltage work was conducted. The results indicated that, except for the Co(III) amines, the coverage of GaAs surfaces with metal ion species was below one-half monolayer coverage. XPS signals from the Co(III) ammine-treated surfaces, however, were much larger; typical signals ranged from two to ten monolayers coverage. The focus of the surface studies was subsequently brought to bear on the reactions of Co(III) amines with GaAs surfaces.

The XPS studies demonstrated that the reaction between GaAs surfaces and Co(III) amines was pH dependent, occurring in aqueous solutions only above pH = 8, and that it involved electron transfer from substrate GaAs to Co(III) ammine complex to yield oxidized substrate and surface bound Co(II) hydroxide. An independent radiotracer study, employing the gamma-ray active nuclide ^{57}Co as the $[\text{}^{57}\text{Co(III)(NH}_3)_6](\text{Br})_3$ complex, verified the pH dependence and coverage estimates derived from XPS analysis. XPS analysis of the relative intensities of Co 2p region and O 1s region signals showed

that the stoichiometry between Co(II) and O (corrected for contributions from sources of O 1s signal intensity due to surface bound water, substrate oxides, and carbonaceous material) was Co(II): O = 1.0: 2.1 ± 0.2 . No evidence for the ligands initially in the inner shell of the reagent Co(III) ammine complex was ever detected at reacted GaAs interfaces. This information ruled out electrostatic or ligand substitutional routes to cobalt metal ion attachment at the GaAs surface.

The identity of the surface bound Co(II) species was unambiguously confirmed by extended x-ray absorption fine structure (EXAFS) experiments. EXAFS analysis provides information on the bond distances and number of ligands in the inner sphere of a particular absorber atom. A comparison of the EXAFS data from model compounds Co(O)(OH) and *roseo*-Co(OH)₂ with the EXAFS obtained from GaAs powders exposed to aqueous basic (pH > 9) solutions of Co(III) ammine complexes established that the surface bound Co(II) species was *roseo*-Co(OH)₂. Taken together, the XPS and EXAFS data made possible the complete determination of the amount and identity of the significant surface constituents at Co(III) ammine-reacted GaAs interfaces.

The overall reaction between Co(III) ammine complexes and GaAs surfaces was determined by quantitative chemical analysis. Solutions of Co(III) ammine complexes were anaerobically-reacted with freshly ground GaAs powder. The solution was filtered off from the GaAs solids, and the eluent analyzed for Co(II) ions, and total Co, As, and Ga content. Using a combination of modified wet chemical analytic protocols and x-ray fluorescence analysis, the reaction stoichiometry was found to be:



The pH dependence of the GaAs/Co(III) reaction was again confirmed by these methods.

XPS and EXAFS analysis also demonstrated that immersion of $\text{Co}(\text{OH})_2$ covered GaAs surfaces into $\text{KOH-Se}^{-/2-}(\text{aq})$ electrolyte resulted in the transformation of $\text{Co}(\text{OH})_2$ to a CoSe_2 -like phase of approximate Co: Se stoichiometry 1.0: 1.8. This CoSe_2 phase is believed to be very closely related to the active electrocatalyst responsible for the reduction of $\text{Se}^{-/2-}$ oxidation/reduction overpotentials at the GaAs/ $\text{KOH-Se}^{-/2-}(\text{aq})$ liquid junction.

The above surface analytic studies were conducted on isolated n-GaAs single crystals or GaAs powders. A naturally arising question concerns the dependence of the surface chemistry at n-GaAs electrodes on the composition of contacting electrolyte, as well as the effects of specific surface compositions on cell current-voltage properties. In order to address these issues, correlations between the current-voltage characteristics of n-GaAs electrodes etched to produce a near stoichiometric (As: Ga) surface, an elemental arsenic (As^0) rich surface, or a uniformly oxidized surface in contact with $\text{KOH-Se}^{-/2-}(\text{aq})$ or acetonitrile/ $\text{LiClO}_4\text{-FeCp}_2^{+/0}$ electrolytes were probed by high resolution XPS. The correlated data from this work also provided for a test of the general applicability of solid state (metal/semiconductor and insulator/semiconductor systems) theories regarding charge carrier dynamics to n-GaAs/liquid interfaces.

High resolution XPS data on specifically etched n-GaAs electrodes demonstrated the reproducible and characteristic nature of each etch. The near stoichiometric surface was found to be free of any sign of elemental arsenic, composed of a nearly 1: 1 substrate As to Ga stoichiometry, and practically free of substrate oxides. n-GaAs electrodes etched to produce an elemental arsenic (As^0) rich surface were observed to be identical to the near stoichiometric etch except for the appearance of *ca.* a full monolayer of As^0 . Uniformly oxidized n-GaAs surfaces were consistently found to be near stoichiometric in substrate As: Ga, free of As^0 signals, and covered with Ga_2O_3 , As_2O_3 , and As_2O_5 substrate oxides.

When any of the specifically etched n-GaAs electrodes were placed in contact with the KOH-Se⁻²⁻(aq) electrolyte and photoelectrochemically cycled, they all displayed the same current-voltage characteristic. Furthermore, the XPS data showed they all possessed the same final surface chemical composition: a near stoichiometric substrate, a surface free of any substrate oxides or As⁰, and having a small (< ca. 1/2 monolayer) Se interface component. The *I-V* behavior and surface chemical composition data are not unwarranted in light of the known solubility behavior of As⁰ and substrate oxides in the KOH-Se⁻²⁻(aq) electrolyte. The data do, however, demonstrate that initial state surface chemical preparations of n-GaAs electrodes are unlikely to survive exposure to the basic selenide electrolyte. It follows, then, that this system is not an ideal one for assessing the role of chemical manipulations of electrically active recombination sites at GaAs/liquid junctions.

XPS analysis of the individually etched n-GaAs surfaces placed in contact with the acetonitrile/LiClO₄-FeCp₂⁺⁰ electrolyte revealed that the initial and final surface compositions were altered very little following photoelectrochemical cycling, showing only slight increases in substrate sub-oxides. Predictably, the *I-V* behavior of the uniformly oxidized substrate was very poor in the acetonitrile-based FeCp₂⁺⁰ electrolyte. The *I-V* characteristic for the near stoichiometric etch and the As⁰ rich etch were, significantly, virtually identical. This is in contrast to the behavior of identically etched electrodes made into Schottky barrier devices by the filament evaporation of thin (< 100 Å) Au overlayers onto the etched n-GaAs surfaces. The Schottky barrier devices displayed, for the same photocurrent density as that employed in the liquid interface experiments, much lower open circuit photovoltages (consistent with solid state theory), as well as clear differences in the *I-V* properties of the near stoichiometric surface and the As⁰ rich surface. The data indicated that the acetonitrile/LiClO₄-FeCp₂⁺⁰ system is, in general, a useful experimental platform for studies of the chemical manipulation of electrically active surface states. The

data also demonstrated that current theories regarding carrier dynamics at solid state GaAs junctions are not generally applicable to n-GaAs/liquid junctions.

The research contained herein has established several important aspects of interfacial chemistry at GaAs/liquid contacts. Foremost among them is the notion that the GaAs surface ought to be viewed as a dynamic chemical entity. The GaAs surface can involve itself in redox active reactions, is sensitive to solution pH, and may be reproducibly prepared with a variety of specific interface compositions. Studies of the reaction chemistry at GaAs (or any other substrate) clearly require a careful accounting of all of the reactant and product species. To this end, careful attention to surface and solution analytic techniques must be made if a detailed picture of the system is to be completed. Finally, the results highlight the inapplicability of current theories of solid state semiconductor junction physics to liquid based systems. In this respect, the need for a more thorough interplay between theory and experiment at semiconductor/liquid junctions is warranted.